# Chapter 6 The Rehabilitation of the Hand – A Review

## 6.1 Introduction

A normal working hand is one of the most important features for independence in an individual's life. The human dependence on fully functioning hands is highlighted most when these integral tools of the body are hindered in some way. The loss of hand function results in a severe compromise of the ability to feed and care for oneself, and limits one's participation in work, social and family life (Scott and Peckham 1995).

There are many injuries or conditions that can result in the loss of hand function. These include paralysis (from central or peripheral nerve injuries), swelling, joint stiffness, pain, burns, scarring or broken bones. For individuals recovering from such conditions, vigilant, appropriate and effective therapy of the hands can significantly improve the outcome of the healing process and the restoration of hand function (Hunter, Mackin et al. 1995). Prior to the prescription of appropriate therapy, comprehensive assessment of hand condition is necessary. Furthermore, ongoing assessment during the course of the applied therapy can ensure the treatment will continue to be appropriate and provide optimal benefits to the patient. In addition, during the recovery process and where no further improvements can be made to the hand, there are technologies available that can improve hand function.

One of the aims of this project is to create a novel human-machine interface to address the abovementioned aspects of hand rehabilitation, namely: assessment, therapy and function.

To the best knowledge of the author, no prior-art technology exists that can provide hand assessment, therapy and function in a single device. However, much work has been conducted in each area over many years. A review of current technology is presented in the following sections. Literature specifically related to the hand rehabilitation device is reviewed in Chapter 7.

## 6.2 Assessment of hand condition and function

Clinical examination the hand includes physical inspection, evaluation of range of motion (ROM), testing of intrinsic and extrinsic muscles, evaluation of motor and sensory functions and assessment of pinch and grip strength. Radiographs, CT scans, MRIs, electro-diagnostics, and specialised laboratory tests are also useful in confirming diagnoses made on clinical bases (Chapter 5, Hunter, Mackin et al. 1995).

### 6.2.1 Range of Motion

Of the assessment procedures listed above, examination of ROM is perhaps the most informative and useful.: *"Rarely, if ever, is assessment of hand function discussed without some reference to the range of motion (ROM) of the involved extremity"* (Chapter 8, Hunter, Mackin et al. 1995). Range of motion assessment is typically undertaken by therapists using goniometers (to measure joint angles) and torque

gauges (to measure torque required to passively* move the joints to end range) (Bromley, Unsworth et al. 1994; Hunter, Mackin et al. 1995; Schultz-Johnson 2002; Glasgow, Wilton et al. 2003). Measurements can be used to determine torque range of motion (TROM) and active range of motion (AROM). In TROM, the therapist applies a known force using a torque gauge or a hanging weight to each joint and measures the resulting joint angle (see Figure 6.1). Using a series of different torques, a distinctive TROM curve can be plotted (see Figure 6.2). TROM results are indicative of joint stiffness and other factors resisting movement in the joints (Swanson, de Groot Swanson et al. 1995). AROM readings (measured by goniometer) are used to assess the abilities of the patients to flex or extend joints actively. Active movement is commonly stopped near the end range of motion by stretching antagonistic muscles. Other factors that could prematurely limit active movement of joints include ligamentous or capsular damage, muscle contractures, pain, fibrous cysts, or joint disorders such as arthritis (Chapter 5, Hunter, Mackin et al. 1995). Identifying structures involved in active movement and comparing those with results from passive movement such as TROM and manual resistive tests helps identify the cause of movement restriction (Swanson, de Groot Swanson et al. 1995).

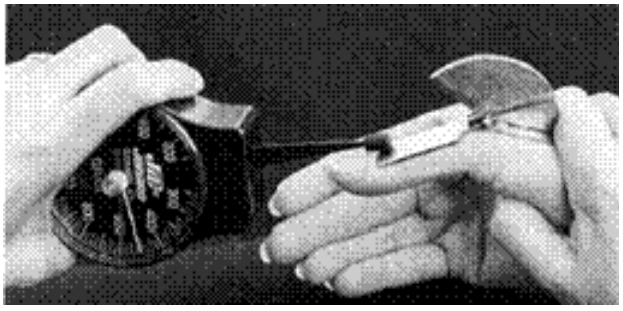

Figure 6.1 A typical method for measuring Torque Range of Motion (TROM).

* Passive movement refers to movements caused by active forces (as opposed to active internal forces from muscles)

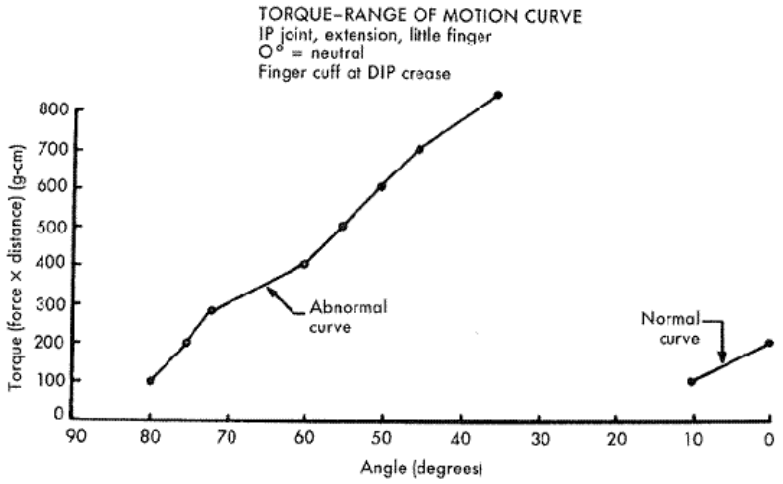


**Figure 6.2 The Torque Range of Motion (TROM) plot.** The position, shape and slope of the TROM curve can provide information about the monitored joint (Adapted from Swanson, de Groot Swanson et al. 1995).

### 6.2.2 Functional assessment of the hand

'Hand function' can be defined as "the ability to use the hand in everyday activities" (Fowler and Nicol 2001). Traditionally, assessment of hand function has focused on grip or pinch strength, range of motion and subjective evaluation of activities of daily living. However, although grip strength can be measured objectively, it may bear little relation to the patient's actual hand function (Agnew and Maas 1982). A more valuable form of functional assessment is conducted through the use of activities of daily living (ADL) assessment boards (Sollerman 1980). Using ADL assessment boards (see Figure 6.4), different types of hand grip and object manipulation can be evaluated. Sollerman (1978, 1980) described eight main types of grasp used by normal hands in activities of daily living. These are listed below:

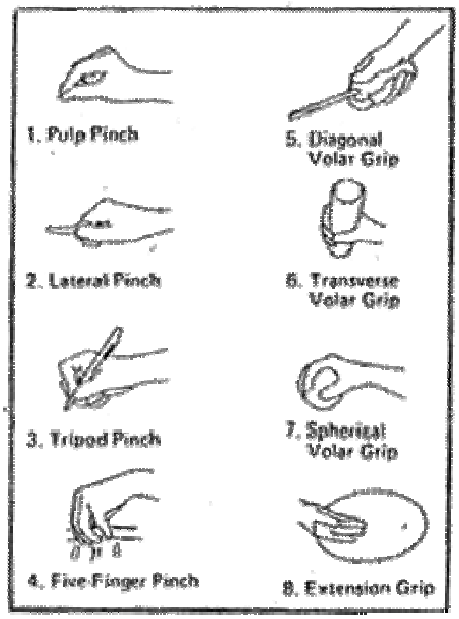


**Figure 6.3 Sollerman's eight categories of functional grasp** (adapted from Sollerman 1980)

Sollerman devised a grip function test in which each of the main grip types listed was performed by the patient and scored by the investigator. The scoring depended on both the performance ability and the patient's choice of grip type. Adaptations of the ADL assessment board (see Figure 6.4) have been used and continue to be used by clinicians and researchers to evaluate hand function (Fowler and Nicol 2001).

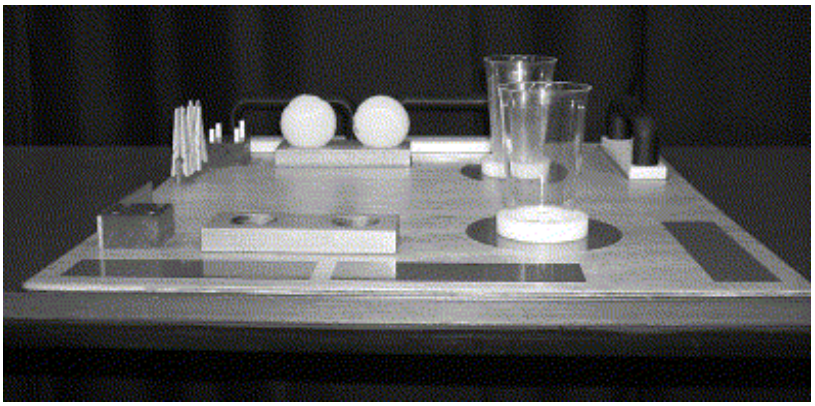

**Figure 6.4 Hand function assessment board.** (Adapted from Fowler et al, 2001). Various objects with particular shapes are grasped and manipulated by the patient. The clinician assesses (scores) hand function based on the performance of the patients taking into account time and accuracy.

## 6.3 Therapy of the hand

The main purpose of therapy following damage to the hands is to reduce impairments and restore functional performance by improving joint range of motion, alleviating pain and reducing inflammation and swelling. Ultimately, the body must heal itself. However, there are many techniques and tools to help facilitate the recovery of the hands. Clinical evidence shows that joint mobilisation, a supervised exercise program and appropriate splinting can all increase joint range of motion (Michlovitz, Harris et al. 2004).

### 6.3.1 Continuous passive motion

Until the middle of the 20th century, immobilisation was the traditional method used to treat wounds and damaged joints. Experiments with animals however, in the latter half of the century produced important studies on the effects of immobilisation and motion on synovial joints (Akeson, Amiel et al. 1987; Dimick 1990; Le Stayo 1995). It was found that immobilisation causes profound alterations in joint structures including intraarticular adhesions, which mature into scar tissues and lead to joint stiffness (Dimick 1990). The main cause of the ensuing adhesion is the formation of irregular cross-links in the newly synthesised collagen during the recovery of the joints (Akeson, Amiel et al. 1987). Early mobilisation of joints has been shown to prevent abnormal cross-links by facilitating orderly deposition of new collagen fibrils while maintaining lubrication-critical fibre distance within the cellular matrix (Dimick 1990).

The concept of continuous passive motion (CPM) as a means to stimulate healing and prevention of join stiffness was introduced in 1970 by R. B Salter. In this form of therapy joints are passively moved in a cyclical manner by a machine interface for hours at a time. The movement enhances the healing process and reduces complications such as muscle and sheath adhesions or non-functional scar tissue formation in the skin, joints, tendons, sheaths and muscles (Bentham, Brereton et al. 1987; Dent 1993; Adams and Thompson 1996). Salter studied the effects of CPM on knee joint of rabbits. He concluded that CPM is well tolerated, has a healing effect on synovial connective tissues and prevents adhesions and joint stiffness (Salter 1996).

CPM is often prescribed and utilized for rehabilitation of larger joints such as the knee, ankle, shoulder, elbow and hip with positive results (Ring, Simmons et al. 1998). It is easier to administer CPM therapy to singular, large joints that can be isolated. For rehabilitation of the small multiple joints of the hand however, although CPM has been proven to be beneficial, the therapy is seldom prescribed or used. This is often due to the limitation of the currently available CPM devices. Hand CPM technology includes devices of varying portability attached to the hand and wrist by the way of braces. Attachment to the fingers is usually at the tips (see Figure 6.5). Most devices work by passively moving the tips of the fingers, pulling them down to a closed clench and then reversing the movement. This movement is repeated slowly for a specified number of hours per day, over a number of days. There are several publications based on the results of the available devices (Bentham, Brereton et al. 1987; Dimick 1990; Dent 1993; Le Stayo 1995; Adams and Thompson 1996).

**Figure 6.5 Hand CPM devices.** *Most such devices are difficult to attach to the fingers and most fail to address individual joints. Movement is typically facilitated by a single motorised mechanism which pulls the finger tips into a clenched hand and reverses the motion.*

### 6.3.2 Dynamic splinting

The dynamic splint is a form of therapy used for improving ROM (see Figure 6.6). This is a type of upper extremity splint in which particular joints are immobilised, while others are free to move (Brand 1995). Rubber bands or other elastic materials are used to apply prolonged therapeutic forces to specific joints to increase the compliance of stiff structures, lengthen shortened soft tissue, increase joint range of motion and help restore functional use of limited joints (Austin, Slamet et al. 2004). One of the factors influencing the effectiveness of dynamic splinting is Total End Range Time (TERT)(Chow, Dovelle et al. 1989; Brand 1995; Chester, Beale et al. 2002; Glasgow, Wilton et al. 2003; Austin, Slamet et al. 2004). TERT refers to the amount of time a joint is held at its passive end range (the joint angle at which passive torque does not cause further movement).

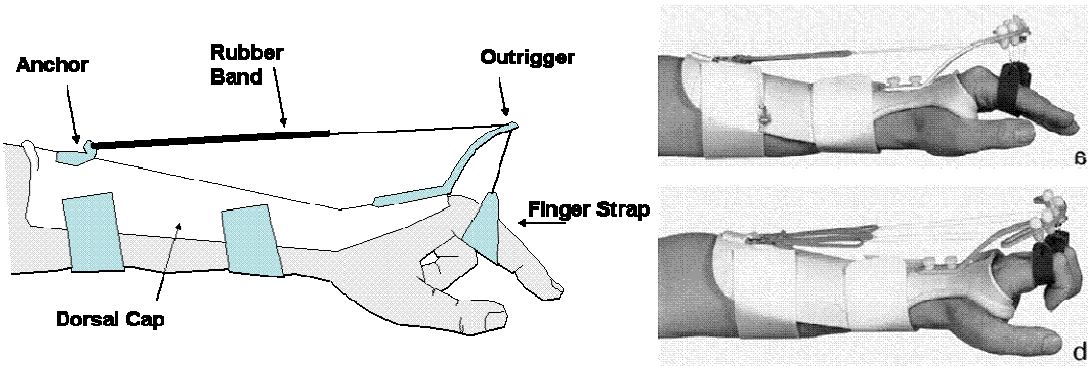


**Figure 6.6 The dynamic splint.** *An outrigger dynamic splint is used to apply a prolonged extension force to the metacarpal joint of the index finger.*

## 6.4 Methods used to improve hand function

Loss of the ability to perform basic grasps as well as individual finger and thumb movement, is likely to lead affected persons to depend on other people or systems to fulfil basic activities of daily living. The degree of this dependence will vary according to the ability of the individual to compensate for the loss of coordinated hand movement and function. For example, many tetraplegic persons have residual wrist, elbow and shoulder mobility. They learn to optimise the coordination of these preserved movements to manipulate objects. One such strategy for regaining function is the tenodesis grasp (Hart, Kilgore et al. 1998): Tenodesis refers to hand closure which is associated by either active or passive wrist extension. This closure of the hand is produced by the passive tensioning of the finger and thumb flexor tendons in the hand during wrist extension (see Figure 6.7).

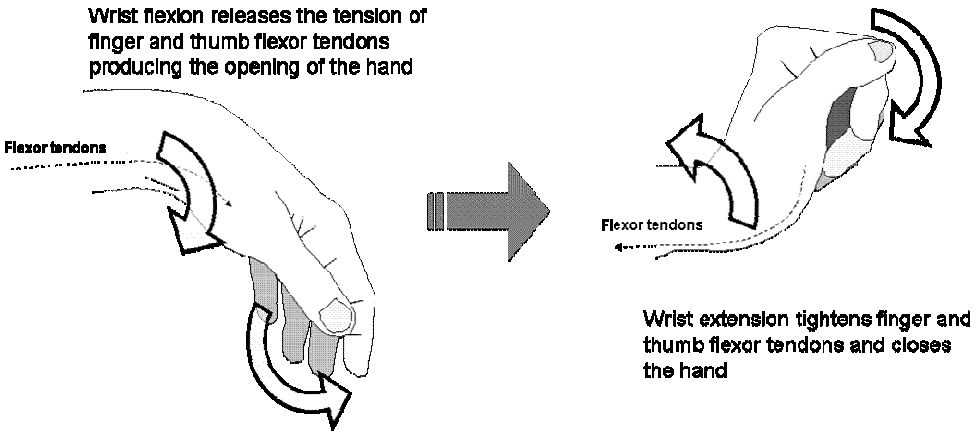


**Figure 6.7 Tenodesis Grasp.** *Extension of the wrist causes the flexor tendons of the fingers to tighten and pull fingers closed. This technique can be used for paralysed hands to achieve light grasps.*

### 6.4.1 Flexor hinge splint

The flexor hinge splint is a splint mechanism that increases the tenodesis movement by transferring mechanical energy from the extension of the wrist into flexion of the metacarpal phalangeal (MCP) joints (Stenehjem and Swenson 1983). These splints may be either purely mechanical or partially motorised to increase force and movement (Moromugi, Koujina et al. 2004).

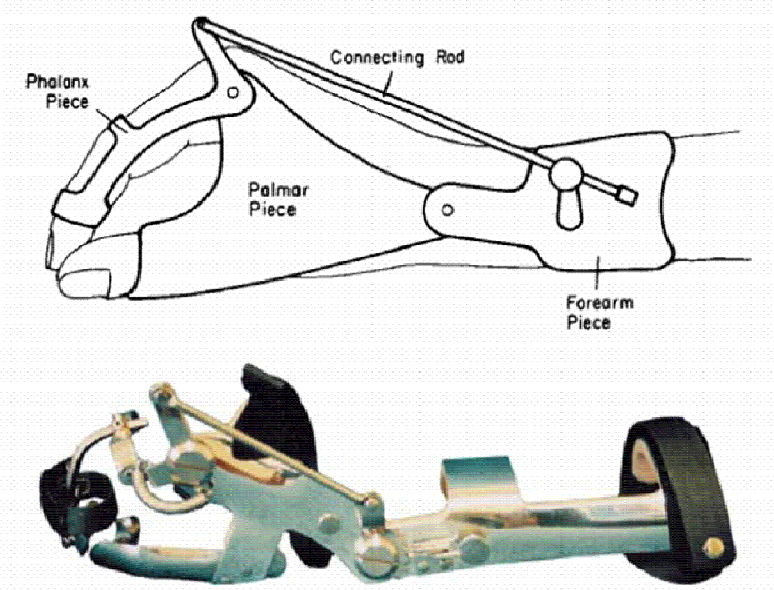


**Figure 6.8 The Flexor Hinge splint.** *Adapted from (Stenehjem, 1983).*

### 6.4.2 Functional electrical stimulation (FES)

FES is primarily suited for the activation of otherwise paralysed* muscles using electrical stimulation to create functional movement. As a functional aid for the hands, it has been used with tetraplegic individuals with little or no active hand flexion or extension to provide grasp and release. Although hand muscles can be functionally stimulated via external electrodes (Prochazka, Elek et al. 1992), the most effective method for coordinated and accurate activation is via an implanted neural prosthesis (Smith, Peckham et al. 1987; Wijman, Stroh et al. 1990; Peckham and Knutson 2005). The prosthesis is a simulator chip implanted within the chest from which internal electrodes travel to the muscles. An external transmitting coil placed on the skin above the neural prosthesis powers and communicates with the stimulator. The carefully coordinated activation of the hand muscles is achieved by a pre-programmed external controller (see Figure 6.9). With an eight channel stimulator, a lateral key pinch and a palmar prehension (traverse volar grip) are possible (see grip types in Figure 6.3). Furthermore, these grasp and release functions can be selected volitionally by the recipient via a shoulder position sensor (Scott, Peckham et al. 1995).

* Where paralysis is due to a lesion in the central nervous system and where peripherally the muscles are nonetheless innervated.

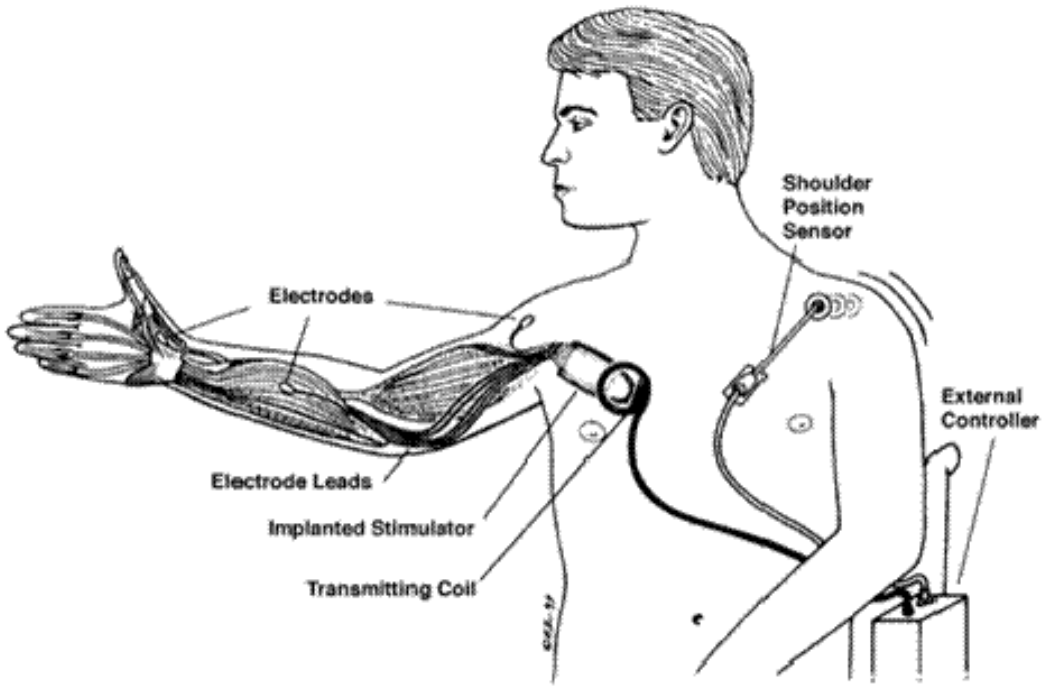


Figure 6.9 Functional Electrical Stimulation (FES) using a neural prosthesis.

FES is a desirable tool for rehabilitation because it is effective in utilising the individual's own muscles. Currently however, its suitability and use are limited by a list of factors:

- The neural prosthesis is invasive and requires surgery
- FES is suited to muscles which are innervated by healthy intact nerves. It is not suited for muscles whose excitability and simulation capacity have been compromised by damage to peripheral motor system (Popovic, et al, 2001).
- Due to high cost and invasive procedures, the method is only suitable for long-term functional aid. The neural prosthesis would not be a feasible option for those recovering from damage to joints or connective tissues, or short-term reversible damage to muscles or nerves.

# Chapter 7 Development of a Finger Harness to Evaluate the Principle Functions of the Hand Rehabilitation Device

## 7.1 Introduction

There are many benefits to developing a powered/instrumented upper extremity exoskeletal interface. Using specialised sensors for force and position feedback, such a device can work safely in parallel to the natural hand to assist or provide movement for activities of daily living as well as for therapy[*]. Furthermore, the system can be used to provide range or movement (AROM or TROM) measurements. In addition, such a system, controlled through software can be adapted to be used as a clinical research tool to optimise the delivery of therapy and rehabilitation to the damaged hand.

In this project, a finger harness and associated electromechanical setup were designed to test the principles of a full hand rehabilitation glove. At this stage, a single joint device has been developed to objectively evaluate the design concepts. A full-hand glove was also constructed, but due to the lack of sufficient actuators and sensors the device was useful only for demonstration purposes. The single joint device showed that using a hybrid torque-angle (or force-position) sensor[†], series

[*] This may include passive movement for therapy, augmentation of active movement for grasp function, resistance to active movement for exercise.

[†] See the FPT, Chapter 3.

elastic actuation (SEA)[†], Bowden-cable tele-actuation[*] and a hybrid torque-angle control algorithm, a safe and effective human-machine interface can be created for hand joints. The interface can passively move, or can resist active movement of the joints according to programmed angle and torque command. It can also assess joint stiffness and splint the joint.

In this chapter the groundwork has been laid for the creation of a portable platform for hand therapy, assessment, function and research.

### 7.1.1 Assessment using an automated system

In Chapter 6, joint range of motion (ROM) assessment methods were presented as indispensable to assessing effectiveness of rehabilitation of the hand. However, reliability and accuracy are difficult to achieve with traditional TROM or AROM measurements. Nicola (2004) found that the reliability of range of motion measurements for patients with rheumatoid arthritis has an error margin of more than 10 degrees. For normal hands the error margin is between 6 and 10 degrees (Marx, Bombardier et al. 1999).

In order to increase reliability, repeatability and, hence, increase the diagnostic value of ROM measurements, the process may be automated (and, hence, standardised). Several groups have successfully attempted this endeavour (Goddard, Dowson et al. 1969; Unsworth, Bey et al. 1981; Unsworth, Yung et al. 1982; Yung, Unsworth et al. 1986; Latash and Zatsiorsky 1993; Bromley, Unsworth et al. 1994; Dionysian, Kabo et al. 2005). However, the application of automated devices to measure ROM or joint characteristics has not acheived wide clinical usage.

---

[*] To allow actuation of a joint independent of the motion of preceding joints.

Recently Dionysian and others (2005) developed a computer-controlled torque-angle plotter (see Figure 7.1) to measure PIP* joint stiffness and energy absorbed during passive flexion and extension. The purpose of the study was to study the relationship between PIP joint stiffness and different common clinical parameters. The authors argued that "*...having an objective measure of PIP joint stiffness will allow us to define the natural course of an injury with respect to stiffness and to compare different treatment modalities scientifically*".

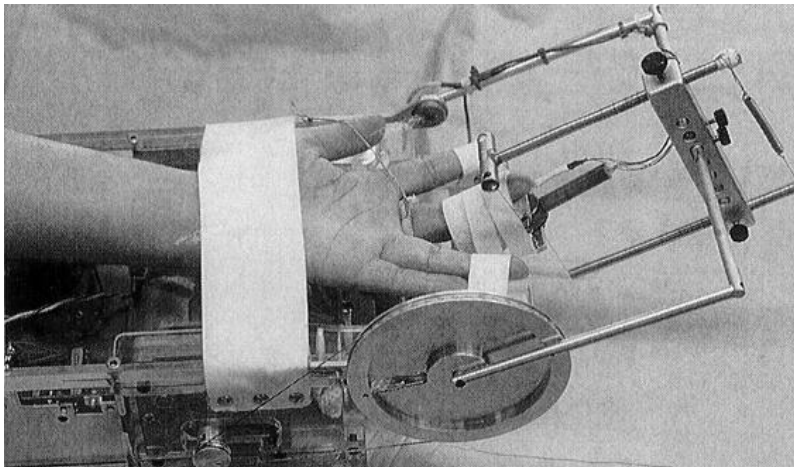

**Figure 7.1 Moment-Angle (MA) Plotter developed by Dionysian and others.** The device was used to apply controlled torques to the subject's PIP joint and measure resulting joint angles. Figure adapted from Dionysian, Kabo et al (2005).

The "moment angle (MA) plotter" works by applying controlled flexion or extension torques (in a cyclical manner) to the subject's joint and measuring the resulting angles. MA measurements create unique hysteresis curves that can provide information about the condition of the joint (see Figure 7.2). These curves differ from TROM curves obtained manually using torque gauges and goniometers (see Figure 6.2, page 126). The predominant difference observed is the hysteresis in moment-

* The Proximal Inter-phalangeal joint

angle plots caused by a loss of energy during flexion and extension parts of the cycle. The energy loss accounts for the friction at the joint surface, the tendon sheath, the ligaments, the skin, and the muscles (Dionysian, Kabo et al. 2005).

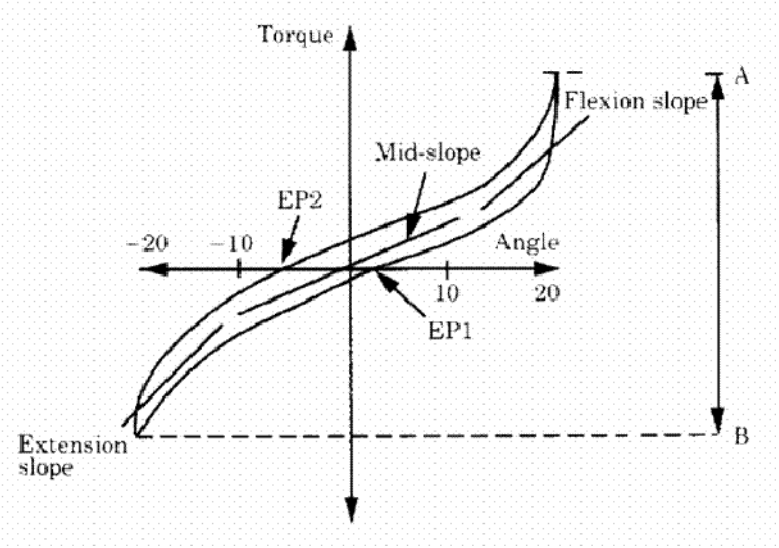


**Figure 7.2 Hysteresis curve measured by moment angle (MA) plotters.** Torque is positive when resisting flection. Angle is shown positive in flexion with reference to the cycle centre. Energy dissipation is related to the area of the hysteresis loop. EP1 and EP2 are mean equilibrium positions. The distance between A and B is the peak to peak difference in torque (Adapted from Bromley, Unsworth et al. 1994).

The authors identified and concentrated on the sections of the curve considered to have clinical significance. Any consistent deviation from a smooth curve may indicate a possible pathological process for which the curve may be considered a signature. Yung, et al. (1986) and Bromley, et al. (1994) used devices similar to the MA plotter (referred to as the "Arthrograph") to measure the effects of short-term and long-term physiotherapy on joints of normal subjects as well as patients with rheumatoid arthritis (RA). Both studies found significant reductions in elastic torque range[*] and dissipated energy following short-term ultrasound and hot wax therapy. However, during the long-term study no significant changes were found.

[*] This parameter refers to the passive torque measured at each joint angle by the MA plotter

#### *7.1.1.1 Limitations of previous studies*

Previous work has presented the potential for improving assessment of hand joints using computer controlled torque-angle measurement. However, the extent of clinical research into the effects of therapy has been limited to subjects with rheumatoid arthritis. Furthermore, the types of therapy studied have been limited to ultrasound, hot wax and active flexion-extension exercises. The devices used for these studies were bulky, difficult to install and not widely available. Ideally, torque-angle measurements should be applied in a wide range of clinical studies with diverse pathologies and therapeutic techniques.

### 7.1.2 Opportunities for new forms of therapy

The ability to externally mobilise hand joints in a controlled manner while measuring resulting joint torque and angle will allow new forms of assessment and therapy. These include therapeutic methods that have been described in literature but are not practiced clinically due to the lack of appropriate tools. Continuous passive motion (CPM) and dynamic splints were previously described in Chapter 6. CPM is not widely used on hands despite indication due to limitations of available technology. Dynamic splints, although simple in design, are bulky and require periodic readjustment of applied tension. Ideally the dynamic splint should apply and maintain a constant therapeutic torque on the joint despite gradual changes in joint angle (as range of movement is recovered). In practice, the applied torque of dynamic splints is highly dependent on joint angle and is not reliably held constant. The rehabilitation device proposed in this thesis aims to address these limitations as well as allow other forms of therapy such as differential tendon gliding (see section 7.1.2.2) and active exercises. In addition, while applying active and passive motion therapy, potential changes in neurological mapping of motor-sensory functions may be investigated.

#### 7.1.2.1 Neural re-mapping potentials

According to recent research, the brain has a greater ability to recover after injury than previously thought. Following brain injury, motor cortical neurological maps have been shown to shrink with inactivity. Subsequent activity, however, has been found to expand the cortical map (Jenkins 1987; Nudo 1996; Nudo and Milliken 1996; Nudo, Wise et al. 1996). Despite their enormous potentials, traditional neurological rehabilitation therapies are very labour intensive and thus prohibited by high cost (Koeneman, Schultz et al. 2004). However, using computer controlled exoskeletons, providing neurologically rehabilitative therapy may become economically feasible and of highly benefitial.

*"The successful motor rehabilitation of stroke, traumatic brain injured and SCI[*] patients requires an intensive and task-specific therapy approach. Budget constraints limit a hand to hand therapy approach, so that intelligent machines may offer a solution to promote motor recovery and obtain a better understanding of motor control"* (Hesse, Schmidt et al. 2003)

#### 7.1.2.2 Differential tendon gliding exercises

Differential tendon gliding exercises were introduced by M. Wehbe and others for use in hand treatment and rehabilitation (Wehbe and Hunter 1985; Wehbe and Hunter 1985; Wehbe 1987). The exercise programs require composite movements of the metacarpal (MCP) and interphalangeal (IP) joints. These movements allow flexor tendons of the hand to glide to their maximum potential and facilitate therapeutic activities when incorporated in a comprehensive program of hand therapy.

---

[*] Spinal chord injured

A number of composite hand movements were studied using radiography (to understand the extent of flexor tendon glide). The two flexor tendons in each finger have different excursions and can glide separately. This is referred to as differential tendon gliding. Following pathology or trauma, loss of tendon gliding due to sheath adhesions leads to loss of joint movement and, therefore, loss of strength and dexterity. Three of the fist positions evaluated by Wehbe (1985) provided maximum differential gliding for both flexor tendons: hook, fist, and straight fist (see Figure 7.3). These exercises require different combinations of flexion or extension for each of the three types of finger joint. The specific position for each joint type is displayed in Table 7.1 and depicted in Figure 7.3.

| | MCP | PIP | DIP |
|---|---|---|---|
| Straight fist | Flex | Flex | Extend |
| Hook | Extend | Flex | Flex |
| Fist | Flex | Flex | Flex |

**Table 7.1 Differential Tendon gliding exercises.** Flexion or Extension for each of the joint types: metacarpal (MCP), proximal interphalangeal (PIP) and distal interphalangeal (DIP) during the different fist positions.

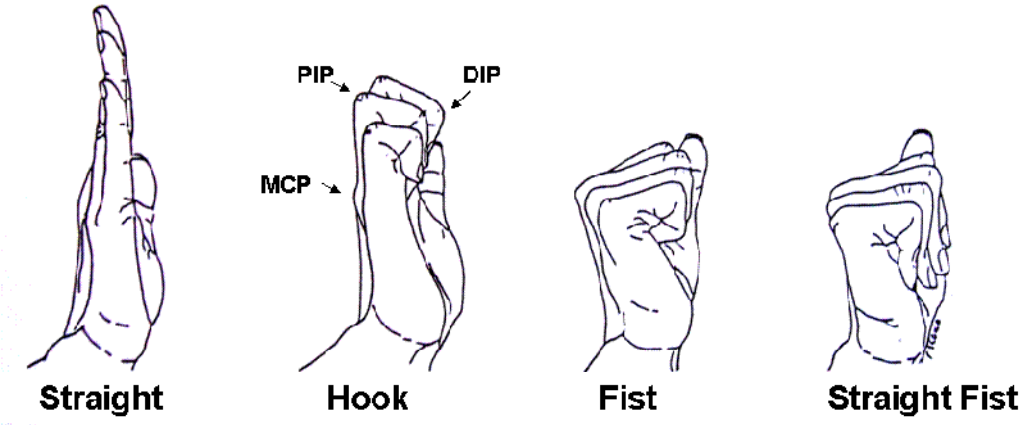


**Figure 7.3 Differential Tendon gliding exercises.** Adapted from Wehbe (1987)

The Wehbe study also showed that such tendon gliding exercises allow maximum excursion of the flexor superficialis and profundus sheath. They also force each of the digital joints to glide through its full potential range. Implications of this process can be extended to tendon and cartilage nutrition and may be valuable in preventing the degenerative process and inflammatory disorders of flexor tendons and joints in the hand. In addition they may have great importance in preventing the formation of adhesions and in promoting tendon healing during rehabilitation of the hand following trauma or surgery. Rozmaryn and others (1998) studied patients presenting for carpal tunnel syndrome by dividing them into two groups. Both groups were treated with standard conservative methods. But one group was also treated with nerve and differential tendon gliding exercises. Of the group receiving standard treatment, 71% underwent surgery. In the experimental group however, only 43% required surgery. Thus a significant number of patients who would otherwise have undergone surgery for failure of traditional conservative treatment were spared carpal tunnel release surgery.

The composite movements involved in tendon gliding exercises may be performed actively by the patient or passively by a therapist or a machine. Current continuous passive motion devices are incapable of providing the entire range of exercises required. Ideally such devices should be able to move each joint type independently to produce composite fists. The technology proposed in this thesis aims to enable such functions.

### 7.1.3 Early demonstrations of the rehabilitation glove technology

Throughout this project, many prototypes were developed to test the principles of an instrumented rehabilitation glove. Each prototype was used to test an isolated aspect of the proposed system. One of the challenges of this project has been the manufacturing of a working human-machine interface working with all the hand joints. Such a device will require multiple micro-actuators and micro-sensors and professional manufacturing capacity. A full hand rehabilitation glove was not within the scope of this thesis.* However, a limited glove-based device was developed with nine micro-actuators and no feedback system. This glove was used to demonstrate the principles of grasp and release capabilities on tetraplegic subjects. The glove was able to passively flex and extend the MCP, PIP and DIP joint of the subject's hand independently† (as required for differential tendon gliding exercises). Furthermore, it was capable of steering the subject's thumb to flex, extend, abduct and adduct. Composite movements of the joints were applied to allow the subject to apply lateral pinch grip and a traverse volar grips (see grip types in Figure 6.3 and the demonstration in Figure 7.4).

---

* Although the project is currently undergoing commercialization and a full prototype is expected in the near future.

† Independent movement here refers to the ability to flex one group of joints (e.g the MCPs) while another group (eg. PIPs) is extended or held still.

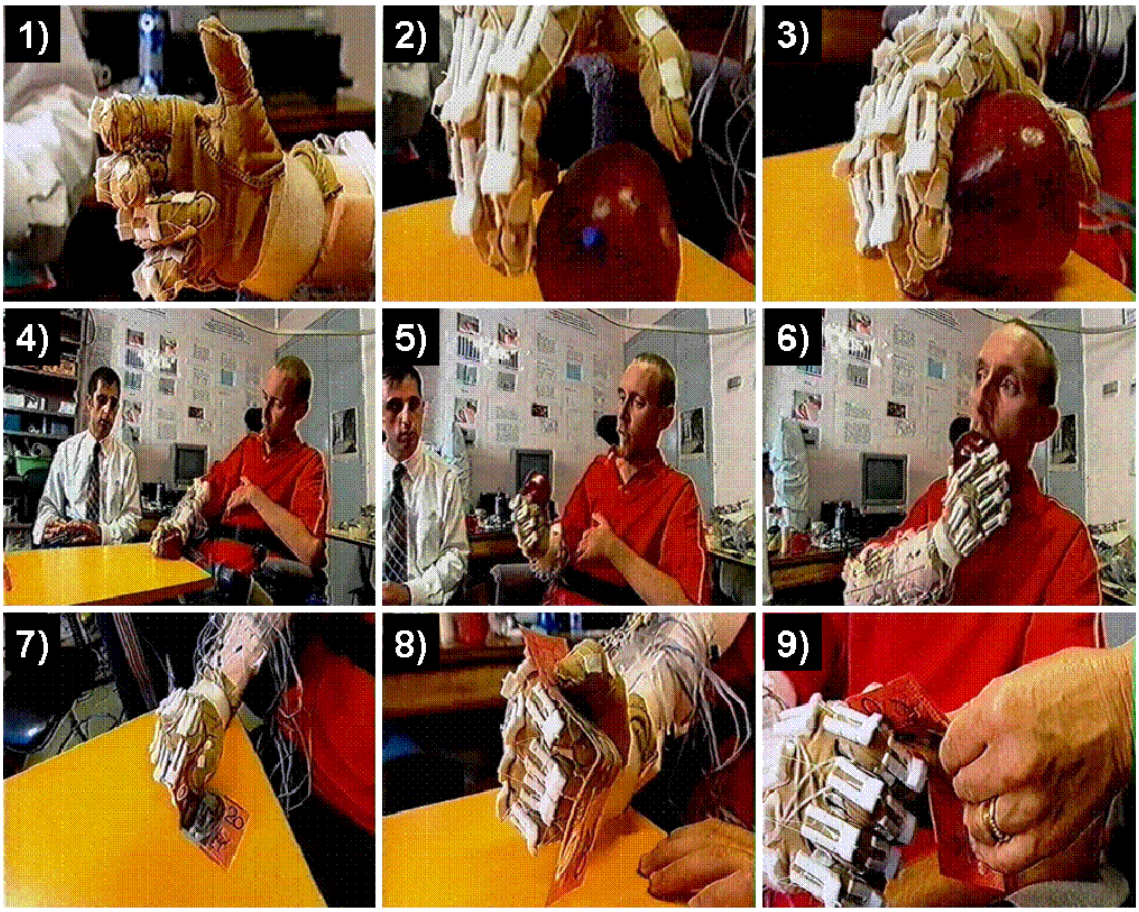


**Figure 7.4 Demonstration of the rehabilitation glove with a tetraplegic subject.** *The subject's hands were paralysed but displayed limited wrist extension. 1) the glove was fitted on the subject's hand. He was able to move his arm within a functional work space and to stabilise his wrist for grasp. 2) Once the subject brought his hand over an apple the glove was activated to grasp it. 5) and 6) The subject was able to bring the grasped apple to his mouth and take a bite. 7) Lateral pinch grip was able to be reproduced by the glove over objects such as a bank note. Pictures courtesy of the Discovery Channel "Medical Marvels" program (aired March 2005)*

This demonstration was highly useful in understanding the challenges involved in external manipulation of a paralysed hand. Moreover, the fundamental principles of the technology regarding independent joint movement and tele-actuation using Bowden cables were shown to work. However, due to lack of sufficient sensors and motors a full-hand device could not be made with torque-angle feedback and independent control of all hand joints. Subsequently, a single joint device was

developed for an objective evaluation of the capabilities and potential of the proposed technology. The results of this evaluation follow.

### 7.1.4 Aims of the single joint electromechanical harness

The aim of this study was to evaluate the potential benefits of newly proposed methods to improve hand therapy and assessment. These new methods are based on the use of series elastic actuation (SEA), hybrid torque-angle feedback, tele-actuation and specialised human-machine interface principles. Furthermore, the study aimed to assess the effectiveness of a unique hybrid torque-angle control system algorithm.

The principles evaluated here will be used to determine the benefit of such techniques for up to 15 joints of the hand. It is hoped that given the successful outcomes of improved clinical application, the principles demonstrated may be used directly as a clinical tool to improve practice.

## 7.2 Methods and Materials

In principle, the hybrid force position transducer (FPT) and the SMA based actuators could have been employed within the experimental platform of this chapter. However, the performance limitations currently present with these early prototypes and proof of concept systems would be a hindrance to the aims of the single joint electromechanical harness. Nonetheless, the principles of the FPT and the SMA-Binary actuator are emulated with an alternate set-up described in the following section. In particular, the hybrid torque-angle control system, as well as series springs,

represent the FPT component, while, step motors used as actuators are representative of the function of the ideal SMA-binary actuator.

### 7.2.1 The experimental platform

The experimental platform consisted of a table-top electromechanical section and a finger harness. The single finger harness was prepared for the right hand index PIP* joint. This harness was actuated via Bowden cables (containing polyester tensile lines) connecting to the electromechanical section. The latter was composed of a box containing two linear stepper motors (as previously described in Chapter 3) series elastics (stainless steel springs with elastic coefficients ~ 0.608 N/mm) and force† and position‡ sensors. A schematic of the setup is displayed in Figure 7.5.

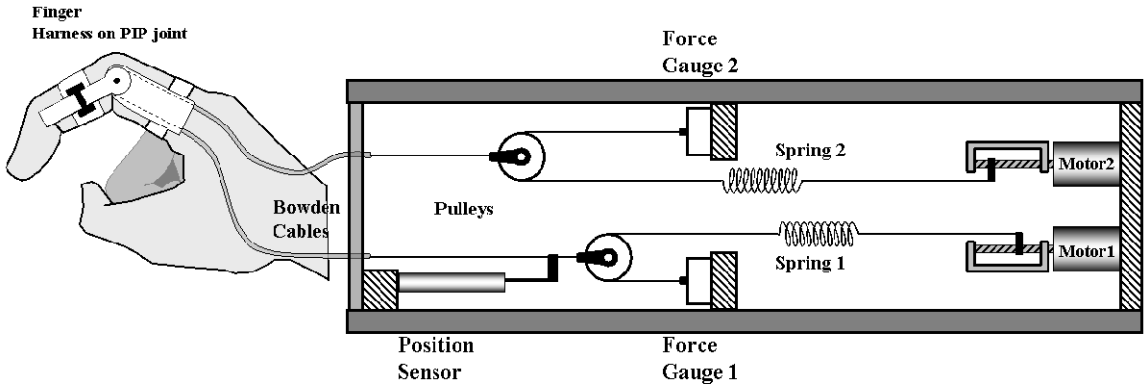


**Figure 7.5 The experimental setup.** A finger harness was actuated by an electromechanical section. The subject's PIP joint was moved through Series Elastic Actuation (SEA) of stepper motors. Torque and joint angle feedback stemmed from sensors in the electromechanical section.

* Proximal Interphalangeal Joint

† Force sensors: 15248A TOCO 4-element DC strain gauge balance circuit and amplifier

‡ Honeywell Potentiometer MLT model, accurate within +/- 0.05mm

#### 7.2.1.1 Finger harness

The Series Elastic Actuators were installed in an antagonistic* configuration (as shown in Figure 7.5). Actuation of Motor-1 caused flexion in the PIP joint. Conversely, Motor-2 was responsible for extension. The motors worked in unison to implement torque and angle control of the finger.

The finger harness (Figure 7.6) consisted of two finger saddles for the proximal and medial segments of the index finger. The proximal saddle was coupled to a pair of thin lateral housings containing the cables and strut joints. From these housings a pair of flat struts travelled to slider slots on the sides of the medial saddle. Pulling on the extensor and flexor cables caused the struts to rotate accordingly. The torque on the struts was transmitted to the medial segment of the finger via the slider slot coupling. The purpose of the sliding slots was to allow for translational shifts of the struts during movement†.

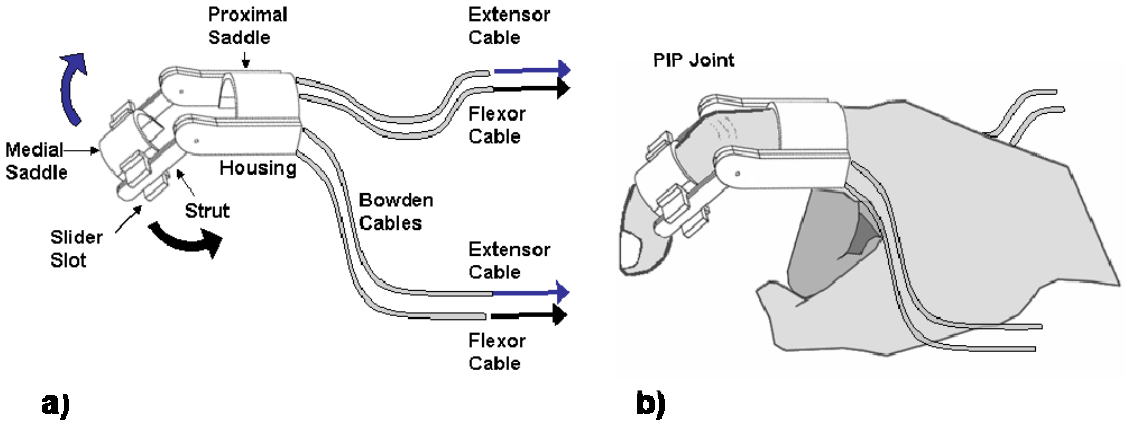


**Figure 7.6 Design of the finger harness.** a) The components of the finger harness used in the study. b) The harness is placed dorsally on the finger and secured using double sided adhesive tape.

* The actuators oppose each other. This allows two uni-directional actuators to control a lever bi-directionally. As an added benefit, a single position sensor suffices for angle feedback.

† This was an important inclusion in the design considerations. Although finger joints do not act as perfect hinges, they can be approximated by them. A certain amount of misalignment is inevitable during the movements.

The saddles were fastened on the subjects' fingers using double sided adhesive on the inner surfaces. This method was effective in keeping the saddles in place during the operation of the setup. More importantly, it allowed the harness to be coupled to the hand without placing material on the palmar side of the finger, minimising obstruction to joint movement. The struts had a range of travel from extension of -20˚ to a maximum flexion of +130˚. The strut joints were thin reels of 10mm diameter to which the cables from the SEAs connected.

Each subject was seated next to the setup with his/her right hand placed on a raised foam block. The hand was positioned in such a way that the index finger protruded from the corner of the foam block and was free to move (the foam was hollow under the finger allowing flexion without obstruction). The wrist of the subject was maintained at a neutral angle (approximately 10˚ when placed on the foam block).

**Figure 7.7 The position and orientation of subjects in respect to the platform.** A non-injured subject is shown with her finger in the experimental harness.

#### 7.2.1.2 Angle and torque measurements

Joint angle was measured from cable position. When the harness was placed over the subject's finger, the angle of the PIP joint was directly proportional to the linear motion of the internal sensor (in the electromechanical setup). Thus, angle could be measured from sensor's voltage output (see figure 4.1). Subsequent to the placement of the harness on the finger of each subject, angle was recalibrated.

The torque between the harness strut joint and the PIP joint was measured from force gauge-1 and force gauge2 (see equation 4.2).

$$A = K_A V_A + C_{ACAL} \qquad \textbf{(7.1)}$$

Where A is the angle, $V_A$ was the voltage from position sensor and $K_A$ and $C_{ACAL}$ are calibration constants.

$$T = K_{F1} V_{F1} - K_{F2} V_{F2} + C_{FCAL} \qquad \textbf{(7.2)}$$

Where T is the applied torque, $V_{F1}$ and $V_{F2}$ are voltages from force gauges 1 and 2 respectively and $K_{F1}$, $K_{F2}$ and $C_{FCAL}$ are calibration constants.

#### 7.2.1.3 Control algorithm

The control algorithm employed in this study and proposed for the control of similar human-machine interfaces was conceived to provide function and safety. In both considerations, the relation between position and force (or angle and torque) is paramount.

Hybrid torque and angle control was implemented using variable sliding windows. As opposed to a single target command, using this algorithm, a window is commanded with upper and lower limits ($A_H$ , $T_H$ and $A_L$ , $T_L$ respectively) for each parameter (see Figure 7.8). In general, narrow windows are used for control of parameter while wide windows are used for specifying boundary limits.

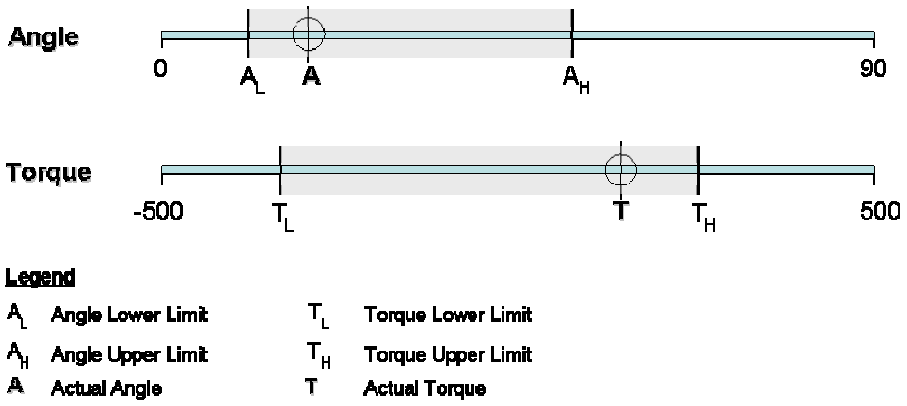


**Figure 7.8 A visual representation of the control command levers used in actuating the finger harness.** Torque and angle are each controlled by two limits (upper and lower). The control system acts to bring the parameters into their respective windows. The windows can be shifted, and their sizes can be adjusted manually or programmatically.

In each program cycle, the system measures actual torque and angle (A and T in Figure 7.8).

- If one parameter is outside of its respective window, the motors are commanded to take a step in the direction that brings the parameter closer towards the window.
- If both parameters are within their windows, no steps are taken.
- If both parameters are out, the control system calculates the necessary step direction for each.
    - If both solutions are in unison (i.e. +1 or -1 step), the step is taken.
    - If they contradict each other, no step is taken.

This control algorithm is illustrated in Figure 7.9.

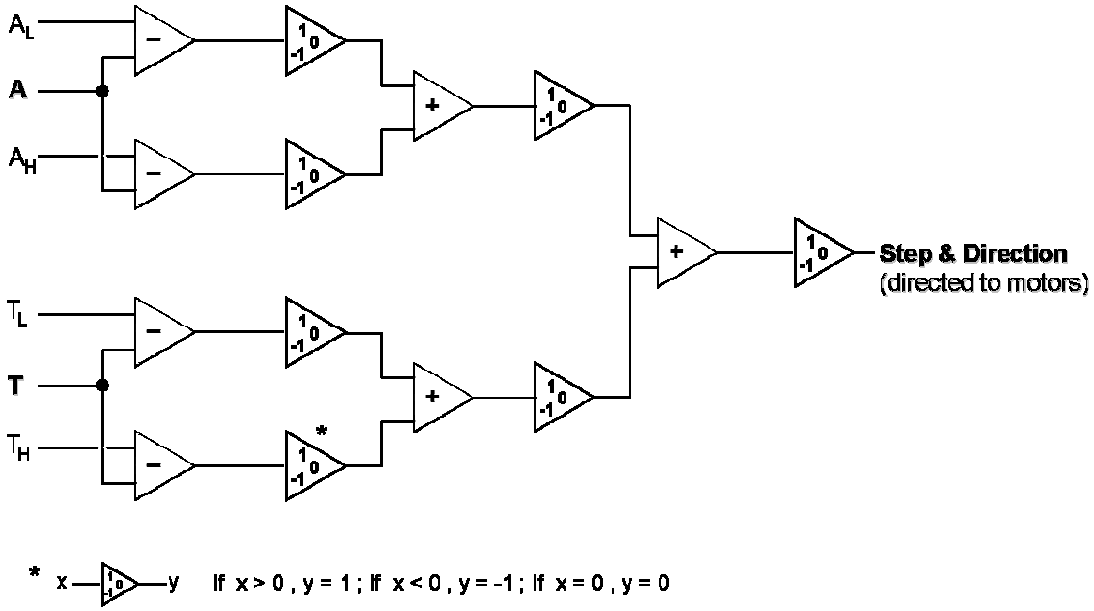


**Figure 7.9 The algorithm of the hybrid torque-angle control system.** In each cycle, the step output to the motors is either -1, +1 or Zero.

### 7.2.2 Calibration

The finger harness was attached to a mock-up finger joint (see Figure 7.10). This finger model exhibited low friction* in its joint (two orders of magnitude lower than the full scale torque applied in the study by the harness. A series of hanging masses were used to test the torque measurement. An electronic goniometer† was used to test the angle measurement of the system.

---

* Average friction force was 0.041N.cm ±0.004N.cm ($p < 0.05$) equal to 5.3% of the load exerted by the lowest calibration mass used (75g or 0.73N). Friction was determined by applying a gradually increasing normal force to the model segment above the joint. The force was applied via a cable attached to the force transducer such that it could be monitored in real time. The force at which joint movement initiated was converted into a torque value and recorded.

†Constructed for this project using a high precision LVTD position sensor. Design details and calibration results of the sensor are presented in Appendix F.

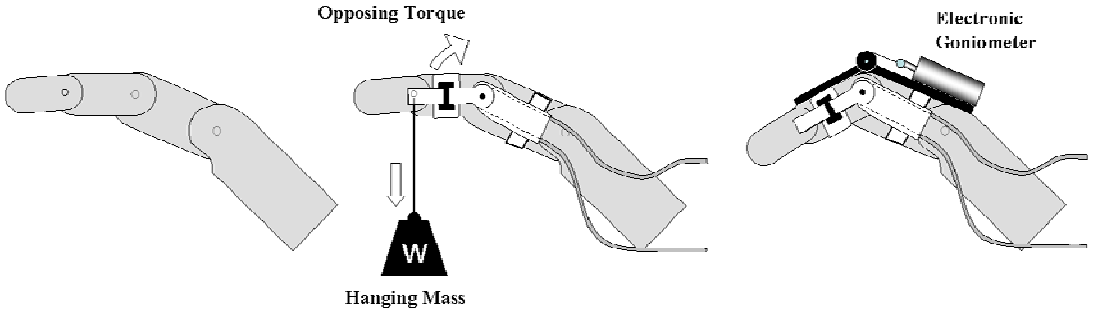


**Figure 7.10 Calibration of Torque and angle**. Calibration was conducted using a low friction finger model to which the harness was coupled.

#### *7.2.2.1 Testing angle control and angle, torque accuracies*

With the harness applied to the finger model, cyclic angle control was conducted. During the movements, angles measured by the internal sensor of the setup were compared to direct angle measurements recorded from the electronic goniometer. In addition, the ability of the control system to track the target angle was evaluated. Using an angle control window gap of 4˚ ($A_H - A_L$), varying cycle speeds were tested. The target window was cycled continuously from -4˚ to 100˚.

Force accuracy was evaluated by applying known torques using hanging masses and comparing values with measured torque.

### 7.2.3 Subject selection and ethics approval

A total of eight volunteer subjects were recruited for this study. These included four non-injured subjects with normal hand function and four high level spinal cord injured subjects with little to no active movement of the right index PIP.

Ethics approval for research involving humans was sought and obtained from the Northern Sydney Health Human Research Ethics Committee.

### 7.2.4 TROM and AROM

For recording purposes, the standard TROM and AROM tests were applied using a force gauge (same model as used in the electromechanical setup). The electronic goniometer was used to record the angles (Figure 7.11).

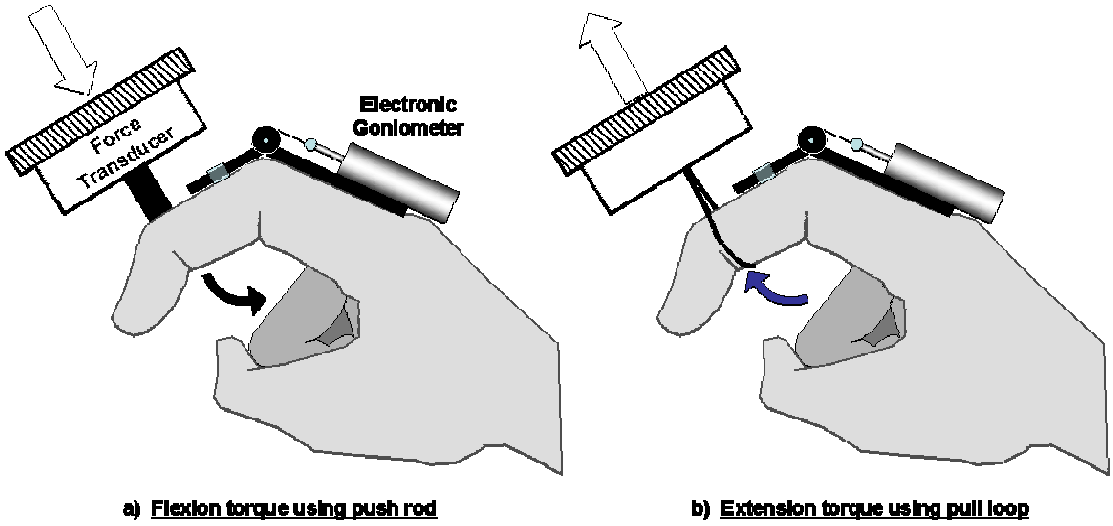


**Figure 7.11 Standard TROM assessment.** Both flexion and extension TROMS are measured. Left: The force gauge is pushed perpendicularly on the dorsal surface and at a measured distance from the joint. The resulting angles are measured. Right: From the same force gauge, a cable is looped around the middle segment allowing extension torques to be applied (by pulling up at right angles).

With both extension and flexion, care was taken to maintain perpendicularity between the force transducer and the finger segment mobilised. Torque was calculated as: [normal force applied in N] x [moment arm length in cm]. The consequence of torque measurement error introduced from angles other than 90˚ is given by E% = (1/cos(α) – 1) where α is the deviation angle from 90˚. To put this error in perspective, 1˚, 5˚, 10˚ and 20˚ deviations result in torque measurement

errors of 0.015%, 0.38%, 1.54%, and 6.42% (in respect to normal force) respectively. Practically, this means that staying within ±10˚ ensures torque accuracy better than 1.54%. Recordings were made continuously at 2 Hz*.

#### *7.2.4.1 Standard Assessment TROM (Figure 7.11)*

- FLEXION:
    1. Using the tip of a force gauge applied perpendicularly to the dorsal surface of the middle phalanx, the PIP joint was passively pushed into flexion towards end range. Care was taken (visually and manually) to maintain a perpendicular contact throughout the range. The moment arm where the force gauge tip was applied was noted. Applied torque was derived (in N.cm).
    2. The electronic goniometer was fixed to the proximal and middle phalanges to measure the PIP angle during the movements.
    3. The measurements from both the force gauge and the goniometer were recorded continuously using the data acquisition setup† and plotted showing a relationship between applied torque and resulting joint angle.
    4. The flexion readings were repeated 10 times.
- EXTENSION:
    1. A cable was looped around the palmar side of the middle phalanx at a known distance away from the joint (placed at the crease between the

---

* 2Hz was selected because typically TROM movement in each direction typically had cycle lengths longer than 5 seconds. This meant that each push or pull could record around 10 points of data.

† An 8-channel digital output, 16-channel analogue input data acquisition card was used: National Instruments DAQ Card Model: PCIMIO 16XE-50

distal and medial segments). The cable was then hooked onto the force gauge tip. Care was taken to maintain a perpendicular orientation between the force gauge tip and the phalanx. The force gauge was pulled to extend the phalanx to its end range.

2. Extension readings were repeated 10 times.
3. Applied extension torque and corresponding joint angles were recorded and plotted on the same graph as above.

- WITH HARNESS:
  1. The above method was first applied without the exoskeleton. Subsequently the same measurements were conducted with the harness secured to the finger. The purpose was to evaluate the obstruction of joint movement by the finger harness.

#### *7.2.4.2 Standard Assessment AROM*

- WITHOUT HARNESS:
  1. Subject with active movement were asked to actively flex the right index finger PIP to maximum angle. The electronic goniometer was used to measure the resulting joint angle.
  2. The subject was asked to extend the PIP maximally. The goniometer was used to measure the resulting joint angle.
- WITH THE EXOSKELETON:
  1. The above standard AROM measurements were repeated with the exoskeleton placed and secured on the finger. Changes in the readings were indicative of the degree of obstruction to free movement presented by the exoskeleton.

### 7.2.5 Joint stiffness characterisation

In the joint characterisation test, the finger harness was employed. The control system applied torques to the PIP joint and simultaneously measured the resulting angles. The reference goniometer was used to test the accuracy of the angle measurements recorded from the electromechanical section.

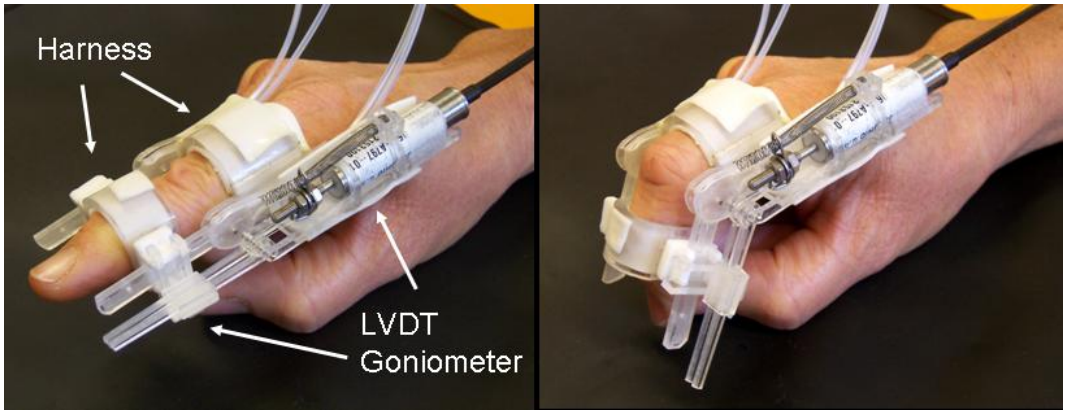


**Figure 7.12 Pictures of a subject's studied finger with the harness and the reference goniometer attached.**

- PASSIVE MOVEMENT:
    1. The harness was placed on, and secured to the subject's right index finger. The proximal saddle of the harness was secured to the dorsal side of the proximal phalanx using high strength double sided adhesive. The medial saddle of the exoskeleton was similarly secured to the dorsal side of the middle phalanx.
    2. The electronic goniometer was coupled to the exoskeleton to provide reference angle measurements during the experiment. The reference measurement allowed comparison of results between standard TROM and AROM measurements and the Joint Characterisation method applied by the device.

3. The forearm, wrist and hand of the subject were rested on a foam bloc to minimise movements (refer to Figure 7.7). The index finger was extended to allow free movement of the PIP joint.
4. Starting from zero torque, the electromechanical system was instructed to gradually ramp up flexion torque causing the PIP to gently flex accordingly. Once maximum flexion was achieved, the torque was reversed and ramped towards maximum extension.
5. Following maximum extension of the finger, the flexion was repeated. Each direction was ramped a total of 10 times.
6. The resulting joint angles were recorded by the system using the device's internal joint angle sensor and plotted against applied torque.
7. The goniometer readings were used to assess the accuracy and reliability of the system and to allow comparisons to readings made during the standard assessment.

- ACTIVE MOVEMENT
    1. With the harness in place, the system was instructed to enter 'Zero Torque Mode' (as described in section 7.2.7). In this setting the harness motors continuously adjusted to minimise force on the PIP joint*. This allowed the subject to actively move the PIP joint (while limited by the maximum speed of the motors).
    2. The subject was asked to actively flex the right index finger PIP to maximum position. A reading was made at this angle.
    3. The subject was asked to extend the PIP maximally. The system was used to measure the resulting joint angle.

* 'Zero Torque' could not be alternatively implemented by disengaging the motors as this would lock the joint in place.

### 7.2.6 Joint-angle and torque control

PIP joint angle and torque of the subject were controlled using the algorithm described in section 7.2.1.3 (page 150).

#### *7.2.6.1 Joint-angle Control*

1. Using results obtained in the joint characterisation test, end-range angles were obtained for the PIP joint of each subject.
2. A cyclic movement program drove the control system with the following characteristics:
    a. The angle control was based on a sine wave with specified amplitude, frequency and offset.
    b. The frequency chosen was 1.5 cycles per minute* (40 seconds per cycle).
    c. Amplitude and offset were selected such that the peak to peak values corresponded with the maximum flexion and extension angles respectively.
3. The movement cycle was continued for 15 minutes.
4. During the session, applied torque and joint angle readings were recorded and plotted against a time axis. Analysis was performed on the resulting graphs to test the ability of the system to achieve the desired angle targets.

* Cycle lengths used in hand CPM are typically between 1-4 cycles per minute (Le Stayo 1995; Adams and Thompson 1996)

5. During the angle cycles, the torque control window ($T_L$ and $T_H$) was narrowed to test the ability of the system to react accordingly to the enforced limits.

#### *7.2.6.2 Torque Control*

1. A torque-control-based cyclic movement program drove the control system with the following characteristics:
    a. The torque-control was based on a sine wave with specified amplitude, frequency and offset.
    b. The frequency chosen was 1.5 cycles per minute (40 seconds per cycle).
    c. The peak to peak values of the control wave were +3N.cm and -3N.cm (corresponding to flexion and extension respectively)
2. The movement cycle was continued for 15 minutes.
3. During the session, the applied torque and joint angle readings were recorded and plotted against a time axis. Analysis was performed on the resulting graphs to test the ability of the system to achieve the desired force targets.
4. During the torque cycles, joint angle limits were enforced by narrowing the angle control window ($A_L$ and $A_H$).

### 7.2.7 Active movement and torque bias

In this test, three modes of torque bias were tested while the subject was asked to actively move his/her PIP joint.

1. Zero Torque Mode – The setup acted to minimise passive torque on the subject's PIP joint. The subject was then asked to slowly flex and extend

his/her finger cyclically for two minutes. The ability of the system to minimise resistance to active movement was evaluated.

2. Flexion bias – The system was instructed to apply and maintain a constant +2N.cm torque on the PIP joint. The subject was then asked to move the PIP joint cyclically as previously against this torque.
3. Extension bias – The system was instructed to apply and maintain a -2N.cm torque on the PIP joint. The subject was then asked to move the PIP joint cyclically against this torque.

## 7.3 Results

The results are based on measurements recorded from the internal control sensors and the external reference sensors (see Figure 7.5 and Figure 7.12).

### 7.3.1 Calibration and accuracy using the finger model

The angle and torque measurements of the setup were calibrated as described in section 7.2.2. The resulting lines of best fit of plotted data were used to provide the calibration constants required for equations 7.1 and 7.2 (page 150).

The results of the calibration are found in Figure 7.13.

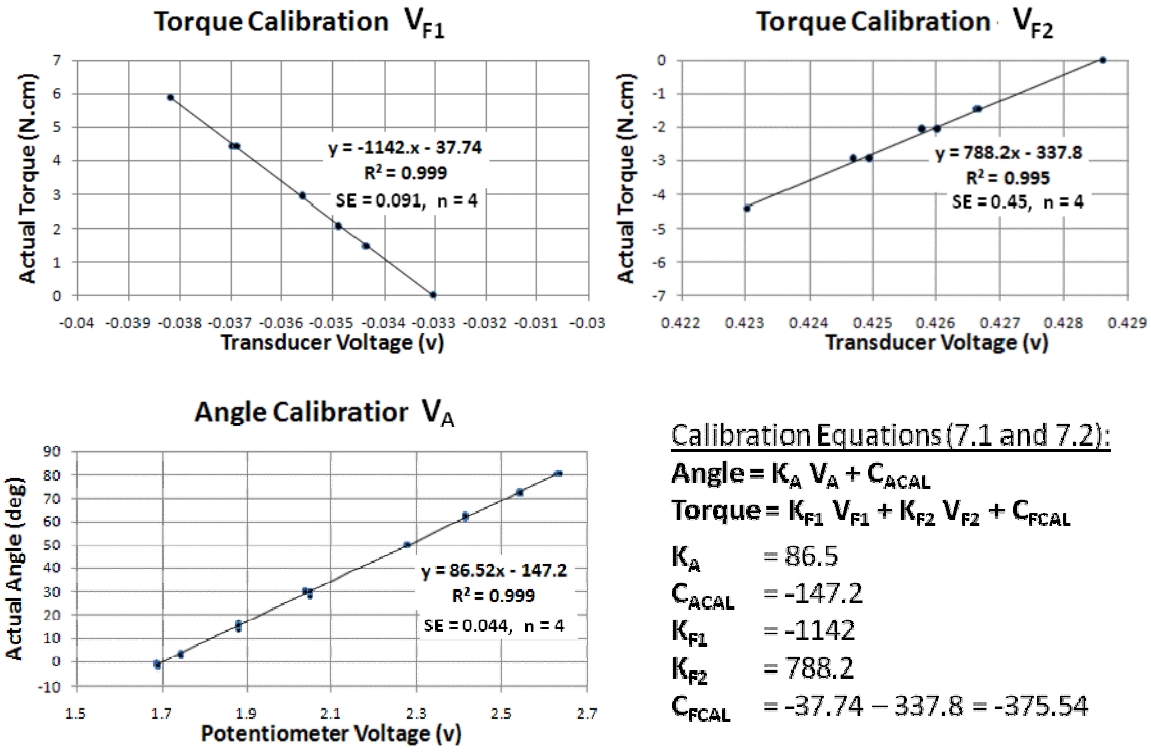


**Figure 7.13 Calibration of angle and torque measurement.** The graphs show angle and torque calibration data of the internal sensors. The resulting lines of best fit provide the constants for the calibration equations 7.1 and 7.2.

Accuracy of the internal sensor was measured during cyclic movements. The graph in Figure 7.14 shows two different speeds: two cycles per minute, followed by four cycles per minute.

The angle error was a recurrent shape and was not random. The mean error was 0.82˚± 0.85˚(standard deviation, n=708).

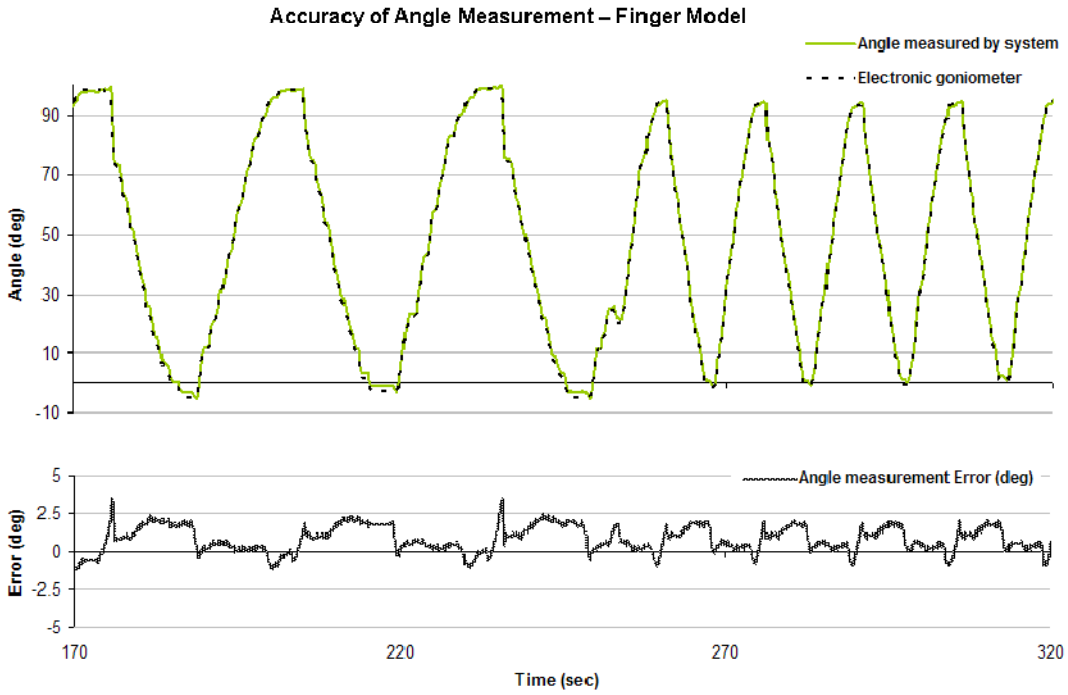


**Figure 7.14 Joint angle accuracy using the finger model.** Top graph: Finger model joint angle was controlled using the setup. Two cycle rates are shown. The control system began with 2 cyc/min and changed to 4 cyc/min. Bottom graph: Accuracy of the internal joint angle sensor (in the electromechanical section) during cyclic movements.

#### *7.3.1.1 Control error*

Control error was defined as the difference between actual angle (as measured by the electronic goniometer) and the closest window limit. Reducing the window size made the system more responsive, but more likely to become unstable (due to overshoots). By trial and error, a window size of 4˚ was found to be a suitable compromise between responsiveness and stability. When the actual angle was within the window, error was considered to be zero. Figure 7.15 shows the control signals ($A_H$ and $A_L$) for the same movements presented in Figure 7.14, superimposed on a plot with actual angle.

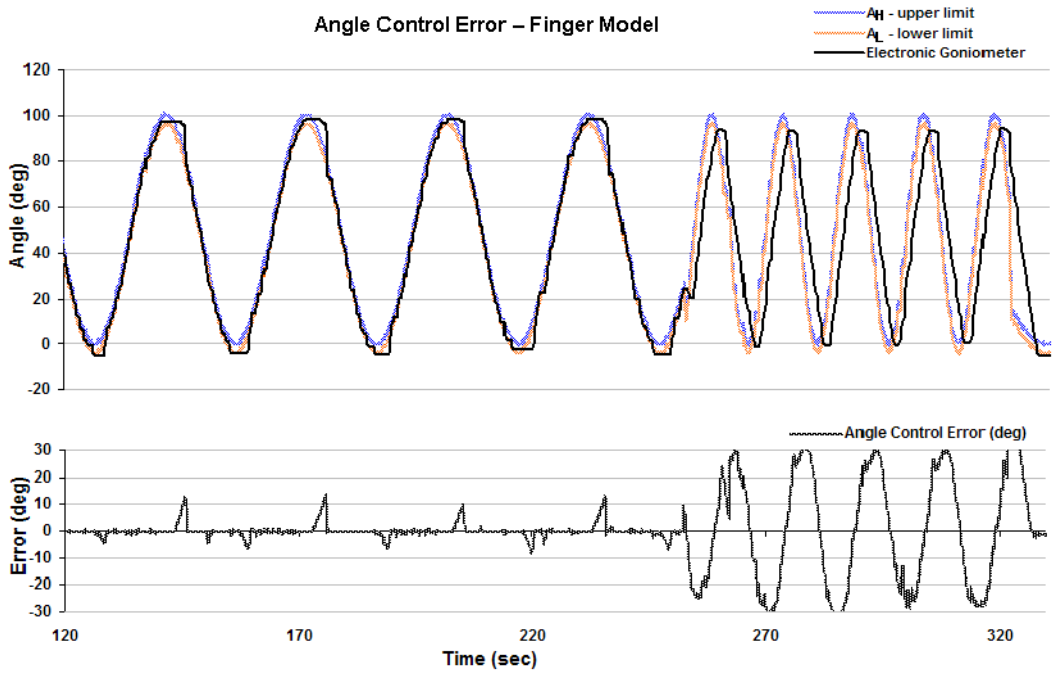


**Figure 7.15 Angle-control error.** The graph presents the same angle control cycle shown in Figure 7.14 with the cyclic control window. $A_H$ and $A_L$ represent the upper and lower limits of the control window respectively.

#### *7.3.1.2 Torque measurements*

Torque measurements were compared to known torques from hanging masses. The results are placed in Figure 7.16. The mean error for flexion torques was -0.14N.cm ±0.1 (std dev, n=8). This is equivalent to -2.8% ±2% of full-scale 4.9N.cm. The mean error for extension torques was -0.017N.cm ±0.1 (standard deviation, n=8). This is equivalent to -0.35% ±2% of full-scale 4.9N.cm..

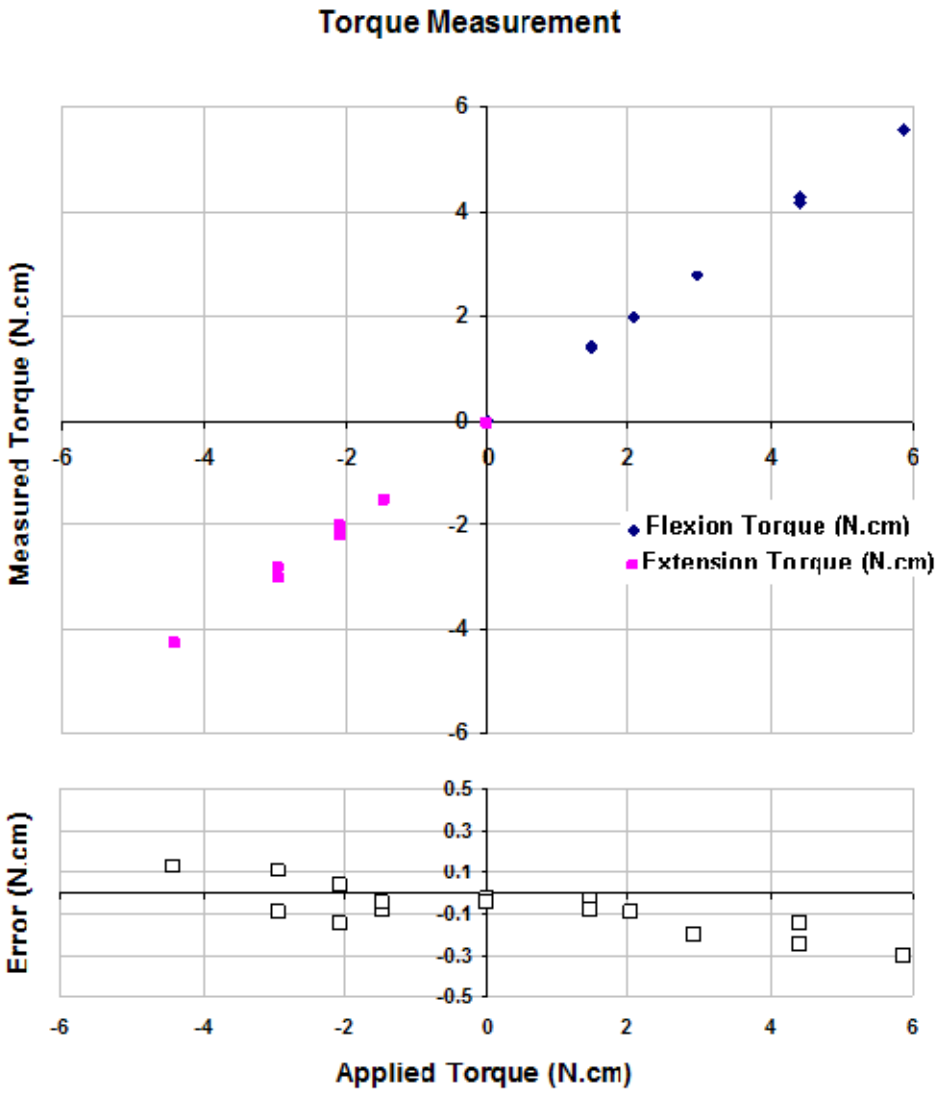


Figure 7.16 Torque measurements following application of calibrated torques.

### 7.3.2 TROM and AROM measurements

TROM and AROM measurements were recorded for all subjects. Of the spinal cord injured subjects, only one was capable of limited active movement of the right index PIP joint.

From the TROM data points, only loading torque measurements were included. These were torque-range measurements when pushing the middle segment of the finger towards flexion and when pulling the segment into extension.

Figure 7.17 shows the TROM and AROM measurements for a healthy subject taken both with and without the harness. The graphs show a nonlinear relationship between torque and joint range of motion. Fourth order polynomial lines of best fit were used to approximate the relationships.

Coupling the harness to the fingers was found to change the TROM readings in all subjects. In all cases, the effect of the harness was to increase the scatter of the readings in both directions. For some subjects, the harness was found to increase the slopes of the loading curves near the end ranges. This increase in slope was observed for subjects whose flexion end-ranges were greater than 90°. The mid range was mostly unaffected by the harness. Figure 7.17 is demonstrative of the effects of the harness. A greater scatter of the torque-range measurements can be observed. This is also indicated by the differences in $R^2$ of the lines of best fit: 0.92 for flexion without the harness compared to 0.72 with the harness. Similarly for extension, the $R^2$ value decreases from 0.88 without the harness to 0.82 with the harness.

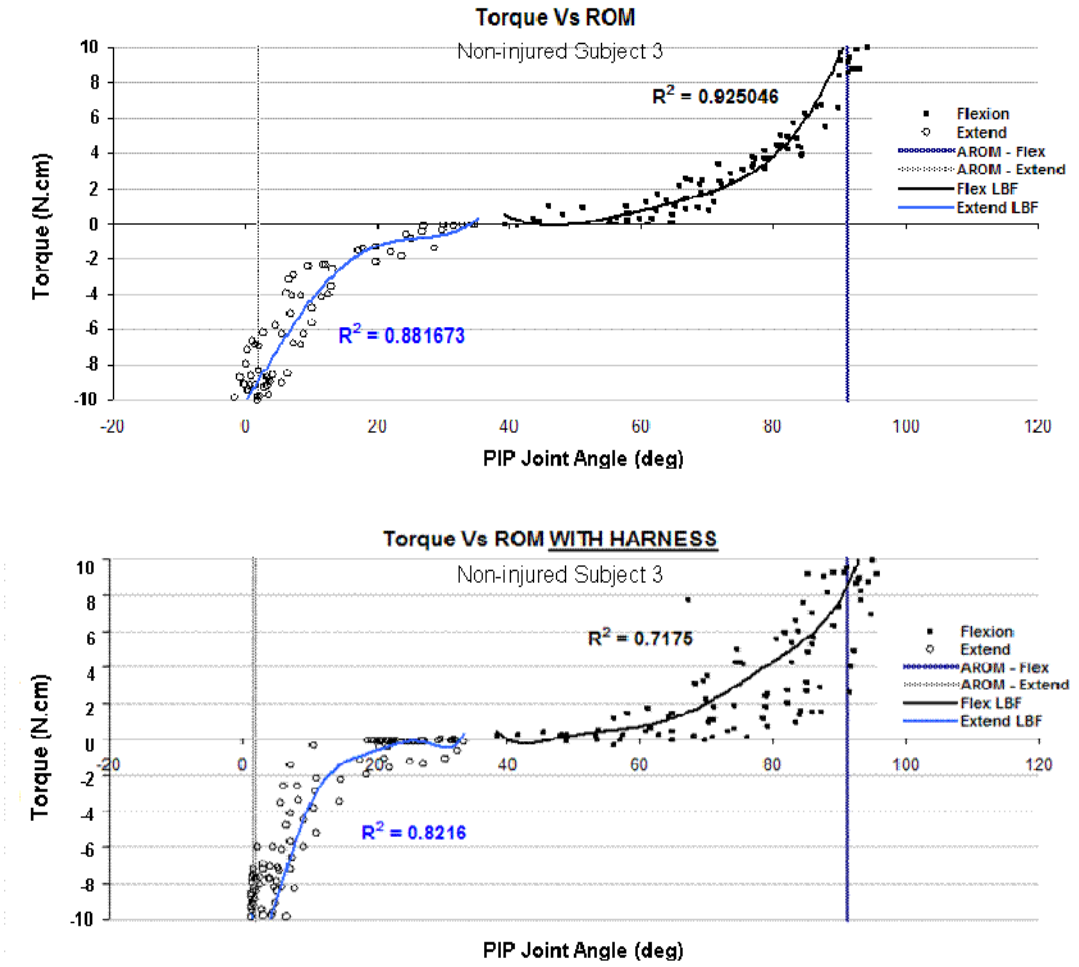


**Figure 7.17 TROM measurements and lines of best fit.** Measurements with (below) and without the finger harness are shown. There is no change in active range of movement. The distribution of the measurements has a higher variance in the TROM with harness.

Figure 7.18 shows a comparison of the polynomial lines of best fit of TROM measurements of an injured and a non-injured subject. The injured subject displayed highly flaccid joints in his right index finger and significant hyperextension in the PIP joint. The non-injured subject had slightly swollen hands and the finger joints were noticeably stiffer.

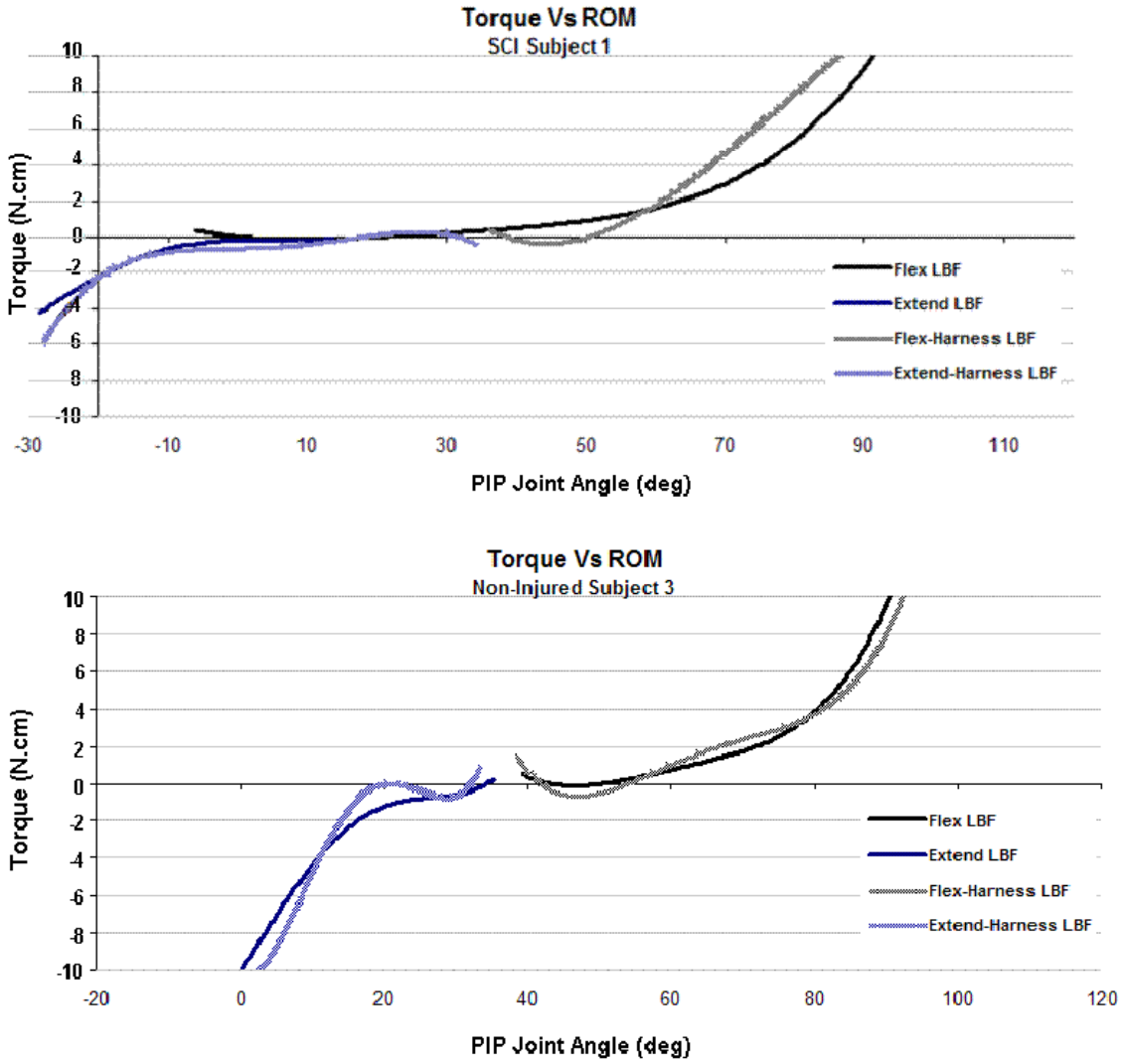


**Figure 7.18 Comparison of TROM results with and without harness for two subjects.** *Spinal cord injured subject (top graph) displayed significant hyperextension of the PIP joint. The relatively gentle slopes measured for this subject matched inspection by palpation of the PIP joint which was observed to be highly flaccid. In contrast, the TROM results of the non-injured subject (lower graph) show relatively stiff joints. During inspection of the non-injured subject's finger some swelling was noted.*

#### 7.3.2.1 Repeatability

Figure 7.19 shows the TROM results of the same subject taken two weeks apart. Comparing the polynomial lines of best fit of the two readings showed consistent curves. Mean difference between the two curves was 2.8% of full-scale 20N.cm ±1.3% (standard deviation, n=120).

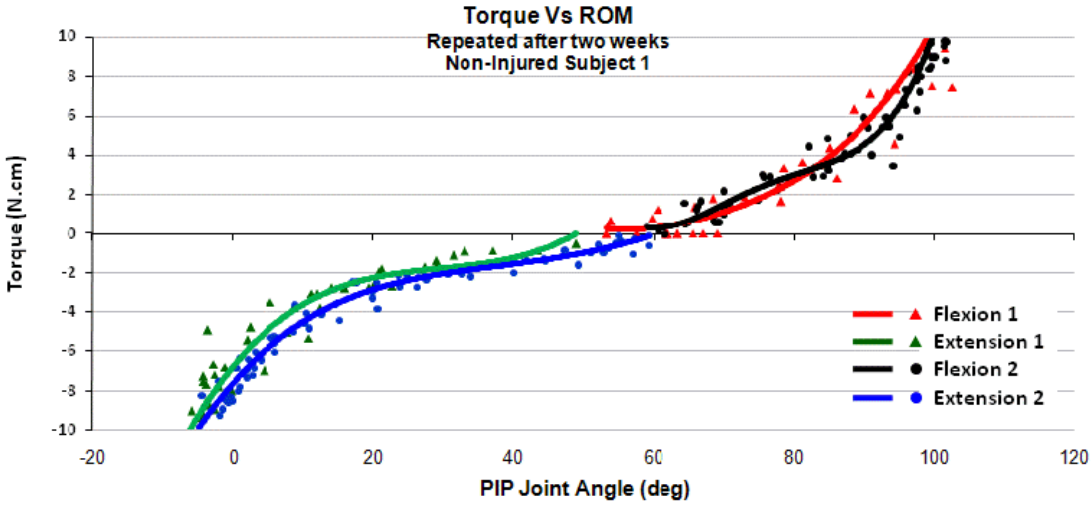


**Figure 7.19 Comparison of TROM curves for the same subject obtained at different times.** Two TROM measurements were recorded from the same subject with a two week separation. Results showed consistent TROM curves.

#### 7.3.2.2 Quantifying joint stiffness using TROM curve slopes

In order to allow a more objective comparison of joint stiffness either between different joints or for the same joint at repeated intervals, the slopes of the TROM curves were calculated (by differentiation of the polynomial lines of best fit). Figure 7.20 returns to the comparison of joint characteristics for spinal cord injured subject 1 (SCI-1) and non-injured subject 3 (NI-3) previously shown in Figure 7.18. In Figure 7.20, TROM measurements of the two subjects superimposed are compared with joint stiffness calculations from the same data. Subject NI-3 displayed greater joint

stiffness for extension end range than subject SCI-1. Flexion end range stiffness curves were relatively closer.

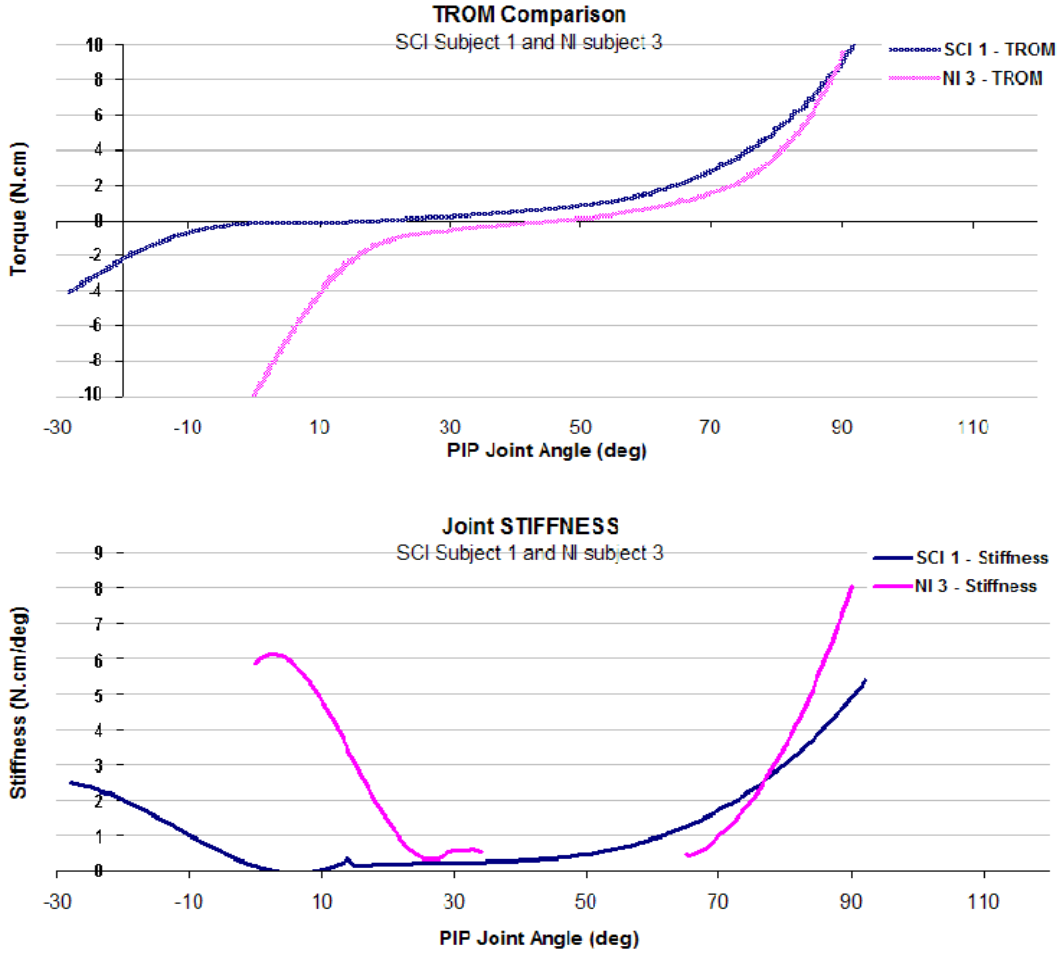


**Figure 7.20 Comparison of TROM curves and joint stiffness plots.** The top graph overlays the TROM (without harness) lines of best fit of spinal cord injured subject 1 (SCI-1) and non-injured subject 3 (NI-3). The lower graph displays information from the same data in the form of joint stiffness curves. These were derived from the TROM curves by differentiation. The stiffness graph suggests that subject NI-3 has greater PIP joint stiffness than subject SCI-1 for the lower joint angles. Both subjects however, displayed similar joint stiffness for the flexion end range.

#### *7.3.2.3 AROM measurements using the alternate setups*

AROM was measured and averaged for all non-injured subjects using three alternate setups. The measurements without the harness were compared to measurements

with the harness on the finger (but inactive). Additionally, the setup was put into zero-torque mode allowing active movement with minimised resistance. The averaged results are found in Figure 7.21.

Although some reductions to active movement were observed with the harness (Figure 7.21), the difference was not considerable. However, due to the small sample size (n = 4), significance could not be established.

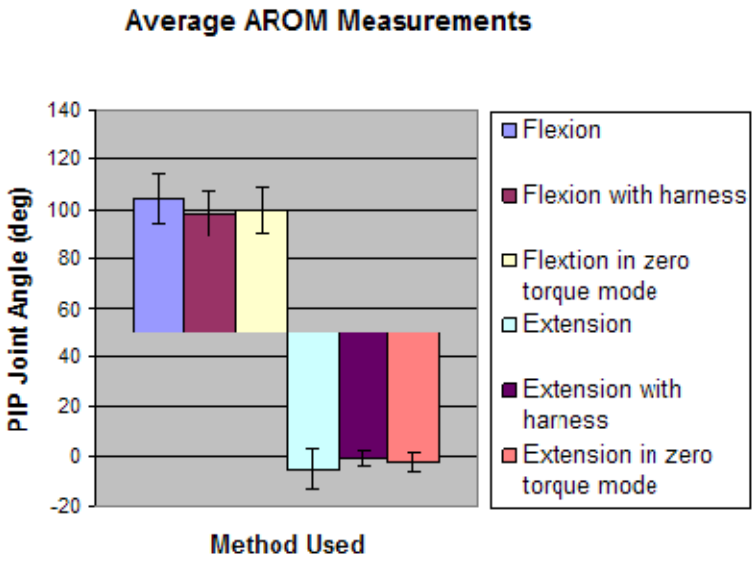


**Figure 7.21 Averaged results from the AROM readings for the alternate protocols.** The first three bars correspond to active flexion. The remaining bars are active extensions. The error bars are standard deviations (n=4).

### 7.3.3 Joint characterisation using the electromechanical setup

TROM-equivalent measurements were made with the finger harness in place. The results were less scattered than the TROM readings. However, a characteristic hysteresis was observed on all readings. In addition, it was noted that the setup was not capable of exceeding ±4 N.cm torque.

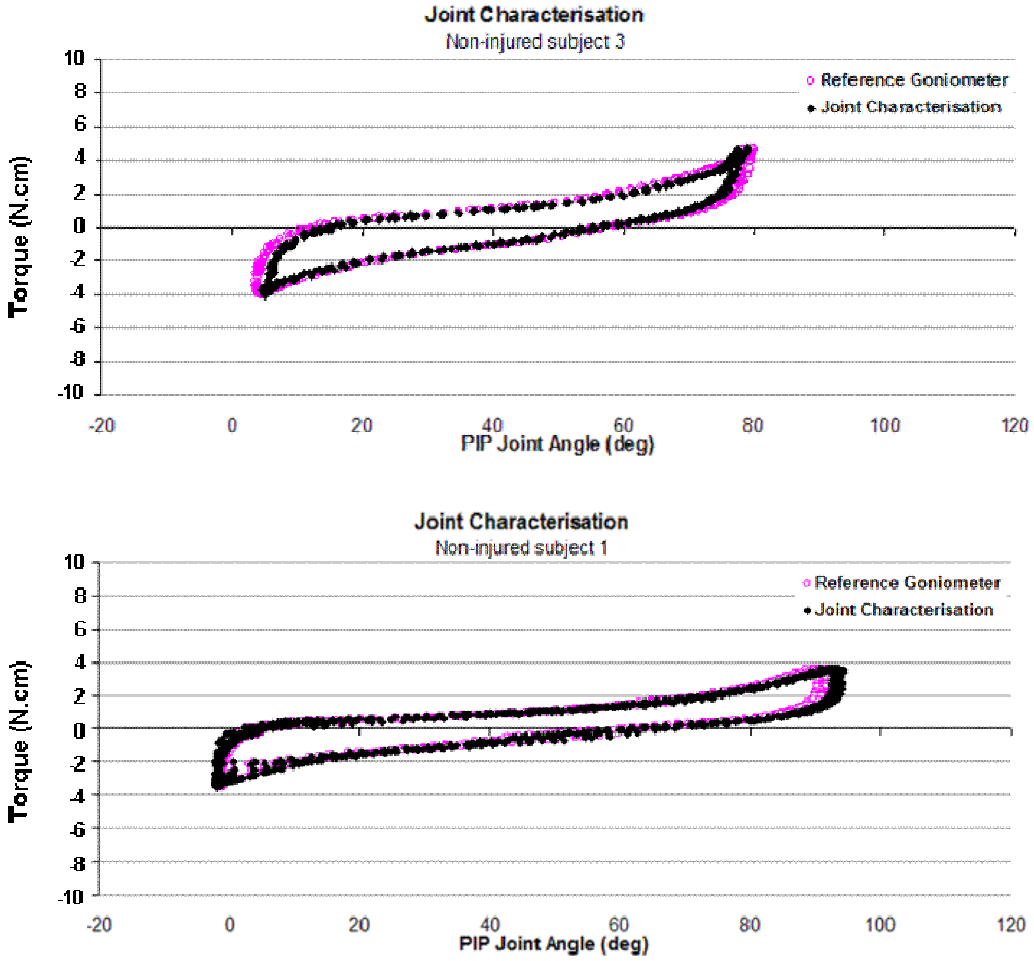


**Figure 7.22 Joint characterisation (JCHAR) readings from two non-injured subjects.** *Each graph shows angle readings made by the internal sensor overlayed by measurements by the electronic goniometer plotted against applied torque.*

### 7.3.4 Passive Motion: Angle control

Figure 7.23 depicts the results of an angle control test with non-injured subject 1. Following joint characterisation (Figure 7.22), end range control parameters were obtained (joint range 0˚-91˚). The control window ($A_H$ - $A_L$) had a width of 4˚. The cycle length was 40sec. The angle control and torque control errors are also shown.

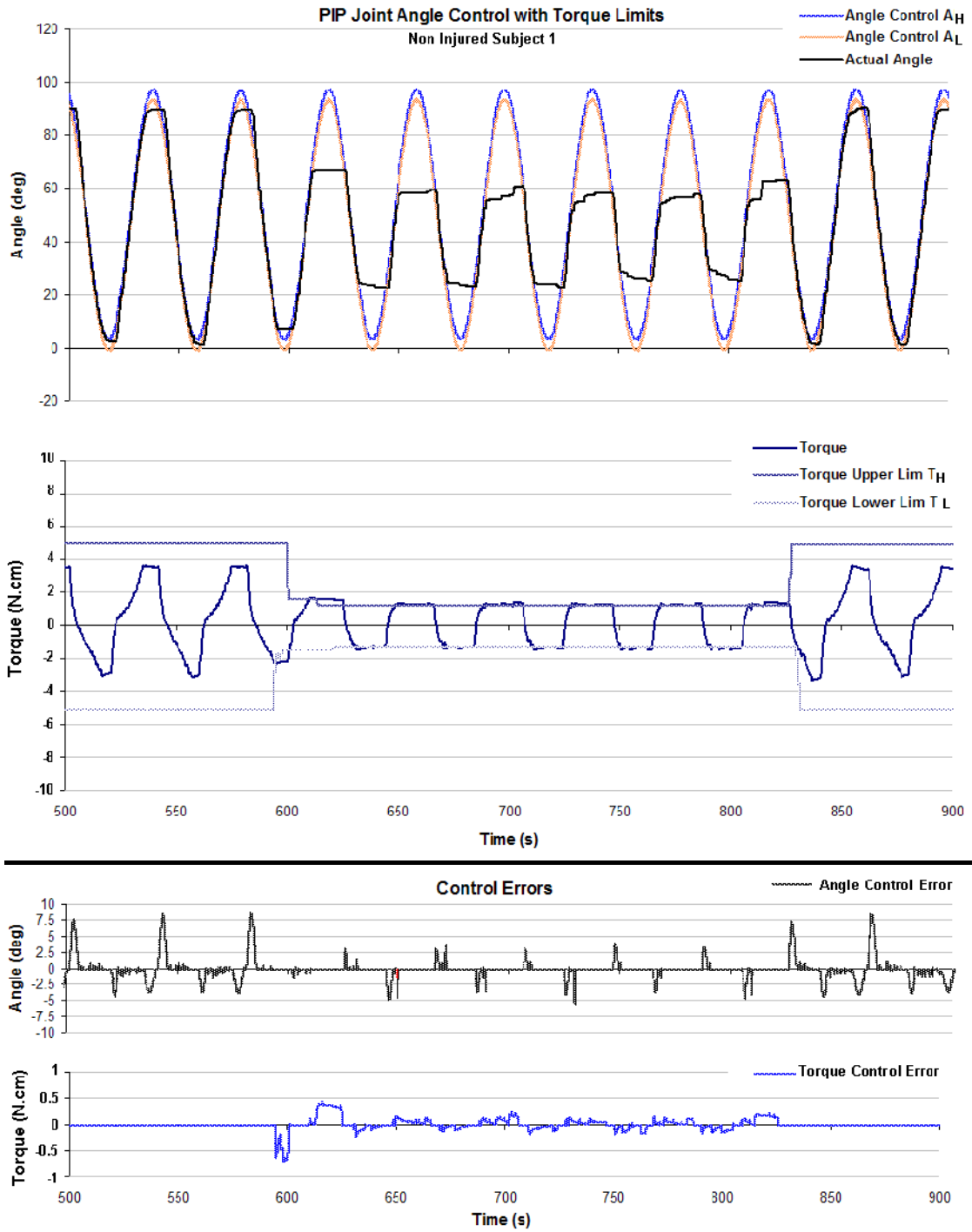


**Figure 7.23 Graphs showing angle control for non-injured subject 1.** Top two graphs show angle and torque measurements with their respective control commands ($A_H$, $A_L$, $T_H$ and $T_L$). The cyclic angle's control parameters were based on end-range limits obtained from the subject's joint characterisations (see lower graph in Figure 7.22). During the cycles, torque control window was narrowed to enforce upper and lower limits. The bottom two graphs show the angle and torque control errors during the cycles. The latter manifests only following the narrowing of the window.

During the session, the torque control window was narrowed to enforce upper and lower limits ($T_L$ = -1.20 N.cm and $T_H$ = 1.20 N.cm selected as suitable example limits). This had the effect of stoping the tracking of the joint angle control command whenever the torque limits were reached. During non-torque-limited cycles, the average angle control error magnitude was 1.1˚± 0.4˚ (standard deviation, n=700). This value was equivalent to ±1.2% of full-scale 90˚. However, the angle control error showed higher magnitudes (greater than 8.3% for flexion and 5% for extension) when the direction of movement was changed. During torque-limited cycles, the angle control error was considered to be zero when the torque limits were reached (otherwise false errors would appear due to the continuing angle commands). However, some artefacts of this algorithm were residual. These appear as vertical lines in the angle control error graph in Figure 7.23. The average torque control error was found to be (during the torque limited section) 0.01 N.cm ± 0.05 N.cm (standard deviation, n=700) or ±1.25% of full-scale 4 N.cm. Although, transient error peaks of 0.15 N.cm (3.75%) were observed.

### 7.3.5 Passive Motion: Torque control

Figure 7.24 shows the results of the torque control test with non-injured subject 1. End-range torques of +3.7N.cm and -3.3N.cm were specified to the control system (with a moving torque control window of 0.4N.cm). Cycle length was 40 sec as before.

During the torque cycles, joint angle limits were enforced by narrowing the angle control window ($A_L$ = 20˚ and $A_H$ = 75˚). The average angle control error within the angle-limited segment of the session was found to be -0.27˚±2.8˚ (or 3.8% of full-scale 90˚, standard deviation, n=1259). This was slightly larger than in the angle control test. The average torque errors were -0.1 N.cm ± 0.44N.cm (or 5.46% of full-

scale 8 N.cm, standard deviation, n=1188) for non-angle-limited and -0.01 N.cm ± 0.22N.cm (or 2.73% of full-scale 8 N.cm, standard deviation, n=1188) for angle-limited cycles. Error peaks exceeding 1 N.cm were observed.

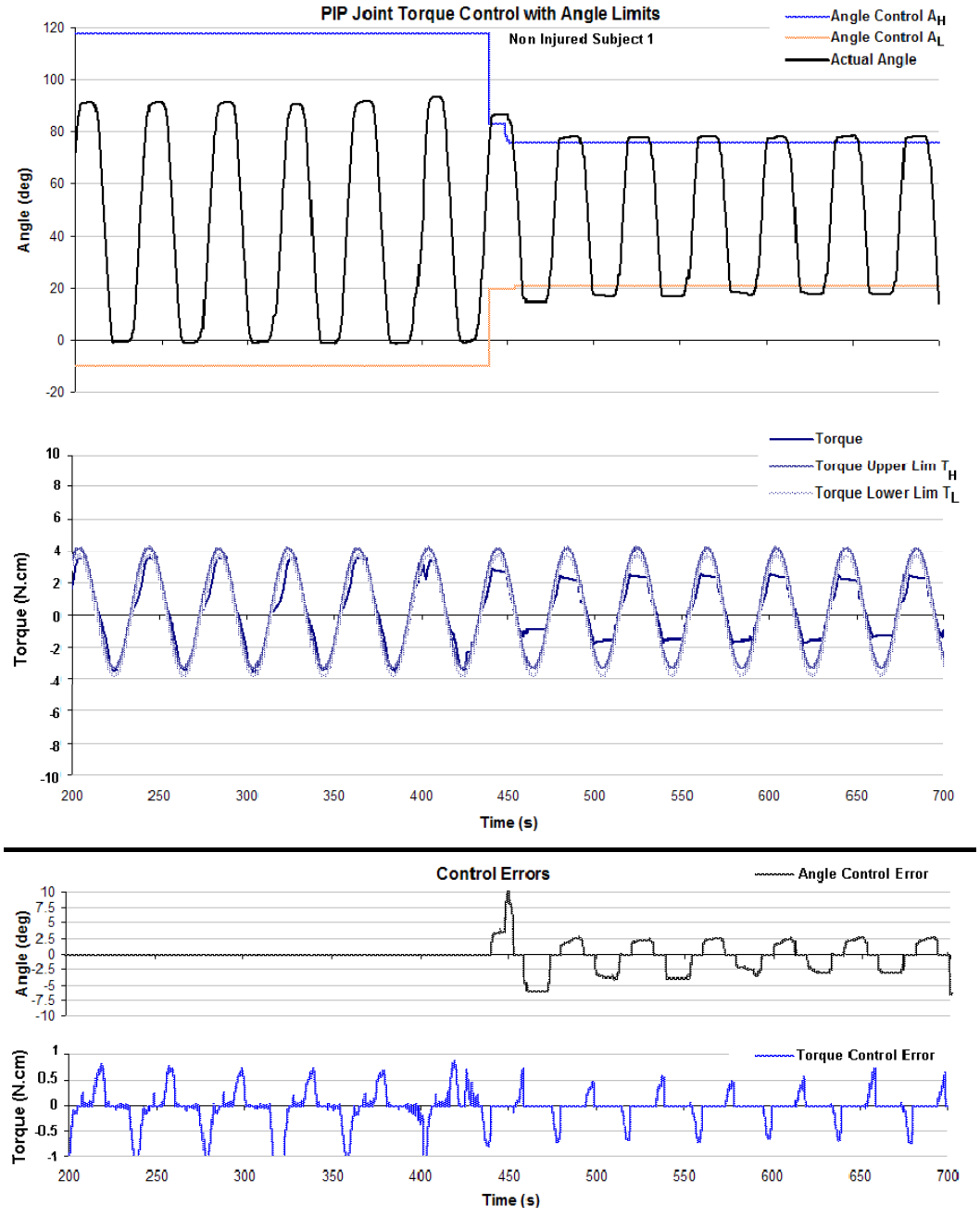


**Figure 7.24 Graphs showing torque control for non-injured subject 1.** The top two graphs show angle and torque measurements with respective control commands ($A_H$, $A_L$, $T_H$ and $T_L$). The cyclic torque control parameters were based on end-range limits obtained from the subject's joint characterisation (see lower graph in Figure 7.22). During the cycles, the angle control window was narrowed to enforce upper and lower limits.

### 7.3.6 Active motion with torque biases

Subjects with active movement were asked to flex and extend their PIP joints while the finger harness applied a controlled torque. The torques applied to the PIP joints during active movements, were recorded and compared to control parameters. During zero torque mode (with the system working to minimise torque), the subjects reported feeling minor resistance to movement from the harness provided such movements were slow. Positive torque biases were perceived as constant forces resistive to extension. Conversely, negative torque biases were felt as resistive to active flexion of the PIP joint.

The system was able to maintain positive and negative constant torque biases commanded to the controller (see Figure 7.25). The applied torque was independent of joint angle. However, the torque tended to remain most stable within the set control window (defined by $T_H$ and $T_L$) for speeds less than ~10˚per second. In Figure 7.26 the torque control errors are plotted against active joint angular speed for two non-injured subjects. The graphs represent measurements from zero-torque, positive torque bias and negative torque bias modes. Measurements for which the subject maintained slower than 10˚ per second movement show much lower torque control errors, 0.005 N.cm ± 0.05 N.cm (0.67% of full-scale, standard deviation n=627). In comparison, active movement speeds greater than 10˚ per second produced an average torque error of 0.02 N.cm ± 0.25 N.cm (3.1% of full-scale, standard deviation n=1270). These differences in torque errors are visible in the graphs in Figure 7.26. The zero torque mode for non-injured subject 1 and negative torque bias for non-injured subject 3 show speeds less than 10˚ per second and lower errors.

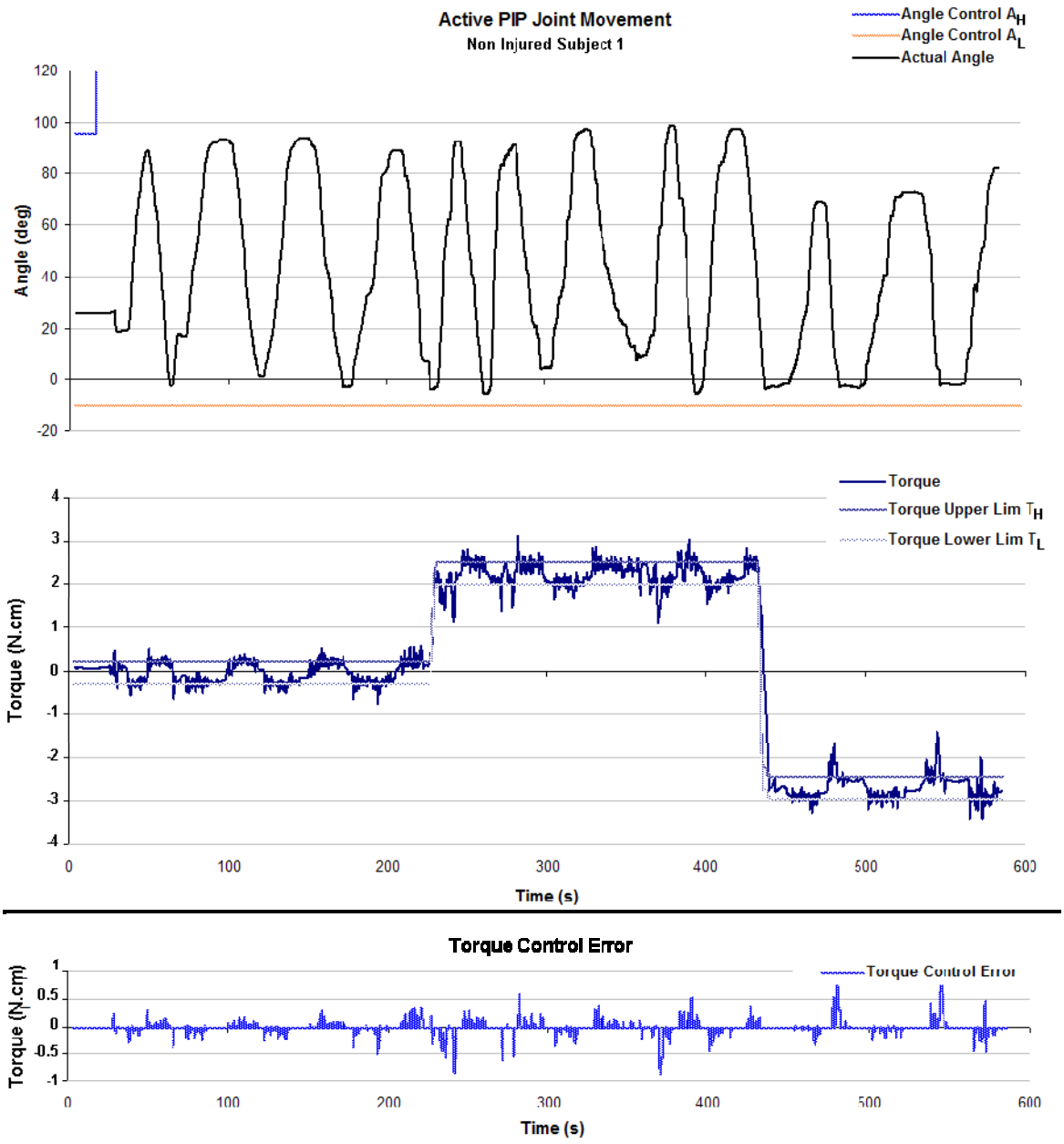


**Figure 7.25** *Measurements from active-joint-movement test. Top: Non-injured subject 1 is actively flexing and extending the PIP joint. Middle: Initially torque in the harness was minimised under zero torque mode. After 220 seconds positive torque (2 to 2.4 N.cm) is applied to the subject's joint (resisting extension). Subsequently, a negative torque bias is applied (-2.55 to -2.95 N.cm). Bottom: Torque control error is recorded.*

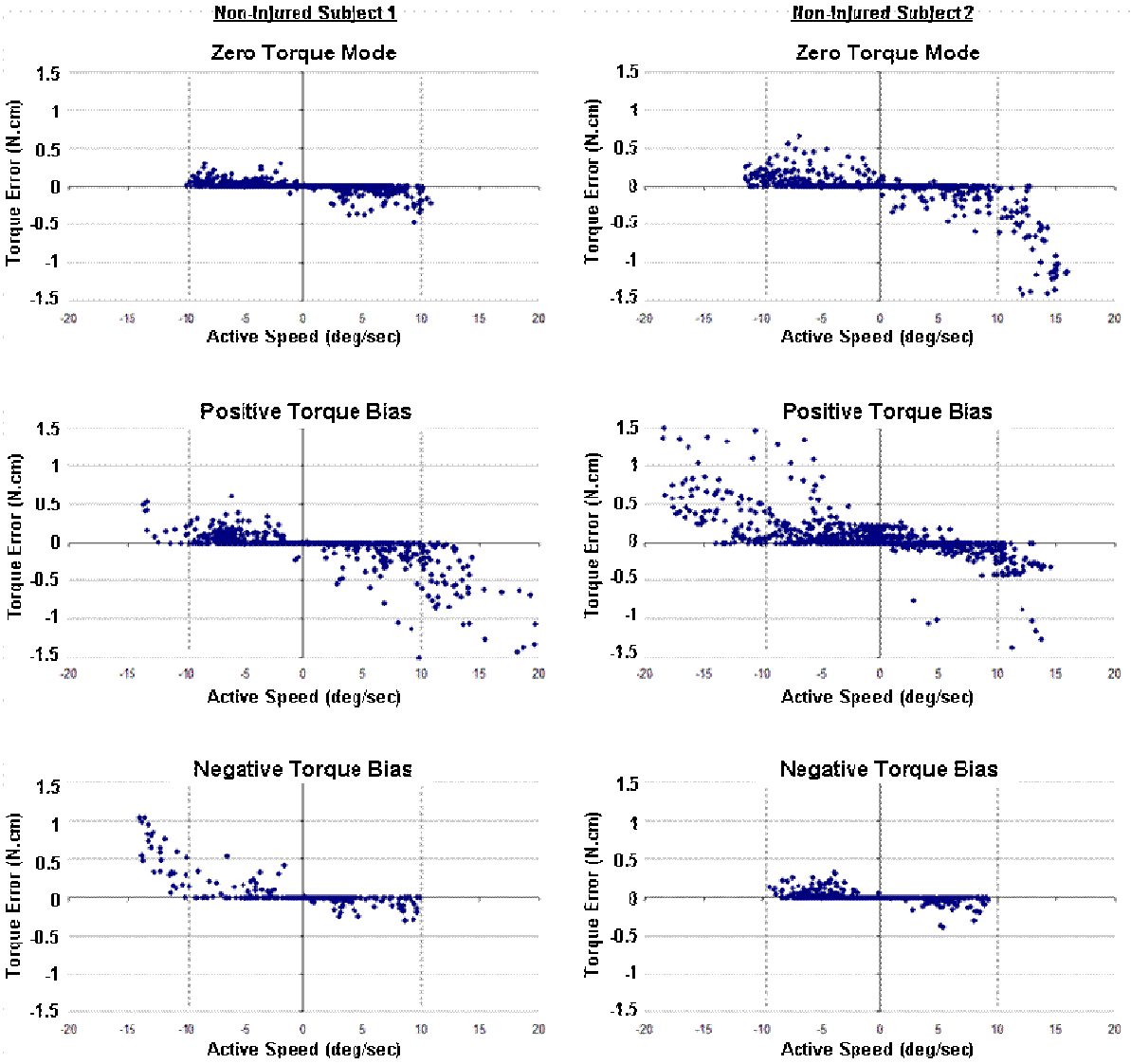


**Figure 7.26 Torque control errors versus active movement speeds.** Results are shown for each of the three torque bias modes for two subjects.

## 7.4 Discussions

The full hand rehabilitation system is expected to be a portable, exoskeletal interface to the hand allowing therapy, assessment and light grasp and release function. Given the presence of its sensory components for torque and range of movement, the device also presents the opportunity to be used as a clinical research tool.

The experiments reported in this chapter tested and showed the viability of the basic building blocks of the envisioned hand rehabilitation system. In doing so, focus was placed on a single joint device and its control system components. The device fitted directly over its target joint and allowed the measurement of torque and joint angle as well as passive control over these parameters. Bowden cable principles were used to allow actuation of the harness independently to the position of proximal joints (in this case the index MCP and the wrist).

### 7.4.1 Calibration and accuracy of the device

The device was calibrated on a model finger and later applied to actual fingers of injured and non-injured subjects. Two types of error were assessed in the experiment: measurement error and control error.

#### *7.4.1.1 Measurement error*

Measurement error (see Figure 7.14) was determined by comparing angle and torque measurements obtained by the internal sensors, with those of the external reference sensors. During cyclic movement of the model finger joint, a recurrent pattern was observed in the angle measurement error. This pattern relates to the effects of the small but noticeable compliance of the Bowden cables. The internal position sensor measures joint angle indirectly from the position of the actuation cable in the electromechanical section. Tensions in the cables lead to minor distortions of the Teflon tubes (Bowden cables) which in turn lead to undesirable movements in the cables. These movements result in errors which increase with tension in the cable. By approximating this relationship to a spring, some error correction can be achieved by taking into account the known tension in the actuation cable (through the internal force transducer) and adjusting the angle measurement by a factor. Correcting the angle in this way does not eliminate the measurement error totally but can reduce it. Following correction, average error dropped from 0.28˚±0.86˚ (standard deviation, n=970) to -0.16˚±0.49˚ (standard deviation, n=970), a drop by approximately 42% (see Figure 7.27).

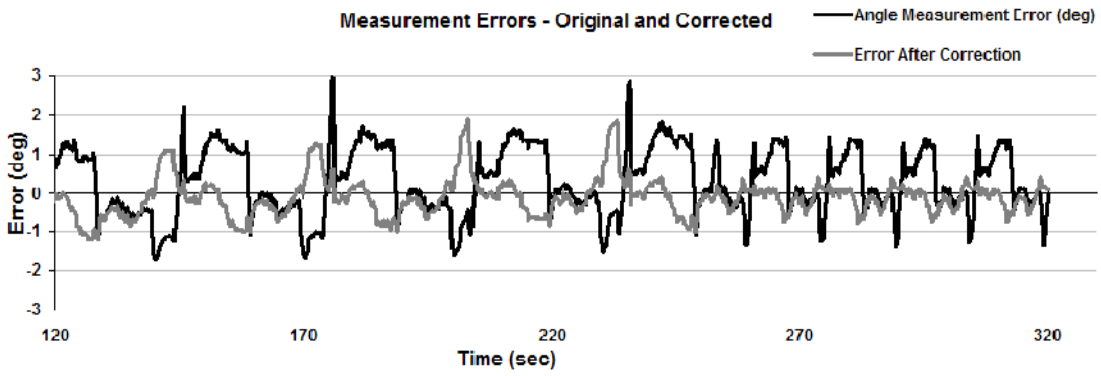


**Figure 7.27 Joint angle measurement errors, raw and corrected.**
Graph shows measurement error before and after correction. The correction can reduce the angle measurement error by up to 50%.

The torque measurement results showed that the indirect sensing method through the Bowden cables and the finger harness is reliable and can be improved. The friction in the system leads to minor hysteresis in the readings.

#### *7.4.1.2 Control error*

Angle and torque control errors are highly dependent on the selected control window width, speed and measurement accuracy. Increasing the window width will increase stability but produce a larger control hysteresis. Angle control error was measured with different speeds using the finger model. For the slower speed in Figure 7.15, the results show higher control errors at the end-ranges. This was caused by friction between the actuation cables and the Teflon cables (the same type of error can be seen in tests with human hands). At control speeds exceeding the limitations of the motors, a lag in movement caused very high control errors. The maximum speed at which the motors were capable of changing the joint angle was ~10˚ per second. The speed of the motors is an important limiting factor in the function of the device (see section 7.4.7, page 192). Generally, it was more difficult for the device to control torque than position. This was attributed to the friction and stiction* in the system causing irregularities in the force transmission to the internal sensor.

---

* A threshold of force caused by the static cohesion between two touching surfaces. Stiction must be overcome before relative movement between surfaces can occur. Stiction is a threshold, not a continuous force.

### 7.4.2 Examination of standard ROM measurements

The TROM and AROM experiments were used to examine the usefulness and reliability of standard forms of measurement. In doing so, standard methods (see section 6.2.1) were adapted to the data acquisition system using the described sensors.

#### *7.4.2.1 TROM measurements*

Standard TROM measurements performed in clinical settings involve discrete measurements of joint angles subsequent to the application of known torques (Swanson, de Groot Swanson et al. 1995; Glasgow, Wilton et al. 2003). Such methods at best produce a limited number of passive joint angles against applied torque. The results in this study show that TROM measurements can vary greatly throughout the range of motion. Thus, there may be large errors associated with standard measurements. The source of this error is the manner by which the measurements are normally obtained. Application of known torques and simultaneous measurements of joint angles are difficult. Applied torque can fluctuate significantly with minor changes in angles of force vectors and moment arm lengths. Friction and hysteresis in the PIP joints also contribute to further error. To many clinicians these errors may not be apparent due to the perceived accuracy of the torque gauges and goniometers used. Despite the potential usefulness of TROM measurements, standard methods are unreliable and may be misleading for use as a form of assessment.

The continuous measurement TROM methods applied in this study were used to produce curves representing the torque versus angle characteristics of the joint. The curves are derived from a large number of readings and are more reliable than single

point measurements. However, they are not necessarily more difficult to obtain than single readings. As shown in Figure 7.19, repetition of the readings after two weeks produces very similar curves.

Applying the TROM measurement to different subjects produced characteristic curves showing total range of movement for specified torque limits and particular curve shapes. The TROM curve of each subject was unique and different to those of other subjects. Steep lines on the curves showed high stiffness and gentle curves showed compliance of the joint studied. In order to obtain a more objective view of the joint stiffness, the slopes of the TROM curves were plotted against joint angles.

The usefulness of TROM measurements has been established in literature (Swanson, de Groot Swanson et al. 1995). This study does not aim to make any objective links between pathology or joint condition and TROM curve shape.

#### *7.4.2.2 Joint stiffness*

Joint stiffness was calculated indirectly from the curves derived using the TROM measurements. Stiffness curves are useful for comparing the stiffness of different joints and monitoring long term changes within the joint. Furthermore, the curve provides specific stiffness values at different joint angles. This type of measurement was proposed by Dionysian and others (2005) and has previously been available only with table-top arthrograph devices.

In Figure 7.20 the TROM curves and joint stiffness of a spinal cord injured (SCI) subject was compared with those of a non-injured (NI) subject. The latter had considerably stiffer joints than the former when examined by palpation. In addition, the SCI subject exhibited substantial hyper-extension of the PIP joint. This comparison

was confirmed by the TROM curves plotted. An average 40˚± 3.5˚ (standard deviation, n=10) difference is observed in extension for a torque of -4 N.cm. However, flexion TROMs appear relatively consistent for the two subjects.

#### *7.4.2.3 Effects of the harness on joint motion*

A certain level of restriction to movement of the joint is inevitable with any measurement system that requires contact with the fingers. However, by standardising the measurement procedure and comparing results from the same platform, useful data can be obtained for assessment. The finger harness used in this study was designed with such considerations in mind. The results presented in section 7.3.2 show that despite the increase in the scatter for the TROM readings with the harness, lines of best fit derived do not greatly differ between measurements with and without the harness. The increase in the TROM measurement scatter is attributed to the friction introduced by the harness as well as the additional hindrance to consistent manual manipulation of the sensors. The resulting increase in the dorsal surface height of finger segments makes it more difficult to maintain a constant angle between the force gauge tip and the middle segment of the finger. The level of obstruction of the harness to free joint movement is also highly dependent on the fit of the saddles. As only two saddle sizes were available (large and medium) the fingers with larger girths were more prone to experiencing restrictions to end range flexion (due to the compression and bunching of the skin and soft tissue).

### 7.4.3 Joint characterisation (JCHAR) using the rehabilitation device principles

Joint Characterisation (JCHAR) measurements are equivalent to TROM in that the device applies torque to the joint and records the applied torque and the resulting joint angles continuously. However, the advantage of the JCHAR method is that the measurements are more controlled and consistent than the latter. The lines of best fit obtained from the loading plots of JCHAR gave an average $R^2$ of 0.996 ± 0.02 (standard deviation, n=8) for flexion and 0.986 ± 0.02 (standard deviation, n=8) for extension. In contrast, the TROM curves produced average $R^2$ values of 0.91 ± 0.05 (standard deviation, n=8) and 0.88 ± 0.06 (standard deviation, n=8) for flexion and extension respectively across the subjects. In JCHAR, the forces are always applied as direct torques via the struts of the finger harness. Hence, the applied torques and their measurements are stable. The same is not true for the TROM in which an attempt is made to manually apply forces perpendicularly to the finger joint at a constant moment arm to produce a known torque. In practice this is very hard to achieve and highly error-prone.

Apart from reliability and accuracy differences, the main distinction between the two measurements is apparent from shape of the resulting plots. TROM produces a scattered series of data points obtained from loading torques. JCHAR however, produces a distinctive hysteresis curve with a highly regular and repeatable shape (see Figure 7.29). This curve includes both loading and unloading torques. The hysteresis shape itself can contain useful information about the energy absorbed by the finger joint during movement. The hysteresis curves produced in this study are consistent with findings in literature. The absorbed energy is related to the friction, stiction and viscoelasticity within the joints. A reduction of this energy often accompanies the recovery of joint range of motion and reduction in joint stiffness (Goddard, Dowson et al. 1969; Unsworth, Bey et al. 1981; Unsworth, Yung et al.

1982; Yung, Unsworth et al. 1986; Latash and Zatsiorsky 1993; Bromley, Unsworth et al. 1994; Dionysian, Kabo et al. 2005).

Attempts were made to overlay TROM and JCHAR measurements from the same subjects to apply objective comparisons. However, four factors considerably hindered the effectiveness of this comparison:

1. The electromechanical setup was incapable of applying torques larger than ±4 N.cm to the PIP joints via the finger harness (whereas the TROM torques spanned beyond ±10 N.cm).
2. The TROM readings were highly unreliable in the middle ranges (~ 30˚ to 60˚)
3. TROM readings were highly scattered and had to be approximated
4. The speed of the TROM measurements could not be easily regulated and typically exceeded the maximum speed of the finger harness during JCHAR readings (see section 7.4.3.1 on effects of viscosity).

The limitations in motor forces result in the reduction in the width span of the hysteresis curve. In a test in which force was deliberately limited to ±2 N.cm, the effect on the hysteresis curve was observed (Figure 7.28). The loading and unloading portions of the curve were identical. However, the width of the curve is limited accordingly. Figure 7.28 shows the JCHAR curves limited to ±2 N.cm and ±4 N.cm as well as a theoretical projection of a curve expected from higher torques. Ideally, the rehabilitation device should be capable of providing the higher torques necessary for characterisation of the joint over its full range. Torques up to ±10 N.cm would be more appropriate in future designs. However, this early prototype is capable of demonstrating the potentials of the device in reliably and consistently characterising the finger joints for assessment and clinical research.

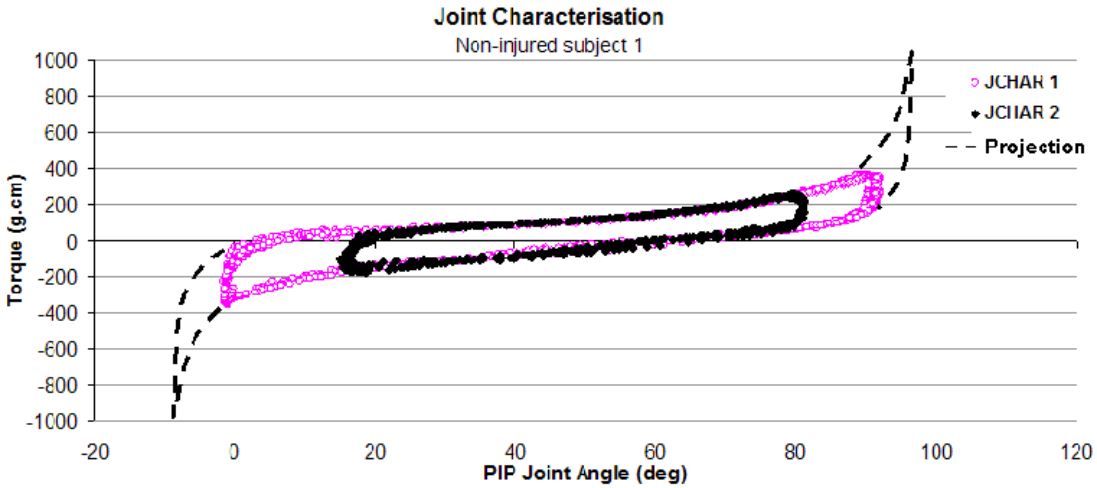


**Figure 7.28 The effect of torque limitations on the JCHAR hysteresis curve.** JCHAR 1 is limited by the systems maximum capability; ±4 N.cm. JCHAR 2 is limited to half the maximum torque at ±2 N.cm. The projection curve presents the type of curve expected from a system with greater torque capability.

Given the factors outlined, only limited segments of the two methods could be compared. This is evident from the results of non-injured subject 3. Figure 7.29 (top graph) presents an overlap of the TROM and JCHAR measurements for the same subject on the same scale. It shows that the height and span of the JCHAR plot is smaller than those of the TROM plots (due to torque limitations of the electromechanical setup). A comparison of the joint stiffness curves (derived from the slopes of the respective plots) presents similar flexion stiffness for a small section of overlap. However, for extension, the joint stiffness curve derived from the TROM plot shows a stiffer joint than the curve from the corresponding JCHAR. This discrepancy may be related to the effects of viscosity within the joints.

#### *7.4.3.1 Possible effects of viscosity*

There are considerable nonlinear forces involved in the movement of joint capsules, tendon sheaths, muscles and connective tissues. These include forces stemming from viscoelastic tissue as well as friction and stiction (Brand, Thompson et al. 1987).

Furthermore, the bone and ligaments contribute to nonlinear limits. Passive forces moving the joints must overcome the viscous restraint of fluids that move around in the tissues (ibid).

Viscoelastic biological materials exhibit time-dependent behaviour, by which their resistance to rapidly applied forces is greater than their resistance to the application of slow or static forces. When comparing JCHAR results with TROM, the higher TROM values may be a direct result of the higher applied speeds.

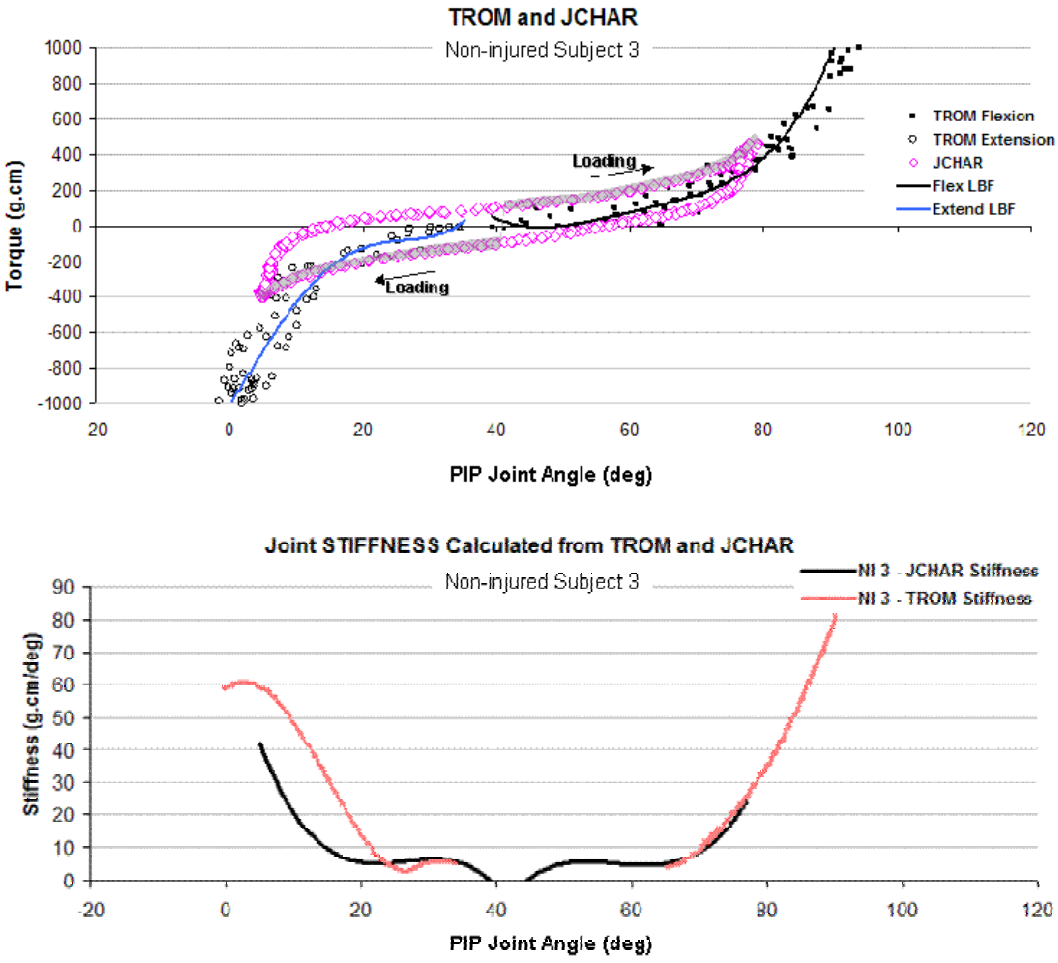


**Figure 7.29 Comparison of the TROM and JCHAR curves for the same subject.** Top graph shows an overlap of the TROM and JCHAR measurements on the same scale. The height and width of the JCHAR plot is smaller than those of the TROM plots due to torque limitations of the electromechanical setup. Bottom graph shows two stiffness curves derived from the TROM and JCHAR data respectively.

### 7.4.4 Effectiveness of a hybrid torque-angle control system

The proposed hybrid control algorithm is appropriate for torque and angle control in a safe and effective way. Results show that torque and angle can be controlled simultaneously.

#### *7.4.4.1 Passive motion: angle control versus torque control*

The results of the passive control tests show that joint angle and passive torque are co-dependent. This is consistent with the TROM and JCHAR findings. In angle control, as the joint was flexed or extended towards its end ranges, the measured torque increased in magnitude (see Figure 7.23). Following the narrowing of the torque safety limits, the increasing torque caused the system to halt movement whenever the limits were breached.

Torque control (angle limited) was effective in applying cyclic forces to the subject's joint and causing passive movement. Narrowing the joint angle limits caused the system to halt torque-increase whenever these limits were breached.

Generally, control errors were higher for torque control than for angle control. This was consistent with finding with the finger model tests. The friction in the system has a more detrimental effect on force measurement than angle measurement. Furthermore, the position sensor used in the setup is more accurate than the force gauges.

### 7.4.5 Significance of hybrid torque-angle control for therapy

The main advantage of hybrid torque-angle control for therapy is that it allows the administration of therapeutic passive motion in a safe manner.

Using the proposed hand rehabilitation system and torque control (within safe angle limits) a novel form of therapy can be applied. Torque control allows gradual stretching and recovery of range of movement while maintaining a therapeutic force. Traditional CPM devices are position controllers with rudimental force safety features (if the force exceeds a set limit, the movement reverses). Although such devices are beneficial, they may not be applying optimal, prescribed and controlled forces to the target joints. Torque control also will allow the application of Total End Range Time or TERT (Chow, Dovelle et al. 1989; Brand 1995; Chester, Beale et al. 2002; Glasgow, Wilton et al. 2003; Austin, Slamet et al. 2004). TERT refers to the amount of time a joint is held at its passive end range. When applied to specific joints, such prolonged therapeutic forces act to increase the compliance of stiff structures, lengthen shortened soft tissue, increase joint range of motion and help restore functional use of limited joints (Austin, Slamet et al. 2004).

### 7.4.6 Advantages of joint-angle-independent torques

The results of the active motion tests show that the system is able to apply angle independent torques (equivalent to position independent forces in SEA, see section 2.1.1.2). This type of torque may be particularly useful in the emulation of dynamic splints and grasp function.

#### 7.4.6.1 Dynamic splinting using the proposed system

One of the drawbacks of traditional dynamic splints is that the therapeutic force applied by the outrigger is highly dependent on finger position. Normally, a therapist tensions the elastic of a traditional dynamic splint to an appropriate level. However, incremental recovery of joint range of motion, creep in the elastic and gradual movement of the outrigger causes this force to decrease with time.

Using the proposed system, a therapeutic torque can be administered to a target joint and held constant. The active motion tests show that such passive torques can be maintained constant despite active or passive movements of the joint. The essential advantage of a traditional dynamic system is its simplicity. However, in a rehabilitation device that delivers a variety of therapeutic programs, dynamic splinting would be an effective and useful addition.

#### 7.4.6.2 Grasp function

A full hand exoskeleton developed on the basis of the proposed design is hoped to produce basic grasp and release functions. For a user with paralysed hands (such as for a tetraplegic individual as presented in 7.1.3) an exoskeleton should be able to close over an object and maintain sufficient forces to prevent the object from slipping. Without involving the user in the intricate and complex control of multiple actuators, a simple proportional close and open function may suffice. Using a single degree of freedom controller (such as a simple shoulder joystick) the user would be able to select a force level for grasp. The control system would then instruct the joints of the exoskeleton to close with the required torque. Using the joint angle independent algorithm, each joint would be free to move until obstruction due to closure of the hand over the object. At the point of obstruction each joint would

maintain the applied torque and self-adjust automatically to any changes due to movement or shape change of the object.

#### *7.4.6.3 Active exercises*

Active exercises are possible using the proposed technology. A patient using a full hand harness can actively work against constant or changing passive torques. This may be a beneficial function for hemiplegic patients who may experience difficulties in extending their hand joints due to partial paralysis and muscle spasms (Koeneman, Schultz et al. 2004). In such cases, a full hand device may be instructed to maintain a constant extension force that can encourage the hand of the patient to open. The function may also have neural remapping benefits (Jenkins 1987; Nudo 1996; Nudo and Milliken 1996; Nudo, Wise et al. 1996). However, in order to fully investigate the possible benefits of such activities further studies will be necessary following the development of a full hand system.

Zero-torque mode will be useful in minimising the obstruction of the device to normal active movement while it is not being used.

### 7.4.7 Errors found in active movement

Relatively high errors were found in the maintenance of constant torques during the active movements. It was found that this error was highly dependent on the speed of active movements. The subjects were asked to flex and extend slowly (in anticipation of the limited speed of the reacting motors). However, this proved difficult for most subjects. Further examination of the relationship between torque control errors and active speed showed a link. The results in Figure 7.26 show that for movements that remained within ±10˚per second control errors were low.

However, once this speed limit was exceeded, the control errors increases significantly causing a disruption to the stability of the control system. Active movement torque control errors can be improved by increasing the speed capabilities of the actuators. Ideally, speed capabilities of actuators should match those required for active movement. Speeds reaching 90˚ per second would be more suited to natural active movement. The combination of such a speed as well as higher torque (ideally above 10 $N.cm^{-1}$) should be feasible with existing technology. However, actuators that could provide the combination of the required torque and speed and simultaneously satisfy the size and weight limitations required for a portable exoskeleton will be highly specialised and expected to be costly.

### 7.4.8 Role of Series Elastic Actuation and Force-Position Transducers

Series elastic actuation (SEA) was found to be compatible with the proposed control algorithm. Although the Force-Position Transducer (FPT) was not used in this experiment (due to current prototype's limitations in accuracy) it can be foreseen that FPTs can replace the springs in the electromechanical system to provide both the elastic elements and position and force feedback (eliminating the need for additional sensors).

### 7.4.9 Role of the harness function in satisfying design objectives

The slot design of the finger harness (see section 7.2.1.1 on page 148) allows the force applied to the medial saddle to be received as a constant torque. This is achieved by allowing the moment arm to change length freely according to the natural movements of the finger segment (as the finger joint is not a perfect hinge). Any increase in moment arm length is accompanied by an inversely proportioned decrease in normal force. As torque = [normal force] x [moment arm], any inversely

proportional changes in normal force and moment will cancel each other allowing torque to remain independent of moment arm length. This design eliminates the need for exact alignment of the finger harness. In addition, a medial saddle placed after a PIP joint can act as a proximal saddle placed before a DIP joint. The DIP harness section can be actuated independently using the Bowden Cable principle. To actuate the MCP, a slightly modified design is used as placement of components lateral to MCP joints is not possible. Actuation of the MCP joint was achieved using crane type levers that travel over the dorsal side of the joints. The evaluated single joint finger harness can be used to work as an independent joint actuator within a multi-linked full hand exoskeleton. Further design work is necessary on the harness coupling mechanism to maximise effectiveness and minimise hindrance to movement and assessment. This is currently underway.

## 7.5 Concluding remarks

In this chapter, a single joint finger harness was developed and used to evaluate design concepts proposed for an electromechanical hand exoskeleton. This device is to act as a human-machine interface used for the rehabilitation of hands following injury or paralysis. In its function, the proposed system aims to bring together several forms of hand therapy currently performed manually by therapists or by rudimentary mechanisms. In addition, the technology can be used for continuous and specialised assessment of hand joints, an important quality that will help enhance the delivered therapy. The demonstration-grade Rehabilitation Glove (see Figure 7.4, 145) used for some simple grasp tests was promising. The single joint experiments reported in this chapter showed that joint torque and angle can be controlled using a feedback system.

Further development of the technology is necessary and underway to produce a portable, full-hand, exoskeletal system. Clinical studies will produce much needed data once the device is commercialised and reaches wider usage.

# Chapter 8 Conclusion

The advent of human-machine interfaces promises to revolutionise the way we interact with our world. Once the subject of science fiction, the technology is creeping ever closer to our everyday lives. All over the world, research facilities are dedicated to creating machines that can enhance human strength and ability. Applications of interest include exoskeletal garments for astronauts, soldiers, nurses, people with disabilities and hobbyist to name a few. However, before such machines can be fully integrated into human life, a number of technical challenges must be overcome.

In this thesis, novel human-machine interface concepts were applied to the rehabilitation of the hand. Of all human parts, the hands are arguably the most complex to interface to, due to the small, intricate and multi-jointed components of the upper extremity. This challenge was riddled with a paradox: to provide enough actuators and sensors to control every joint in the hand, yet keep the interface and working area of the hand light and flexible enough to be feasible. This problem has already been solved by nature using highly efficient actuators in the form of muscles, tiny multifunctional sensors and an ingenious biomechanical design that allows powerful, yet dexterous, tele-actuation of hand joints.

This project was inspired by nature's elegant solutions to its engineering problems. The mechanisms developed and presented in this work use tendon-like cables to enable tele-actuation in multi-linked exoskeletons. This will allow the heavier actuation components to be kept away from the distal end of the upper extremity, easing hand movement. Sensors (FPT) are also kept away from the distal end by measuring the torque and angle of each joint indirectly from its corresponding

actuation cable. In addition, the FPT sensors introduce an elastic component between each actuator and joint. This is an important development allowing series elastic actuation (SEA). SEA is currently gaining wider usage in robotics, particularly with human-machine interfaces. SEA reduces the rigidity in the contact between machine and human parts and optimises function and safety. In addition, the FPT sensors allow joints to be controlled by torque, angle or both. A hybrid torque-angle control algorithm was developed for this purpose and tested in Chapter 7.

The actuation problem is related to the shortcomings of available motor technology. As potential alternatives to standard motors, Smart Materials promise muscle-like actuation with optimal volume and weight. However, the potentials are evident only in small sized materials with actuation outputs far beneath those required in a human- machine interface. In this thesis, it was shown that smart-material-based actuators can be used as small sized units combined to obtain a collective output. A simple method was proposed and used to summate the mechanical work of multiple SMA- based actuators. This method also allowed the combined output to be realised in a step wise manner, leading to part actuation. This was a significant finding, particularly for SMA-based actuators which are difficult to control proportionally. The resolution of this form of actuation can be improved by increasing the total number of active units grouped in this manner.

In the final study, the fundamental components of the envisioned rehabilitation device (see Figure 8.1 adapted from Figure 1.1) were brought together and tested on the hands of human subjects. The study showed that the tele-actuator harness can be placed to mobilise hand joints in a controlled and coordinated way. The device was able to control both joint angle and torque using the same algorithm. The system has the potential to bring several forms of therapy and assessment into one device which can also be used as clinical research tool. As a human –machine

interface, the system can work in parallel to the active movements of the user. This may make the device useful for assisting the movement of weak hands.

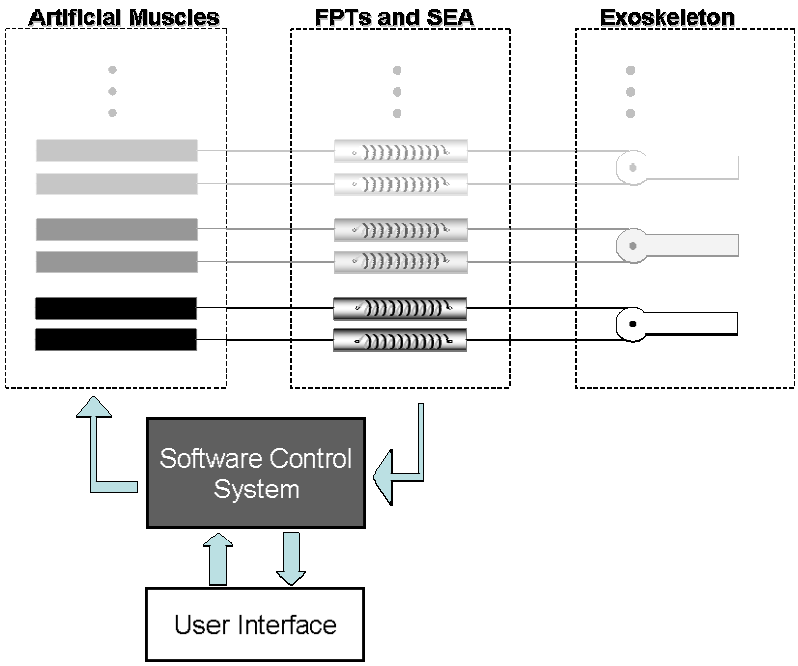


**Figure 8.1 The components of a human-machine interface using concepts developed in this thesis.**

In the course of this study, due to limitations in time and manufacturing resources, it was not possible to produce a truly portable rehabilitation glove which combined all the above components, namely the exoskeleton, FPT and SEA and SMA based muscles[*]. Further development is required to achieve such a milestone. Such an endeavour is likely to require miniaturisation and fabrication of integrated Binary-SMA actuators and FPT based sensors. A lever-based work-summation system (as described in section 5.4.7.1, page 121 and Appendix B) is a promising replacement of the pulley-based method more suited to miniaturisation and manufacturability. Once

[*] A semi-portable glove based device (as described in section 7.1.3, page 143) was made which contained a limited number actuators and no feedback.

this is achieved, it is envisaged that modular, integrated artificial muscle units comprised of the work-summation assembly and FPT can be developed. These modules may then be placed distally and actuate exoskeletal segments via cables. Of further significant challenge will be the improvement of the energy efficiency of SMA based systems and the portable supply of power. Any battery-based power supply is likely to be heavy, compromising the portability of the exoskeleton. Future advances in energy supply and smart material technology should play an important role in realising the aforementioned vision.

The Rehabilitation Glove is currently undergoing further development and commercialisation. The first generation of such a device is expected to utilise standard actuation technology (in the form of miniature dc motors). Once a viable full hand prototype is available, patient trials will be underway to investigate the clinical benefits of the device.

The principles investigated in this work can also be applied for other joints of the body. It is hoped that with improvement in material science and further development a full body harness can one day be made available to assist with movement.

# References


Abolfathi, P., T. Scott, et al. (2004). A novel rehabilitation glove with embedded artificial muscles enabling specific therapeutic and functional options. 11th Combined Orthopaedic Associations Meeting, Sydney.

Abolfathi, P., T. Scott, et al. (2006). Movement Faciliation Device. United States, 20060094989.

Adams, K. M. and S. T. Thompson (1996). "Continuous passive motion use in hand therapy." Hand Clinic **12**(1).

Agnew, P. J. and F. Maas (1982). "Hand function related to age and sex." Archives of Physical Medicine and Rehabilitation **63**(6): 269-271.

Akeson, W. H. M. D., D. D. I. Amiel, et al. (1987). "Effects of Immobilization on Joints." Clinical Orthopaedics & Related Research **219**: 28-37.

Arai, K., S. Aramaki, et al. (1994). Continuous system modelling of shape memory alloy (SMA) for control analysis. 1994 5th International Symposium on Micro Machine and Human Science Proceedings, Nagoya, Japan.

Arai, K., S. Aramaki, et al. (1995). Feedback linearization for SMA (shape memory alloy).

Austin, G., M. Slamet, et al. (2004). "A Comparison of High-profile and Low-profile Dynamic Mobilization Splint Designs." Journal of Hand Therapy **17**(3): 335.

Bar-Cohen, Y., Ed. (1999). Proceedings of the SPIE's Electroactive Polymer Actuators and Devices (EAPAD) Conf., 6 th Smart Structures and Materials Symposium, Vol 3669.

Bar-Cohen, Y. (2002). "Electroactive Polymers as Artificial Muscles: A Review." Journal of Spacecraft and Rockets **39**(6): 822-827.

Bar-Cohen, Y. (2004). "Turning Heads." Spectrum, IEEE **41**(6): 28-33.

Baughman, R. (2005). "MATERIALS SCIENCE: Playing Nature's Game with Artificial Muscles." Science **308**(5718): 63-65.

Baughman, R., A. Zakhidov, et al. (2002). "Carbon Nanotubes--the Route Toward Applications." Science **297**(5582): 787-792.

Bay, L., K. West, et al. (2003). "A Conducting Polymer Artificial Muscle with 12 % Linear Strain." Advanced Materials **15**(4): 310-313.

Bentham, J., W. Brereton, et al. (1987). "Continuous passive motion device for hand rehabilitation." Archives of physical medicine and rehabilitation **68**(4): 248-50.

Brand, P. (1995). The forces of dynamic splinting: Ten questions before applying a dynamic splint to the hand. Rehabilitation of the Hand: Surgery and Therapy. J. Hunter, E. Mackin and A. Callaghan. St Louis, Mosby. **2:** 1581-1587.

Brand, P., D. Thompson, et al. (1987). The Biomechanics of the Interphalangeal Joints. The Interphalangeal Joints. W. Bowers. London, Churchill Livingstone. **1:** 21-54.

Bromley, J., A. Unsworth, et al. (1994). "CHANGES IN STIFFNESS FOLLOWING SHORT- AND LONG-TERM APPLICATION OF STANDARD PHYSIOTHERAPEUTIC TECHNIQUES." Rheumatology **33**(6): 555-561.

Brooks, R. and L. Stein (1994). "Building Brains for Bodies." Autonomous Robots.

Bundhoo, V. and E. Park (2005). Design of an artificial muscle actuated finger towards biomimetic prosthetic hands. Advanced Robotics, 2005. ICAR '05. Proceedings., 12th International Conference on.

Caldwell, D. and N. Tsagarakis (2002). "Biomimetic actuators in prosthetic and rehabilitation applications." Technology and Health Care - European Society for Engineering and Medicine **10**(2): 107-120.

Caldwell, D., N. Tsagarakis, et al. (2000). "Bio-mimetic actuators: polymeric Pseudo Muscular Actuators and pneumatic Muscle Actuators for biological emulation." Mechatronics **10**(4-5): 499-530.

Carpenter, B., R. Head, et al. (1995). Shape memory actuated gimbal. Industrial and Commercial Applications of Smart Structures Technologies: Proceedings of SPIE - The International Society for Optical Engineering. San Diego, CA, USA. **2447:** 91-101.

Carr, J.J, and J.M. Brown (2001). Introduction to biomedical equipment technology. New Jersey, Prentice Hall.

Charles Racine, J. (2003). Control of a lower extremity exoskeleton for human performance amplification. Mechanical Engineering Department. Berkeley, University of California. **PhD Thesis**.

Chester, D. L., S. Beale, et al. (2002). "A Prospective, Controlled, Randomized Trial Comparing Early Active Extension With Passive Extension Using A Dynamic Splint In The Rehabilitation Of Repaired Extensor Tendons." The Journal of Hand Surgery: Journal of the British Society for Surgery of the Hand **27**(3): 283-288.

Cho, K. and H. H. Asada (2006). "Architecture design of a multiaxis cellular actuator array using segmented binary control of shape memory alloy." Robotics, IEEE Transactions on [see also Robotics and Automation, IEEE Transactions on] **22**(4): 831-843.

Cho, K., J. Rosemarin, et al. (2006). Design of vast DOF artificial muscle actuators with a cellular array structure and its application to a five-fingered robotic hand. Robotics and Automation, 2006. ICRA 2006. Proceedings 2006 IEEE International Conference on.

Chow, J. A., S. Dovelle, et al. (1989). "A comparison of results of extensor tendon repair followed by early controlled mobilisation versus static immobilisation." The Journal of Hand Surgery: Journal of the British Society for Surgery of the Hand **14**(1): 18-20.

Damle, R., R. Lashlee, et al. (1994). "Identification and robust control of smart structures using artificial neural networks." Smart Materials and Structures **3**(1): 35-46.

Del Cura, V., F. Cunha, et al. (2003). "Study of the Different Types of Actuators and Mechanisms for Upper Limb Prostheses." Artificial Organs **27**(6): 507-516.

Dent, J. (1993). "Continuous passive motion in hand rehabilitation." Prosthetics and orthotics international **17**(2): 130-5.

Dickinson, M. H., C. T. Farley, et al. (2000). "How Animals Move: An Integrative View." Science **288**(5463): 100-106.

Dimick, P. (1990). Continuous passive motion for the upper extremity. Rehabilitation of the Hand. J. Hunter, E. Mackin and A. Callaghan, Mosby. **2:** 1140-1146.

Ding, J., L. Liua, et al. (2003). "High performance conducting polymer actuators utilising a tubular geometry and helical wire interconnects." Synthetic Metals **138**(3): 391-398.

Dionysian, E., J. M. Kabo, et al. (2005). "Proximal interphalangeal joint stiffness: measurement and analysis." The Journal of Hand Surgery [NLM - MEDLINE] **30**(3): 573.

Durfee, W. and K. Palmer (1994). "Estimation of force-activation, force-length, and force-velocity properties in isolated, electrically stimulated muscle." Biomedical Engineering, IEEE Transactions on **41**(3): 205-216.

Ebron, V., Z. Yang, et al. (2006). "Fuel-Powered Artificial Muscles." Science **311**(5767): 1580-1583.

Elahinia, M., J. Koo, et al. (2005). "Backstepping Control of a Shape Memory Alloy Actuated Robotic Arm." Journal of Vibration and Control **11**(3): 407-429.

Farahat, W. and H. Herr (2005). "An Apparatus for Characterization and Control of Isolated Muscle." Neural Systems and Rehabilitation Engineering, IEEE Transactions on **13**(4): 473-481.

Fowler, N. K. and A. C. Nicol (2001). "Functional and biomechanical assessment of the normal and rheumatoid hand." Clinical Biomechanics **16**(8): 660-666.

Gharaybeh, M. A. and G. C. Burdea (1995). "Investigation of a shape memory alloy actuator for dextrous force-feedback masters." ADVANCED ROBOTICS **9**(3): 317.

Gilbertson, R. (2000). Muscle Wires. San Rafael, CA, Mondo-tronics.

Glasgow, C., J. Wilton, et al. (2003). "Optimal daily total end range time for contracture: Resolution in hand splinting." Journal of Hand Therapy **16**(3): 207.

Goddard, R., D. Dowson, et al. (1969). "The measurement of stiffness in human joints." Rheologica Acta **V8**(2): 229-234.

Gorbet, R. and R. Russell (1995). "A Novel Differential Shape Memory Alloy Actuator for Position Control." Robotica **13**(4): 423.

Gorbet, R. and D. Wang (1995). General stability criteria for a shape memory alloy position control system. Robotics and Automation, 1995. Proceedings., 1995 IEEE International Conference on.

Grant, D. (1999). Accurate and rapid control of shape memory alloy actuators. Department of Electrical and Computer Engineering, McGill University: 158.

Grant, D. and V. Hayward (1995). Design of shape memory alloy actuator with high strain and variable structure control. Robotics and Automation, 1995. Proceedings., 1995 IEEE International Conference on.

Grant, D. and V. Hayward (2000). Constrained force control of shape memory alloy actuators. Robotics and Automation, 2000. Proceedings. ICRA '00. IEEE International Conference on, San Francisco, CA.

Hagan, K., M. Hillman, et al. (1997). The design of a wheelchair mounted robot. Computers in the Service of Mankind: Helping the Disabled (Digest No: 1997/117), IEE Colloquium on.

Hart, R., K. Kilgore, et al. (1998). "A comparison between control methods for implanted FES hand-grasp systems." Rehabilitation Engineering, IEEE Transactions on **6**(2): 208-218.

Hashimoto, M., M. Takeda, et al. (1985). "Application of shape memory alloy to robotic actuators." Journal of robotic systems **2**(1): 3-25.

Herr, H. and R. Kornbluh (2004). New horizons for orthotic and prosthetic technology: artificial muscle for ambulation. Proceedings of SPIE - Smart Structures and Materials 2004, SPIE.

Hesse, S., H. Schmidt, et al. (2003). "Upper and lower extremity robotic devices for rehabilitation and for studying motor control." Current Opinion in Neurology **16**(6): 705-710.

Hill, A. V. (1953). "The Mechanics of Active Muscle." Proceedings of the Royal Society of London. Series B, Biological Sciences **141**(902): 104-117.

Honma, D., M. Yoshiyuki, et al. (1989). Micro robots and micro mechanisms using shape memory alloy. Integrated Micro Motion Systems, Micro-machining, Control and Application, The Third Toyota Conference, Aichi Japan.

Huang, W. (2002). "On the selection of shape memory alloys for actuators." Materials & Design **23**(1): 11-19.

Hunter, I. and S. Lafontaine (1992). A comparison of Muscle with Artificial Actuators. Solid-State Sensor and Actuator Workshop, 1992. 5th Technical Digest., IEEE.

Hunter, J., E. Mackin, et al. (1995). Rehabilitation of the Hand: Surgery and Therapy. St Louis, Mosby.

Ikuta, K. (1990). Micro/miniature shape memory alloy actuator. Robotics and Automation, 1990. Proceedings., 1990 IEEE International Conference on, Cincinnati, OH

Inganäs, O. and I. Lundström (1999). "MATERIALS SCIENCE:Carbon Nanotube Muscles." Science **284**(5418): 1281-1282.

Jacobsen, S., M. Olivier, et al. (2004). "Research Robots for Applications in Artificial Intelligence, Teleoperation and Entertainment." The International Journal of Robotics Research %R 10.1177/0278364904042198 **23**(4-5): 319-330.

Jacobsen, S. C., E. K. Iversen, et al. (1996). The Design of the Utah/MIT Hand. Proceedings of the IEEE International Conference on Robotics and Automation, San Francisco, CA.

Janocha, H. (1999). Adaptronics and Smart Structures: Basics, Materials, Design, and Applications New York, Springer.

Jenkins, W. M. (1987). "Reorganization of neocortical representations after brain injury: a neurophysiological model of the bases of recovery from stroke. ." Progress in Brain Research **71**: 249-66.

Jiping, H., E. J. Koeneman, et al. (2005). RUPERT: a Device for Robotic Upper Extremity Repetitive Therapy. Engineering in Medicine and Biology Society, 2005. IEEE-EMBS 2005. 27th Annual International Conference of the.

Jun, H. Y., O. K. Rediniotis, et al. (2007). "Development of a fuel-powered shape memory alloy actuator system: I. Numerical analysis." Smart Materials and Structures **16**(1): S81-S94.

Jun, H. Y., O. K. Rediniotis, et al. (2007). "Development of a fuel-powered shape memory alloy actuator system: II. Fabrication and testing." Smart Materials and Structures **16**(1): S95-S107.

Kawamura, K., S. Bagchi, et al. (1995). "Intelligent robotic systems in service of the disabled." Rehabilitation Engineering, IEEE Transactions on **3**(1): 14-21.

Klute, G., J. Czerniecki, et al. (2002). "Artificial Muscles: Actuators for Biorobotic Systems." The International Journal of Robotics Research **21**(4): 295-309.

Kobayashi, H. and H. Suzuki (2005). Development of a new shoulder mechanism for a muscle suit. Mechatronics and Automation, 2005 IEEE International Conference.

Koeneman, E., R. Schultz, et al. (2004). A pneumatic muscle hand therapy device. Engineering in Medicine and Biology Society, 2004. EMBC 2004. Conference Proceedings. 26th Annual International Conference of the.

Kornbluh, R., R. Pelrine, et al. (1998). Electrostrictive polymer artificial muscle actuators. Robotics and Automation, 1998. Proceedings. 1998 IEEE International Conference on, Leuven

Kuribayashi, K. (1986). "A New Actuator of a Joint Mechanism Using TiNi Alloy Wire." The International Journal of Robotics Research **4**(4): 47-58.

Kuribayashi, K. (1991). "Improvement of the Response of an SMA Actuator Using a Temperature Sensor." International Journal of Robotics Research **10**(1): 13-20.

Kyu-Jin, C. and H. H. Asada (2004). Segmentation architecture of multi-axis SMA array actuators inspired by biological muscles. Intelligent Robots and Systems, 2004. (IROS 2004). Proceedings. 2004 IEEE/RSJ International Conference on.

Kyu-Jin, C., J. Rosemarin, et al. (2006). Design of vast DOF artificial muscle actuators with a cellular array structure and its application to a five-fingered robotic hand. Robotics and Automation, 2006. ICRA 2006. Proceedings 2006 IEEE International Conference on.

Latash, M. L. and V. M. Zatsiorsky (1993). "Joint stiffness: Myth or reality?" Human Movement Science **12**(6): 653-692.

Le Stayo, P. (1995). Continuous passive motion for the upper extremity. Rehabilitation of the Hand: Surgery and Therapy. J. Hunter, E. Mackin and A. Callaghan. St Louis, Mosby. **2:** 1545-1560.

Lee, Y.-J., H.-m. Son, et al. (2006). "Design and control of multi-step SMA actuator." International Journal of Applied Electromagnetics and Mechanics **00023**(00001): 119-125.

Lewis, T., S. Moulton, et al. (1997). "Optimisation of a polypyrrole based actuator." Synthetic Metals **85**(1-3): 1419-1420.

Lu, A., D. Grant, et al. (1997). Design and comparison of high strain shape memory alloy actuators. Robotics and Automation, 1997. Proceedings., 1997 IEEE International Conference on Albuquerque, NM.

Ma, N. and G. Song (2003). "Control of shape memory alloy actuator using pulse width modulation." Smart Materials and Structures **12**: 712-719.

Madden, J. (2006). "MATERIALS SCIENCE: Artificial Muscle Begins to Breathe." Science **311**(5767): 1559-1560.

Madden, J., B. Schmid, et al. (2004). "Application of polypyrrole actuators: feasibility of variable camber foils." Oceanic Engineering, IEEE Journal of **29**(3): 738-749.

Madden, J., N. Vandesteeg, et al. (2004). "Artificial muscle technology: physical principles and naval prospects." Oceanic Engineering, IEEE Journal of **29**(3): 706-728.

Marx, R. G., C. Bombardier, et al. (1999). "What do we know about the reliability and validity of physical examination tests used to examine the upper extremity?" The Journal of Hand Surgery [NLM - MEDLINE] **24**(1): 185.

Mavroidis, C., C. Pfeiffer, et al. (2002). Prosthetic, orthotic, and other rehabilitative robotic assistive devices actuated by smart materials United States Rutgers.

Meijer, K., M. Rosenthal, et al. (2001). Muscle-Like Actuators? A Comparison Between Three Electroactive Polymers. Proceedings of the SPIE 8th Annual Symposium on Smart Structures and Materials: Electroactive Polymer Actuators and Devices, Newport Beach, CA, SPIE Press.

Michlovitz, S. L., B. A. Harris, et al. (2004). "Therapy interventions for improving joint range of motion: A systematic review." Journal of Hand Therapy **17**(2): 118.

Miller, D. (1998). Assistive Robotics: An Overview Assistive Technology and Artificial Intelligence: Applications in Robotics, User Interfaces, and Natural Language Processing V. Mittal, H. Yanco, J. Aronis and R. Simpson. Berlin / Heidelberg, Springer **1458/1998:** 126-136.

Morita, T. and S. Sugano (1995). Development of One D.O.F. Robots Arm equipped with Mechanical Impedance Adjuster. Proceedings of IEEE/RSJ International Conference on Intelligent Robotics and Systems, Pittsburgh, PA.

Moromugi, S., Y. Koujina, et al. (2004). "Muscle stiffness sensor to control an assistance device for the disabled." Artificial Life and Robotics **8**(1): 42-45.

Nakamura, T., N. Saga, et al. (2003). Development of a pneumatic artificial muscle based on biomechanical characteristics. Industrial Technology, 2003 IEEE International Conference on.

Nakazato, Y., T. Kato, et al. (1993). "Control of push-pull-type shape memory alloy actuators by fuzzy reasoning

" Transactions of Japan Society of Mechanical Engineers, Part C **59**(568): 226-232.

Nef, T. and R. Riener (2005). ARMin - design of a novel arm rehabilitation robot. 9th International Conference on Rehabilitation Robotics, 2005. ICORR 2005..

Nicola, M.-W. (2004). "Measurement of Hand Joint Range of Motion in Rheumatoid Arthritis: Repeatability and Variability." Journal of Hand Therapy **17**(4): 438.

Noritsugu, T. and T. Tanaka (1997). "Application of rubber artificial muscle manipulator as a rehabilitation robot." Mechatronics, IEEE/ASME Transactions on **2**(4): 259-267.

Nudo, R. J. (1996). "Use-dependent alterations of movement representations in primary motor cortex of adult squirrel monkeys." Journal of Neuroscience **16**(2): 785-807.

Nudo, R. J. and G. W. Milliken (1996). "Reorganization of movement representations in primary motor cortex following focal ischemic infarcts in adult squirrel monkeys." Journal of Neurophysiology **75**(5): 2144-9.

Nudo, R. J., B. Wise, et al. (1996). "Neural substrates for the effect of rehabilitative training motor recovery after ischemic infarct." Science **272**: 1791-1794.

Otsuka, K. and K. Shimizu (1970). "Memory effect and thermoelastic martensite transformation in Cu—Al—Ni alloy." Scripta Metallurgica **4**(6): 469-472.

Peckham, P. H. and J. S. Knutson (2005). "Functional electrical stimulation for neuromuscular applications." Annual Review of Biomedical Engineering **7**(1): 327-360.

Pelrine, R., R. Kornbluh, et al. (2000). "High-Speed Electrically Actuated Elastomers with Strain Greater Than 100%." Science **287**(5454): 836-839.

Popovic, M., A. Curt, et al. (2001). "Functional electrical stimulation for grasping and walking: indications and limitations." Spinal Cord **39**(8): 403-412.

Pratt, G. and M. Williamson (1995). Series Elastic Actuators. Intelligent Robots and Systems 95. 'Human Robot Interaction and Cooperative Robots', Proceedings. 1995 IEEE/RSJ International Conference on, Pittsburgh, PA.

Pratt, J. E. and B. T. Krupp (2004). Series Elastic Actuators for legged robots. Proceedings of the SPIE, Unmanned Ground Vehicle Technology VI, Orlando, FL, USA SPIE.

Prior, S. and P. Warner (1990). A review of world rehabilitation robotics research. High-Tech Help for the Handicapped, IEE Colloquium on

Prochazka, A., J. Elek, et al. (1992). "Attenuation of pathological tremors by functional electrical stimulation I: Method." Annals of Biomedical Engineering **20**(2): 205-224.

Ring, D., B. P. Simmons, et al. (1998). "Continuous passive motion following metacarpophalangeal joint arthroplasty." The Journal of Hand Surgery **23**(3): 505-511.

Robinson, D., J. E. Pratt, et al. (1999). Series Elastic Actuator Development for a Biomimetic Walking Robot. Proc. IEEE/ASME International Conference on Advanced Intelligent Mechatronics, Atlanta, GA.

Roch, I., P. Bidaud, et al. (2003). "Fabrication and characterization of an SU-8 gripper actuated by a shape memory alloy thin film." Journal of Micromechanics and Microengineering **13**(2): 330-336.

Romer, G. R. B. E., H. J. A. Stuyt, et al. (2005). Cost-savings and economic benefits due to the assistive robotic manipulator (ARM). Rehabilitation Robotics, 2005. ICORR 2005. 9th International Conference on

Rozmaryn, L. M., S. Dovelle, et al. (1998). "Nerve and tendon gliding exercises and the conservative management of carpal tunnel syndrome." Journal of Hand Therapy **11**(3): 171-9.

Salisbury, K., B. Eberman, et al. (1989). The Design and Control of an Experimental Whole-Arm Manipulator. Proceedings of the 5th International Symposium On Robotics Research.

Salter, R. B. (1996). "History of rest and motion and the scientific basis for early continuous passive motion." Hand Clinic **12**(1).

Schultz-Johnson, K. (2002). "Static progressive splinting." Journal of Hand Therapy **15**(2): 163.

Schulz, S., C. Pylatiuk, et al. (2001). A new ultralight anthropomorphic hand. Robotics and Automation, 2001. Proceedings 2001 ICRA. IEEE International Conference on.

Scott, T. and P. Peckham (1995). Functional electrical stimulation and its application in the management of spinal cord injury. Diagnosis and Management of Disorders of the Spinal Cord. R. Young and R. Woolsey. Orlando, FL, WB Saunders & Co: 377-396.

Scott, T., P. Peckham, et al. (1995). "Upper etremity neuroprostheses using functional electrical stimulation." Bailliere's Clinical Neurology **4**(1): 57-75.

Scott, T., V. Vare, et al. (2003). Rehabilitation applications for the hand using artificial muscle. IPRI International Workshop "Electronic Fibres and Textiles", University Wollongong

Selden, B., C. Kyu-Jin, et al. (2004). Segmented binary control of shape memory alloy actuator systems using the Peltier effect. Robotics and Automation, 2004. Proceedings. ICRA '04. 2004 IEEE International Conference on.

Selden, B., C. Kyu-Jin, et al. (2006). "Segmented shape memory alloy actuators using hysteresis loop control." Smart Materials and Structures **15**(2): 642.

Shadmehr, R. and M. Arbib (1992). "A mathematical analysis of the force-stiffness characteristics of muscles in control of a single joint system." Biological Cybernetics **66**(6): 463-477.

Smela, E. (2003). "Conjugated Polymer Actuators for Biomedical Applications." Advanced Materials **15**(6): 481-494.

Smith, B., P. Peckham, et al. (1987). "An externally powered, multichannel, implantable stimulator for versatile

control of paralyzed muscle." IEEE Trans Biomed Eng **34**(7): 499-508.

Sollerman, C. (1980). Assessment of grip function: Evaluation of a new test method. Hand grip function: Analysis and evaluation and a new test method. C. Sollerman. Gothenburg, University of Gothenburg: pp1-21.

Spillman, W., J. Sirkis, et al. (1996). "Smart materials and structures: what are they?" Smart Materials and Structures **5**: 247–254.

Spinks, G., T. Campbell, et al. (2005). "Force generation from polypyrrole actuators." Smart Materials and Structures **14**: 406-412.

Spinks, G., L. Liu, et al. (2002). "Strain Response from Polypyrrole Actuators under Load." Advanced Functional Materials **12**(6-7): 437-440.

Stalmans, R. and J. Van-Humbeek (1995). Shape Memory Alloy: Functional and Smart. Smart Materials and Technologies - Sensors, Control Systems and Regulators, Prague, Czech Republic.

Stenehjem, J. and J. Swenson (1983). "Wrist driven flexor hinge orthosis: linkage design improvements." Arch Phys Med Rehabil **64**(11): 566-8.

Sulzer, J., M. Peshkin, et al. (2005). MAMONET: An exotendon-driven rotary series elastic actuator for exerting joint torque. Rehabilitation Robotics, 2005. ICORR 2005. 9th International Conference on.

Surdilovic, D., R. Bernhardt, et al. (2003). STRINGMAN: A New Wire Robotic System for Gait Rehabilitation. Proceedings of the 8th International Conference on Rehabiliation Robotics.

Swanson, A., G. de Groot Swanson, et al. (1995). Evaluation of Impairement of Hand Function. Rehabilitation of the Hand: Surgery and Therapy. J. Hunter, E. Mackin and A. Callaghan. St Louis, Mosby. **2:** 1839-1896.

Unsworth, A., P. M. A. Bey, et al. (1981). "Stiffness in the metacarpo-phalangeal joints of young adults." Clinical Physics and Physiological Measurement **2**(2): 123.

Unsworth, A., P. Yung, et al. (1982). "Measurement of stiffness in the metacarpophalangeal joint: the arthrograph." Clinical Physics and Physiological Measurement **3**(4): 273.

Wehbe, M. A. (1987). "Tendon gliding exercises." Am J Occup Ther **41**(3): 164-7.

Wehbe, M. A. and J. M. Hunter (1985). "Flexor tendon gliding in the hand. Part I. In vivo excursions." The Journal of hand surgery **10**(4): 570-4.

Wehbe, M. A. and J. M. Hunter (1985). "Flexor tendon gliding in the hand. Part II. Differential gliding." The Journal of hand surgery **10**(4): 575-9.

Wijman, C., K. Stroh, et al. (1990). "Functional evaluation of quadriplegic patients using a hand neuroprosthesis." Archives of physical medicine and rehabilitation **71**(13): 1053-7.

Yashin, V. V. and A. C. Balazs (2006). "Pattern Formation and Shape Changes in Self-Oscillating Polymer Gels." Science **314**(5800): 798-801.

Yung, P., A. Unsworth, et al. (1986). "Measurement of stiffness in the metacarpophalangeal joint: the effects of physiotherapy." Clinical Physics and Physiological Measurement **7**(2): 147-156.

Zhang, L. (2001). Solid Mechanics for Engineers. Hampshire, Palgrave.

Zinn, M., O. Khatib, et al. (2002). Towards a human-centered intrinsically-safe robotic manipulator. IARP Workshop on Technical Challenges for Dependable Robots in Human Environments.
http:// citeseer.ist.psu.edu/article/zinn02towards.html

# Appendix A

# –

# Design and Calibration of the Force Position Transducer

## Basic principles of the FPT

The central component of the FPT is a spring within a fixed chamber placed in series with the actuating cable. The spring is free to move with the cable. Its length changes in response to tension of the cable. This introduces compliance in the cable. Hence the actuator must now travel a greater distance to accommodate for the length change of the spring and transmit the required force to the load (see Figure 3.2 in Chapter 3). The cable connecting the actuator to the FPT spring is referred to as the actuator segment.

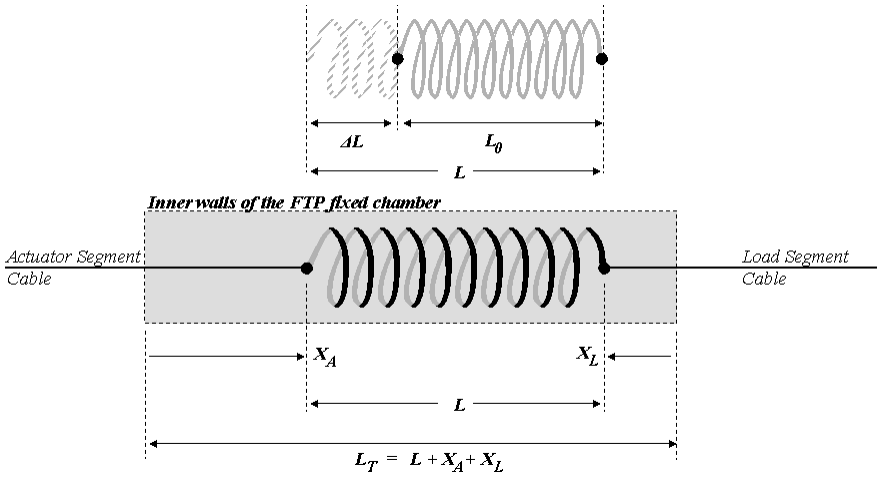


**Figure A.1** $X_A$ and $X_L$ represent the distances of the two ends of the free moving spring from the respective ends of the chamber. The chamber contains sensor that measure these two positions continuously. The length of the spring L can be calculated by subtracting $X_A$ and $X_L$ from the chamber length $L_T$. This length can be used to find the tension F in the cable.

The chamber inside which the spring is free to move, and through which the cable passes, contains sensors to measure the absolute positions of the two ends of the spring (with respect to the chamber). These are $X_A$ and $X_L$ (see Figure A.1), where $X_A$ corresponds to the position of the cable connected to the actuator end and $X_L$ refers to the position of the load end of the spring.

Using the values of $X_A$ and $X_L$, the length of the spring can be calculated. This length is directly related to the tension in the cable given by the equation:

$$F = K_S \times ( L - L_0 ) \qquad \textbf{(A.1)}$$

Where F is the force (tension), L is the varying spring length, $K_S$ the spring constant and $L_0$ the resting length of the spring.

$$\text{But, } L = L_T - X_A - X_L \qquad \textbf{(A.2)}$$

Where $L_T$ is the total internal fixed length of the FPT chamber.

$$\text{Therefore, } F = K_S \times ( L_T - L_0 - X_A - X_L ) \qquad \textbf{(A.3)}$$

### Obtaining force and position information

The position of the load segment of the cable is $X_L$. Given that there is minimal compliance in this segment, actual position of the load can be deduced from this value. By knowing the constants in equation (A.3), force can be calculated based on the measurements of $X_A$ and $X_L$.

## The Polar Disc method – Relationship between voltage and position

Cylindrical linear sliders were prepared to fit into each end of the FPT spring. These sliders were coupled to the optical sensing mechanisms in the following manner:

- The movement of each slider caused a pair of polarised films to rotate in respect to each other, thus causing an attenuation of light passing through.
- The attenuations were measured using phototransistors
- The linear sliders were shaped in such a way to produce a linear relationship between slider displacements and corresponding light attenuations.

As shown in Figure A.2, rotating one disc relative to the other has an attenuating effect on light passing through the pair. This was exploited as an effective method to measure movement via the voltage reading across the light detector.

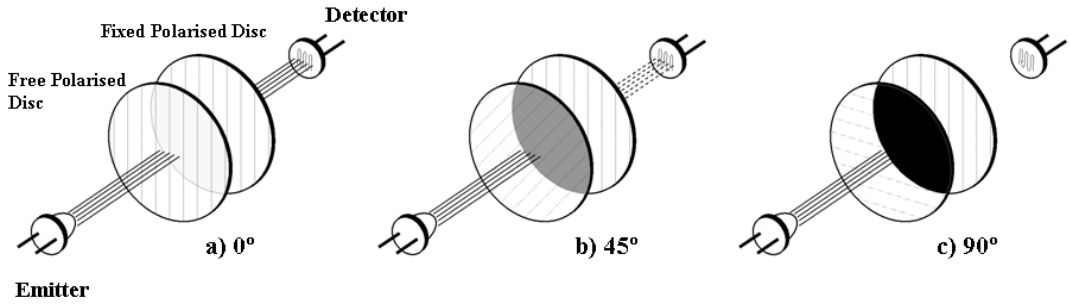


**Figure A.2** The polarised disc attenuation method. The relative rotation of one polarised disc against the other is coupled to the linear movement of one end of the FPT spring. a) When the angle is zero, the polarised orientations are aligned and maximum transparency occurs. b) As one disc is rotated against the other, the light path through the disc pair attenuates and voltage reading drops at the receiver. 45° orientation attenuates the light path by half of maximum. c) At 90°, no light passes through and voltage across receiver is minimal.

Figure A.3 shows the simple circuit used to optically couple a light emitter to a detector. The emitter used was a surface mount high intensity Yellow LED (660 mcd, 20mA 595nm). The matching detector was the Agilent APDS-9002 Miniature Surface-Mount Ambient Light Phototransistor, selected for its high sensitivity and small size. The voltage V measured across the phototransistor's load resistor versus the polarised disc angle is sinusoidal and can be approximated by the equation:

$$V = V_{max} \times \frac{(\text{Cos } 2\alpha + 1)}{2} \qquad \textbf{(A.4)}$$

Where α is the angle between the polarised orientations and $V_{max}$ is the maximum voltage measured when the discs are fully aligned (i.e. α = 0°)

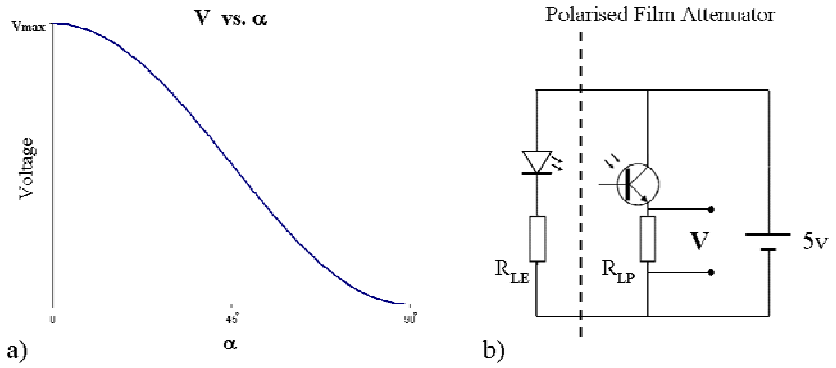


**Figure A.3** a) The relationship between voltage V vs. angle α is described by equation (A4). b) The circuit is a simple optical coupling of a LED light source and a phototransistor with appropriate load resistors. The polarised film pair attenuates the amount of light that passes from the LED to the phototransistor and alters the voltage across the load resistor $R_{LP}$.

The maximum voltage was experimentally found to exceed 2.5V, satisfying the requirement for DC output without amplification. However, the relationship between the angle and the voltage is not linear. To obtain a linear relationship between the slider position and the phototransistor output, the Slider Window can be shaped appropriately. The ideal relationship is a simple linear model:

$$V = K \times X_s + C \qquad \textbf{(A.5)}$$

Where $X_s$ is the position of the slider and K and C are constants.

To achieve this relationship, at each position $X_s$, the cross sectional opening of the slider window must be such that the resulting angle α can equate to the following value:

$$\alpha = \frac{1}{2} \times \text{ArcCos}\left(\frac{2K \times X_s + 2C}{V_{max}} - 1\right) \qquad \textbf{(A.6)}$$

## FPT Calibration Method

The following three steps are used to calibrate the FPT using a single known position and a single known force.

### ① X = 0, F = 0

The position of the load is brought to its minimum with tension equal to zero.

$X_L = 0$,
$X_A = X_{Amax}$ (its maximum position)
$V_A$ and $V_L$ are measured:

$V_L = V_{L1}$
$V_A = V_{A1}$

### ② X = $X_{CAL}$, F = 0

Position is brought to a known calibrated value $X_{CAL}$. Tension is equal to zero.

$X_L = X_{CAL}$,
$X_A = X_{Amax} - X_{CAL}$ (shifted by $X_{CAL}$)
$V_A$ and $V_L$ are measured:

$V_L = V_{L2}$
$V_A = V_{A2}$

### ③ X = $X_{CAL}$ - ΔL, F = $F_{CAL}$

While the actuator end of the FPT is locked into place (e.g. by locking the actuator cable), a known calibrated force is applied to the load end (e.g. using a hanging weight).

$X_L = X_{CAL} - \Delta L$ (shifted towards the load by ΔL)
$X_A = X_{Amax} - X_{CAL}$
$V_L$ is measured:

$V_L = V_{L3}$

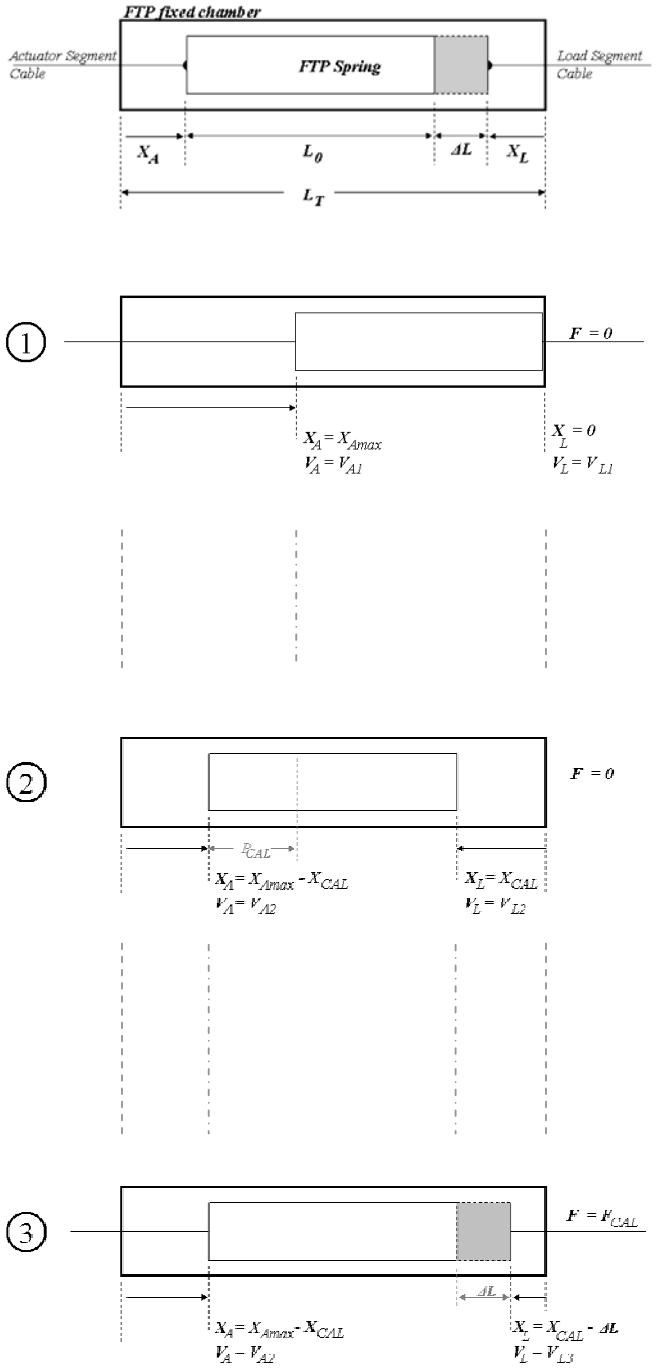


**Figure A.4** FPT Calibration steps

*Calculations*

If the slider voltages are made linearly proportional to the slider positions, we can expect the following equations to hold true:

$$X_L = K_L \times V_L + C_L \qquad \textbf{(A.7)}$$

$$X_A = K_A \times V_A + C_A \qquad \textbf{(A.8)}$$

Where $X_L$ is the same as X (position measured by FPT), $K_X = K_L$ and $C_X = C_L$.

From steps **1** and **2,** the calibration constants for $X_L$ can be derived:

$$K_X = K_L = \frac{X_{CAL}}{V_{L2} - V_{L1}} \qquad \textbf{(A.9)}$$

$$C_X = C_L = \frac{X_{CAL} \times V_{L1}}{V_{L1} - V_{L2}} \qquad \textbf{(A.10)}$$

Also from steps **1** and **2,** $K_A$ and $C_A$ can be derived:

$$K_A = \frac{X_{CAL}}{V_{A1} - V_{A2}} \qquad \textbf{(A.11)}$$

$$C_A = X_{Amax} - \frac{X_{CAL} \times V_{A1}}{V_{A1} - V_{A2}} \qquad \textbf{(A.12)}$$

In order to present Tension as functions of $\mathbf{V_A}$ and $\mathbf{V_L}$ as presented in equation (2.2), equation (A.3) is expanded.

$F = K_S \times ( L_T - L_0 - X_A - X_L )$ (from (3))

When $F = 0$ and $X_L = 0$, $X_A = X_{Amax}$ (see Figure A.4 step 1)

Therefore, $L_T - L_0 = X_{Amax}$ **(A.13)**

$$F = K_S \times ( X_{Amax} - X_A - X_L ) \qquad \textbf{(A.14)}$$

The final unknown value $K_S$ can be determined from step **3**.

$$K_S = \frac{F_{CAL}}{\Delta L_{CAL}} = \frac{F_{CAL}}{F_{CAL} - C_X - (K_X \times V_{L3})} \qquad \textbf{(A.15)}$$

Now, by substituting the derived expressions for $K_S$, $X_A$ and $X_L$ equation (A.14) can be expanded:

$$F = \left(\frac{K_S \times X_{CAL}}{V_{A2} - V_{A1}}\right) \times V_A - \left(K_S \times K_X\right) \times V_L - \left(\frac{K_S \times V_{A1} \times X_{CAL}}{V_{A1} - V_{A2}} - K_S \times X_{CAL}\right) \qquad \textbf{(A.16)}$$

Based on equations (A.7), (A.9) and (A.10), the Position equation is derived as:

$$X = \left(\frac{X_{CAL}}{V_{L2} - V_{L1}}\right) \times V_L + \left(\frac{X_{CAL} \times V_{L1}}{V_{L1} - V_{L2}}\right) \qquad \textbf{(A.17)}$$

Where the values in parenthesis are the derived constants defined in equations (2.1) and (2.2).

In summary, the three calibration steps enable position calibration constants [$K_X$ and $C_X$ for equation (2.1)] to be obtained from equations (A.9) and (A.10). Using equation (A.16), the force calibration constants [$K_{FA}$, $K_{FL}$ and $C_F$ for equation (2.2)] can be derived.

## The FPT assembly CAD models

The FPT body was constructed using CNC cutting based on 3D model drawings. The most critical construction details requiring high accuracy were the slider windows.

The window-cut-paths were derived by modelling the 3D geometry of the polarised disc pins and the dynamic interaction between the pins and the slider window walls.

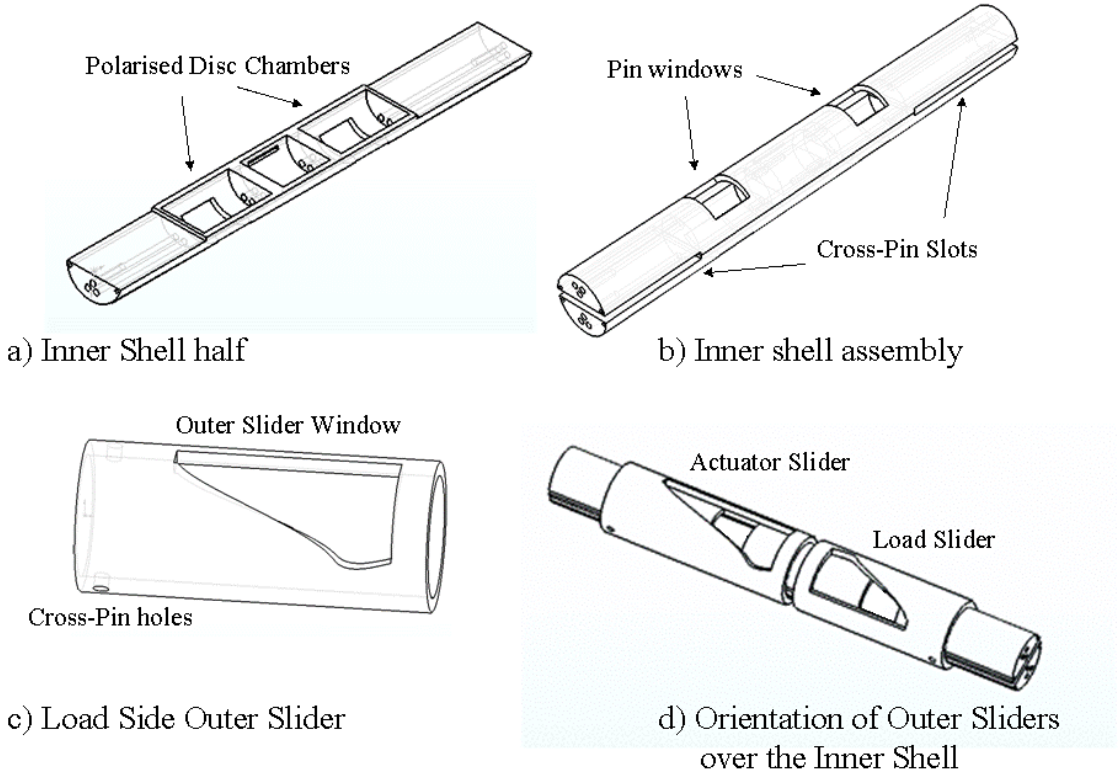


**Figure A.5** 3-D CAD drawings of the FPT body and assembly. a) The Inner shell was made in two half sections. The polarised discs, the emitter and phototransistors, and shaft bearings were placed in the chambers of the lower half before: b) assembling the Inner shell. c) The Outer Slider window shape for each side was calculated to yield a linear output proportional to the slider position. The Cross-Pin holes aligned the slider with the slots in the Inner Shell. d) The sub-assembly depicted before the FPT spring is placed over the sliders and connected at each Cross-Pin.

# Appendix B

–

# The Pulley-based Work-Summation System

## Pulley-based work-summation and descriptions of its function

The mechanical assembly is based on pulleys. The pulleys may be either cables around wheels or they may be cables going through low friction conduits:

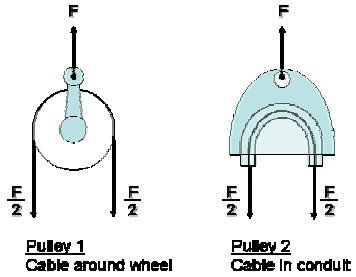


**Figure B.1** Alternate ways to create pulleys

The pulleys can be interconnected in various ways with different effects on the output. A simple force-adder can be represented by the following arrangement:

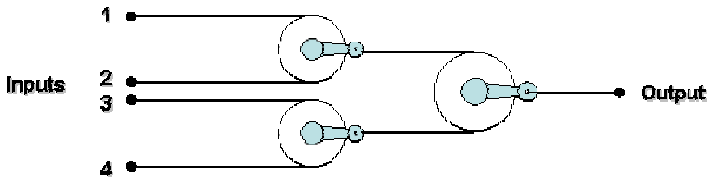


**Figure B.2** Basic pulley arrangement.

Using the arrangement in Figure B.2, four actuators each with linear travel $D_1$, $D_2$ $D_3$ and $D_4$ respectively, can be combined to produce a movement $(D_1+D_2+D_3+D_4)/4$ at the output at force F. Each actuator feels a quarter of the overall force. Furthermore, each of the actuators can contribute discretely to the output by incremental movements of $D_i/4$. Thus, if in a scenario, actuators 2, 3 and 4 are inactive and only actuator 1 is activated, the resulting movement at output would be $D_1/4$ at force F. Subsequently, if actuator 2 is activated, a further movement of $D_2/4$ will be added to the output and so on.

## Force feedback opportunities

For feedback to a control system, actuation force can be measured using an addition to the pulley system. Two examples are shown in Figure B.3. The first example shows a second pulley placed subsequent to the first combined output. The second pulley has two functions: firstly, it amplifies the output force by a factor of two and secondly, it allows the output force to be measured by a fixed force gauge. In the second example, a reversed pulley is used following the first output. This method allows the amplification of displacement (with the attenuation of force) and the measurement of force using a fixed sensor.

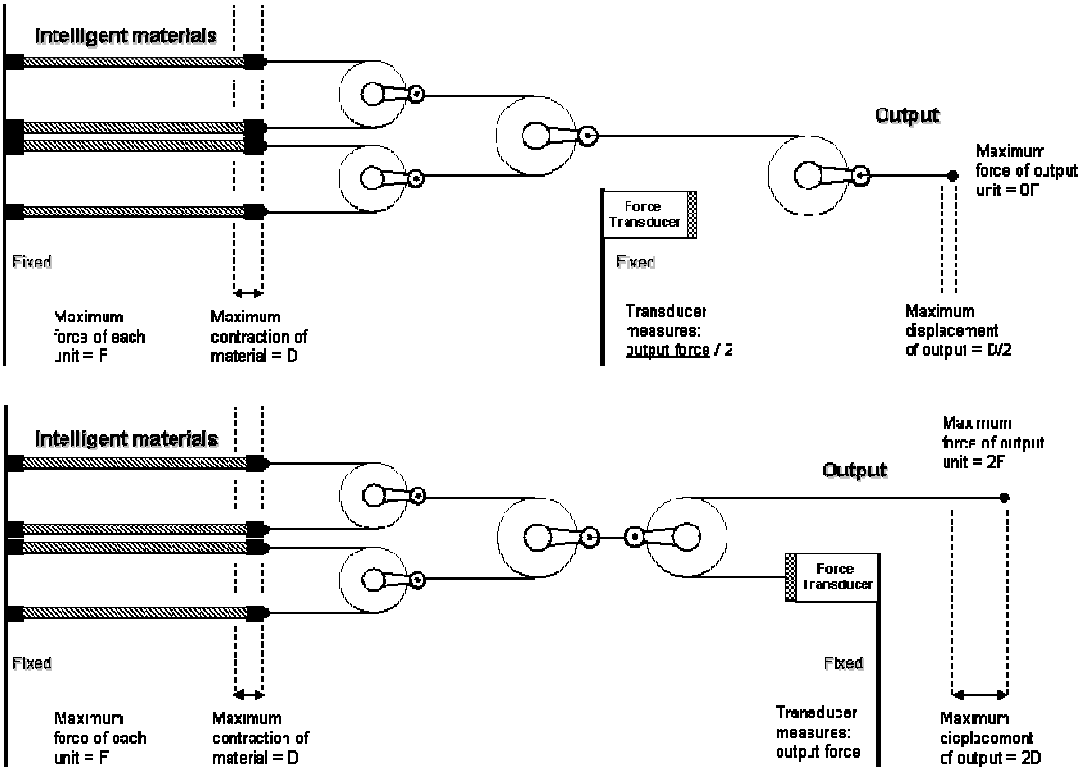


**Figure B.3** Two examples for using the work-summation pulley system with force feedback.

## Lever-based network: An alternative work-summation system

The use of the lever system proposed here will be most suited for applications where only limited linear or rotational motion is required and summation of multiple inputs is necessary. As levers are simpler and more compact than pulleys, this method also presents a potential for the system to be further miniaturised.

The mechanical assembly proposed is based on the interconnection of levers. In this context, the basic unit is a lever which is defined as a simple bar fixed at one point with force applied at one or more other points to create a turning moment about the fixed point or pivot. The following diagram depicts a simple example of the lever:

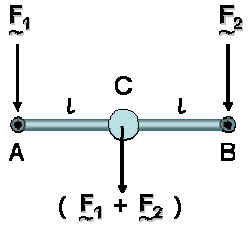


**Figure B.4** Lever centre point C is the basic output. Force at point C is equal to $F_1 + F_2$.

The lever is analogous to the pulley with the centre point C being equivalent to the centre of the pulley and the two arm-ends A and B equivalent to the pulley cables. Figure B.5 presents the same concept shown in Figure B.2 but replacing pulleys with levers.

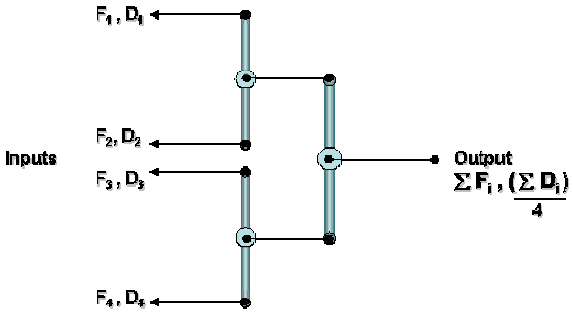


**Figure B.5** A basic 4-input lever-based system

As with the pulley arrangement incremental displacement can be added to the output. It must be noted that with rotation of each individual lever, the force/displacement transmission of each actuator will change (according to changing force vector angles). The levers are most effective (optimal force vectors) when parallel (or near parallel) to each other. Uneven movements at the two ends of a lever cause a change in the angle of the lever. With the change in angle the forces are not transmitted as effectively. The most effective function occurs when a lever is perpendicular to the lever forces. With actuators that activate with small movements relative to the size of the levers, unequal movements will not cause a significant change in the angle of the levers. *Hence this system is advantageous and most useful for actuators with very limited movement* (as with most intelligent polymer based actuators discussed).

Due to their simplicity, the levers can be interlinked directly to reduce the number of elements used in the assembly where failures can occur, to reduce unwanted friction and to reduce the overall weight and size of the system (as shown in Figure B.6). This is also easier than the pulley method to manufacture and to miniaturise.

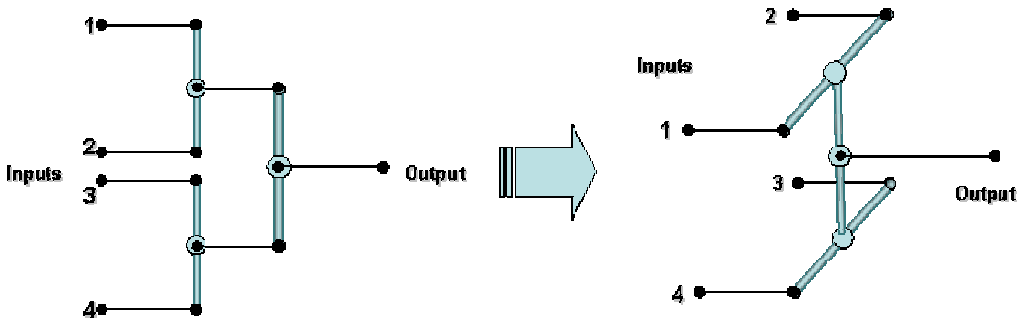


**Figure B.6** The lever-based system can be simplified to reduce the number of joints and components.

Another simpler form of the lever system can be made in the manner depicted in Figure B.7. This is effectively the primary lever adder described in Figure B.4 but with the ability of amplifying the output force (at the cost of movement by increasing the length of the output lever).

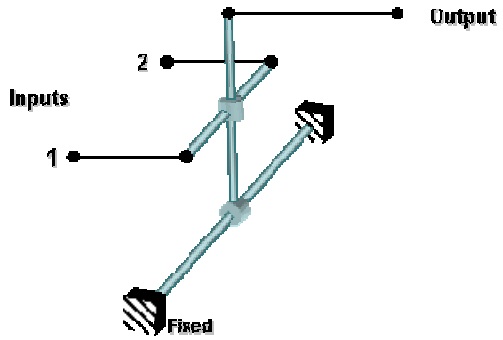


**Figure B.7** The lever based system can be simplified to reduce the number of interconnecting cables. This system combines two inputs into one output. The relationship of output force to summated input force is varied by placing the output vector further away from the fixed hinge than the input.

The system in Figure B.7 can be expanded by introducing additional levers at the input arms. This increases the number of inputs (Figure B.8).

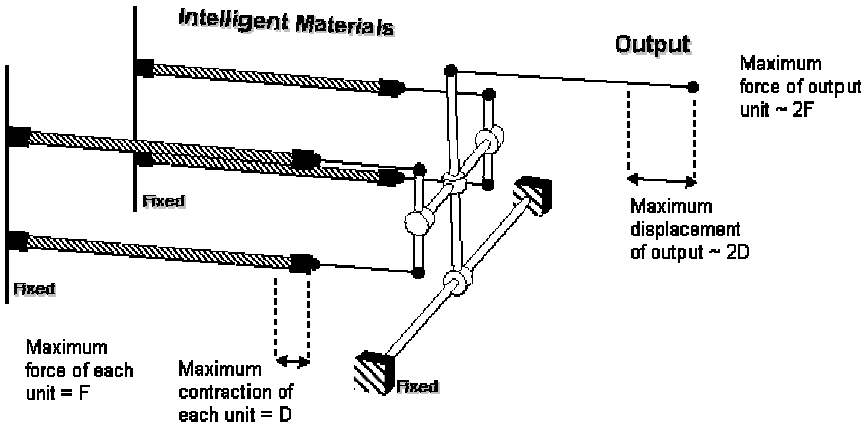


**Figure B.8** The lever-based system is expanded to include four input actuators.

The lever system can be continuously expanded by adding further links to input points. Figure 5.25 in Chapter 5 shows a 32-input system developed by the author for use with multiple conducting-polymer-actuators.

# Appendix C

# –

# Construction of the 4WP and SMA-BA setups

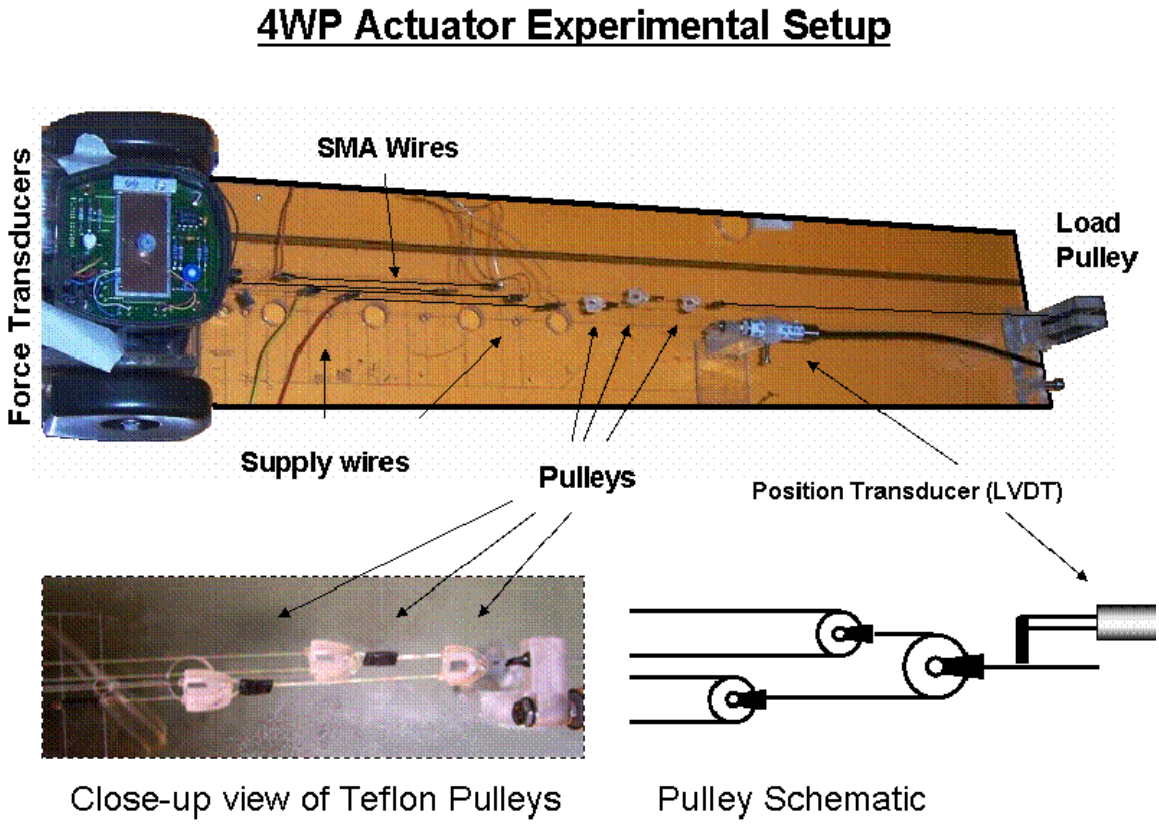


**Figure C.1** *The 4WP experimental setup showing schematic and close-up photo of the work-summation pulley system.*

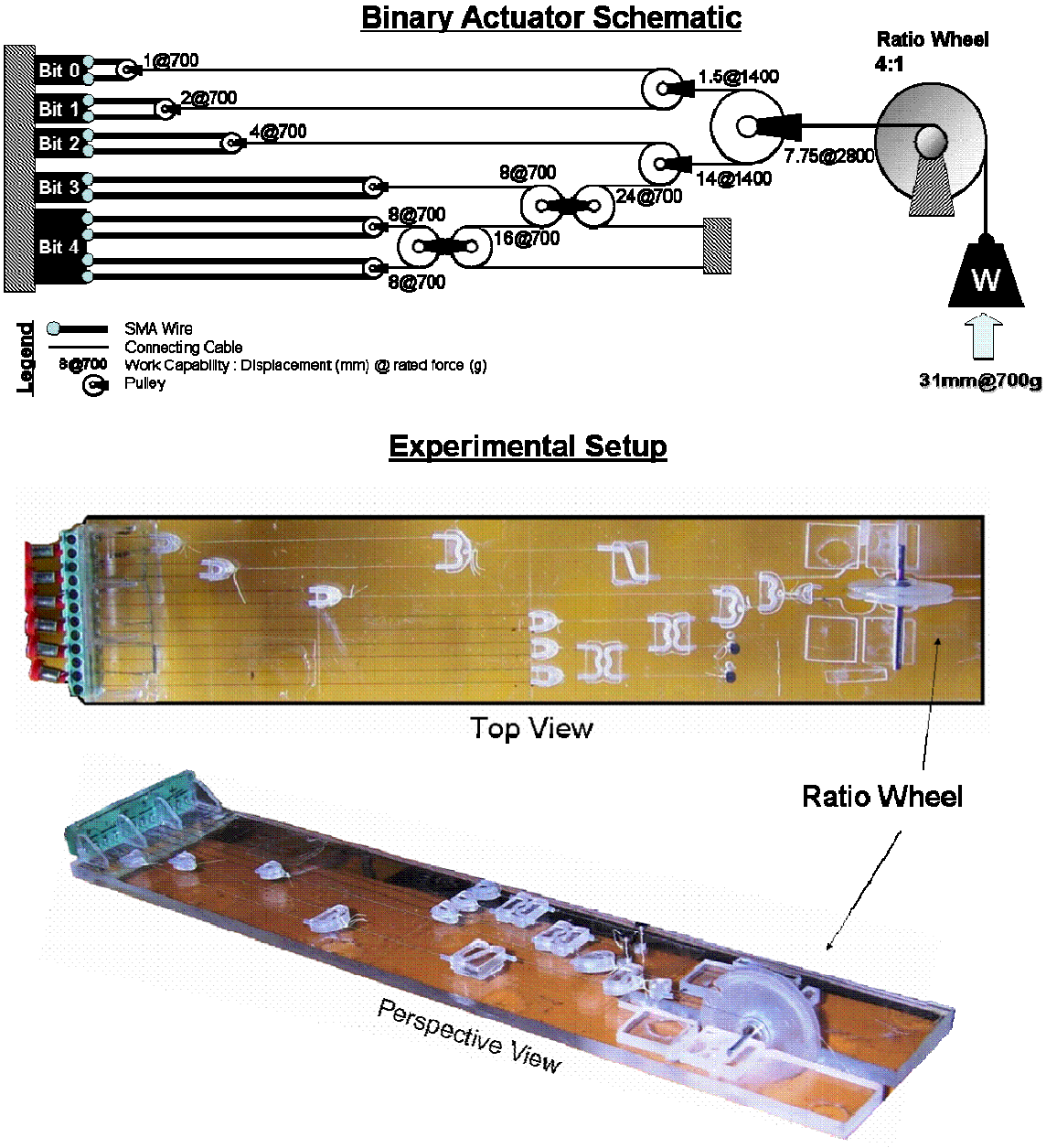


**Figure C.2** The Binary Actuator experimental setup schematic and photos of the actual constructed assembly.

# Appendix D

# –

# SMA Actuator Control Circuits

Transistor based SMA activation channels

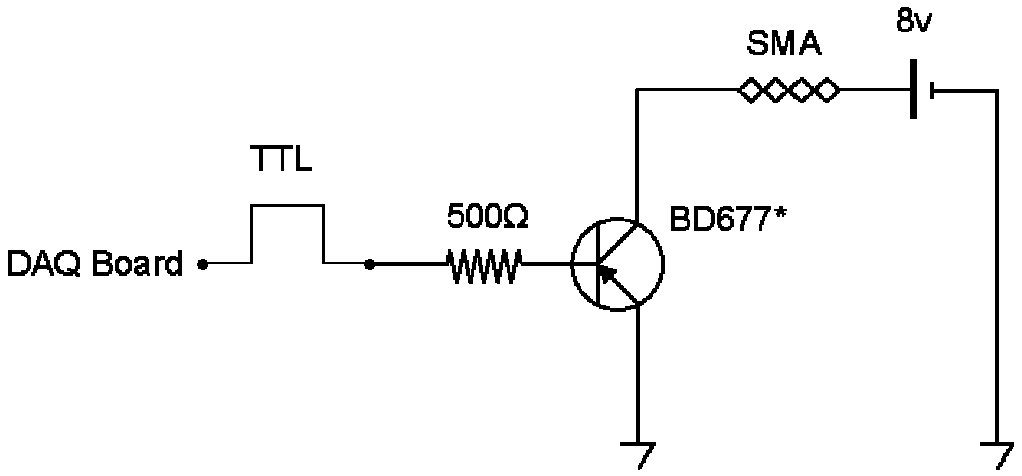


* Power Darlington Transistor (NPN)

SMA wires were activated using transistor circuits turned on by digital (TTL) signals. The data acquisition board controlled by software written in Labview™ featured eight analogue channels, each driving a separate transistor circuit.

# Appendix E

-

# Comparison of Artificial Actuators with Natural Muscle

## Comparison of various actuator technologies and natural muscle

*(Adapted from Herr, et al 2004 and Roch, et al 2003)*

| | Actuator Type (specific example) | Typical (Max.) Strain (%) | Typical (Max.) Stress (MPa) | Typical (Max.) Specific Elastic Energy Density (J/kg) | Typical (Max.) Elastic Energy Density ($kJ/m^3$) | Typical (Max.) Avg. Specific Power Density at 1 Hz (W/g) | Peak Strain rate (%/s) | Est. Max. Efficiency (%) | Relative Speed (full cycle) |
|---|---|---|---|---|---|---|---|---|---|
| NATURAL MUSCLE | Mammalian Skeletal Muscle | 20 (40) | 0.1 (0.35) | 41 (80) | 41 (80) | 0.041 (0.08) | > 50 | 20% | Medium |
| ELECTROACTIVE POLYMER | Dielectric elastomer | 25 (> 300) | 1.0 (7.0) | 100 (3400) | 100 (3400) | 0.1 (3.4) | > 450 | 60–90 | Med. - Fast |
| | Electrostrictive Polymer | 3.5 (7.0) | 20 (45) | 170 (> 530) | 300 (> 1000) | 0.17 (> 0.53) | > 2000 | 60–90 | Fast |
| | Electrochemo-mechanical Conducting Polymer | 2 (20) | 5 (200) | 100 (1000) | 100 (1000) | 0.1 (1.0) | 1 | < 5 | Med. -Slow |
| | Ionic Polymer Metal Composite | 0.5 (3.3) | 3 (15) | (4.0) | (6.0) | 0.004 | 3.3 | 1.5–3 | Med. - Slow |
| | Mechano-chemical Polymer/Gels (Polyelectrolyte) | > 40 | 0.3 | 60 | < 60 | < 0.06 | < 1 | 30 | Slow |
| | Piezoelectric Polymer (PVDF) | 0.1 | 4.8 | 1.3 | 2.4 | 0.0013 | ? | 60–90 | Fast |
| OTHER | Liquid Crystal Elastomer (Thermal) | 19 (45) | 0.12 (0.45) | 3.0 (60) | 3.0 (60) | < 0.003 | 37 | < 5% | Slow |
| | Shape Memory Polymer | 100 | 4 | 2000 | 2000 | < 0.2 | ? | < 10 | Slow |
| NONPOLYMER ACTUATORS | Electromagnetic | | | | | | | | |
| | Direct (Voice Coil) | 50 | 0.10 | 3.0 | 25 | 0.003 | > 1000 | > 80 | Fast |
| | Motor/transmission | 50 | NA | NA | NA | 0.5 | < 200 | > 50 | Medium |
| | Piezoelectric | | | | | | | | |
| | Ceramic (PZT) | (0.2) | (110) | (13) | (100) | (0.013) | > 1000 | > 90 | Fast |
| | Single Crystal (PZN-PT) | (1.7) | (131) | (130) | (1000) | (0.13) | > 1000 | > 90 | Fast |
| | Shape Memory Alloy (TiNi) | > 5 | > 200 | >4000* | > 27000* | < 15 | 300 (one direction only) | < 10 | Slow |
| | Thermal (Expansion) | 1 | 78 | 150 | 400 | < 0.15 | Depends on heat transfer | < 10 | Slow |
| | Magnetostrictive (Terfenol-D, Etrema Products) | 0.2 | 70 | 2.7 | 25 | >0.0027 | >1000 | 60 | Fast |

*The reported energy density of Nitinol varies greatly in literature. Kornbluh (1998) reported 5000 $kJ/m^3$, Roch (2003) reported 27000 $kJ/m^3$ and Madden (2004) reported 1000 $kJ/m^3$. This variation may be due to the different assumed strain/stress points at which the calculations have been made. The author's own measurements have been 9500 $kJ/m^3$ for this study.

# Appendix F

# –

# Calibration and Accuracy of the Electronic Goniometer

## Construction if the reference goniometer

An accurate reference goniometer was developed for this project. The LVDT rod connects to a cable that translates the rotational motion of the goniometer lever into linear motion. The LVDT is spring biased to maintain a light tension in the cable at all times. The electronic goniometer can be placed dorsally (on the back) or laterally (on the side of the finger). The goniometer lever couples to the middle finger segment via a slider housing. This component maintains the lever parallel to the dorsal surface while at the same time allowing the lever to slide during movement.

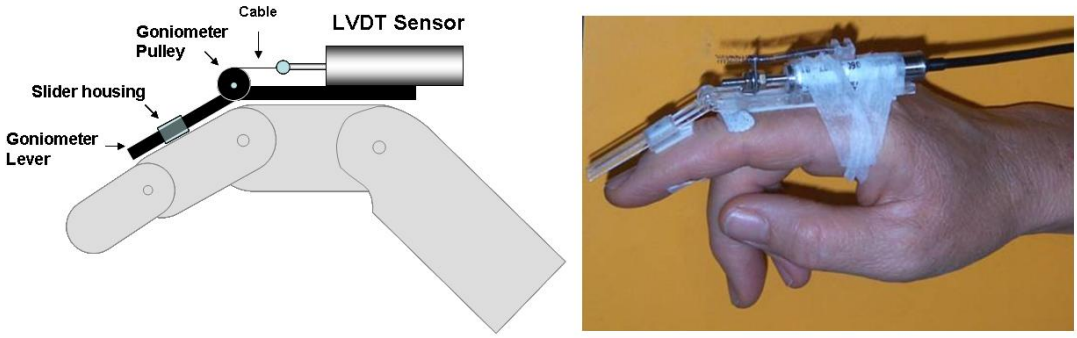


**Figure F.1** Side view of the LVDT-based Electronic Goniometer. Left: Schematic of the device shown on the finger model. Right: actual placement on a subject's finger during the standard TROM and AROM assessments.

## Accuracy of the electronic goniometer

The LVDT-based electronic goniometer was calibrated using two known angles, 0˚ and 90˚. Subsequently, the goniometer reading was compared to calibrated angles. The readings are shown in Figure F.2.

Accuracy was good with a maximum full-scale (90˚) error of 0.39%

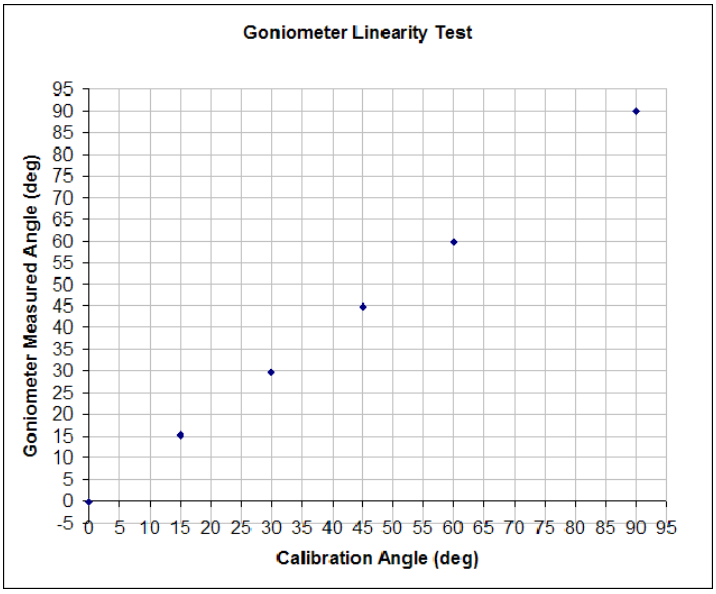


**Figure F.2** Plot of the LVDT goniometer accuracy test.